

**BAX-MEDIATED COORDINATION OF COGNATE ORGANELLE CELL
DEATH SIGNALING CASCADES DETERMINES CELL DEATH PHENOTYPE
AFTER TRAUMA IN THE NEONATAL RAT CORTEX**

APPROVED BY SUPERVISORY COMMITTEE

Dean, Graduate School

For my Babczy

**BAX-MEDIATED COORDINATION OF COGNATE ORGANELLE CELL
DEATH SIGNALING CASCADES DETERMINES CELL DEATH PHENOTYPE
AFTER TRAUMA IN THE NEONATAL RAT CORTEX**

BY

MARTIN BARTHOLOMEW GILL, B.A.

DISSERTATION

Presented to the Faculty

of the University of Texas

Graduate School of Biomedical sciences at Galveston

in Partial Fulfillment

of the Requirements

for the degree of

DOCTOR OF PHILOSOPHY

THE UNIVERSITY OF TEXAS MEDICAL BRANCH

AT GALVESTON

JULY, 2007

Acknowledgements

There is no possible way for me to put in one page all of those who are deserving of thanks for their help and guidance during my graduate career at the University of Texas Medical Branch. First and foremost, I am indebted to my mentor, Dr. Regino Perez-Polo, for his constant encouragement and willingness to give experimental independence to a self-acknowledged loony, as well as, for his genuine compassion for all matters in my life, science or otherwise. In addition, I owe a huge amount of thanks to Dr. Olivera Nesic-Taylor, who played a huge role in teaching me to design experiments that would ask and answer key questions. I would, also, like to thank Karin Werrbach-Perez for passing on to me over 20 years of tissue culture experience and for her great sense of humor. To my dissertation committee, I am extremely thankful for the constant availability for guidance and invaluable critique. I owe all of the administrative personnel, in particular Donna Masters, a huge 'thank you,' as without them, none of my experiments could have ever been accomplished. I would like to thank my lab mates, past and present, as well as my friends, for being with me in the trenches, and their willingness to put up with my antics. I owe a special thanks to my family, especially my mother and father, who always gave me love and support no matter avenue of life I traveled. Last and certainly not least, I am extremely thankful to my best friend and wife, Cassie, who has been a rock on which I could lean, an ear in which I could confide and an angel which I can cherish forever.

**BAX-MEDIATED COORDINATION OF COGNATE ORGANELLE CELL
DEATH SIGNALING CASCADES DETERMINES CELL DEATH PHENOTYPE
AFTER TRAUMA IN THE NEONATAL RAT CORTEX**

Publication No. _____

Martin Bartholomew Gill, Ph.D.

The University of Texas Medical Branch at Galveston, 2007

Supervising Professor: J. Regino Perez-Polo, Ph.D.

Bax translocation to the mitochondria has been well-characterized to induce apoptotic cell death in multiple injury paradigms. However, pro-cell death actions for Bax outside of the mitochondria remain understudied. Bax's pro-cell death role at other non-mitochondrial locales in response to oxidative stress and energy depletion injury paradigms were investigated in *in vitro* and *in vivo* neonatal cortical models.

The aims of this project were: 1) measure Bax multi-organelle localization after *in vivo* HI-injury and its correlation with cognate organelle cell death

signaling, 2) measure Bax multi-organelle localization after *in vitro* rotenone-induced injury and its correlation with cognate organelle cell death signaling and 3) using FK506 and 100% O₂ interventions, investigate the coordinating role for Bax in the activation of multi-organelle cognate cell death signaling cascades and the effects it has on the resulting cell death phenotype.

In vivo, hypoxia-ischemia (HI) induces a distinct subcellular time course for Bax in the neonatal cortex, localizing first to the nucleus, then to mitochondria and, finally, to the ER with Bax localization to these organelles coordinating with the activation of each organelle's cognate cell death cascade, suggesting a new role for Bax in coordinating the cell death signaling at multiple subcellular organelles.

In vitro, using necrotic-like and apoptotic stimuli, we observed both treatments induced early nuclear Bax localization, the apoptotic stimulus increasing mitochondrial Bax localization and caspase-mediated cleavage of α -fodrin, and the necrotic-like stimulus increasing ER Bax localization and calpain-mediated cleavage of α -fodrin. Based on these findings, we concluded apoptotic and necrotic-like stimuli promote differential Bax localization and subsequent differential activation of cognate cell death signaling cascades to induce expression of their characteristic phenotypic cell morphologies. Furthermore, these data suggest that the nuclear localization of Bax early after trauma to be a common mechanism across multiple CNS trauma models.

Finally, we provide novel mechanistic *in vitro* and *in vivo* evidence for Bax coordination of multiple cognate organelle cell death signaling cascades. *In vitro*, we found 1h pretreatment with immunosuppressive and neuroprotective FK506 inhibited high and low dose rotenone-mediated Bax relocalization and cell death signaling, *in toto*. *In vivo*, using 100% O₂ as an intervention, we showed 100% O₂ increases T2-weighted MRI lesion volumes, via increased inflammatory and necrotic signaling, with no amelioration of cortical apoptotic signaling when compared to HI alone. Furthermore, 100% O₂ increased ER calpain activation and increased ER Bax protein levels, suggesting that 100% O₂ increases HI-induced Bax-mediated activation of ER cell death signaling to increase inflammation and injury by increasing necrotic-like cell death. Taken together, these findings are the first to show Bax-mediated coordination of multi-organelle cell death signaling, demonstrate a link between ER Bax, ER cell death signaling and necrotic-like cell death, and provide evidence for a general trauma-induced Bax relocalization mechanism.

TABLE OF CONTENTS

TABLE OF CONTENTS	viii
FIGURES	xiii
CHAPTER I	
INTRODUCTION	1
Neonatal HI and its dysfunctional consequences in childhood development	1
Epidemiology of neonatal HI	1
Causes of neonatal HIE	2
Detrimental outcomes after HIE	4
Neonatal inflammation and adult injury	5
Oxidative stress in the neonatal CNS	6
Sources and Consequences of Reactive Species (RS) in the CNS	6
Susceptibility of the neonatal brain to oxidative stress	9
In vitro oxidative stress and energy depletion models mimic in vivo HI	10
Apoptosis, necrosis and points in between	13
Apoptosis: non-inflammatory, cell death by design	13
Necrosis: unregulated, explosive cell death triggering inflammation	14
Aponecrosis and necroptosis: cell death phenotypes in between	15
Cognate organelle cell death signaling	17
Nuclear cell death signaling cascades	17
Caspase-dependent and –independent mitochondrial cell death signaling	20
Overwhelming the UPR promotes ER cell death signaling	24

Cross-talk between cognate organelle cell death signaling cascades	25
Bcl-2 family of proteins: regulators of cell death	26
General review of the Bcl-2 family of proteins	26
Bax and activation of mitochondrial cell death signaling	29
Bcl-2 family proteins localize to organelles other than mitochondria	30
Neonatal models of HI	32
Project Aims	34
CHAPTER II	
HI INDUCES NUCLEAR, MITOCHONDRIAL AND ER BAX LOCALIZATION TO ACTIVATE COGNATE ORGANELLE CELL DEATH SIGNALING CASCADES	38
Introduction	38
Materials and Methods	41
Results	54
HI induces contralateral cortical injury to a lesser extent than ipsilateral cortical injury	54
Bax in sham-treated animals is mostly in cytosol	56
HI induces cell death in the ipsilateral cortex via activation of mitochondrial- and ER- mediated cell death	58
HI shifts Bax sequentially to the nucleus and then to mitochondria and ER	60
HI-induced mitochondrial Bax	62
HI-induced ER Bax	65
HI induces Bax translocation into nuclei, coincident with maximal nuclear p53 phosphorylation	65
Discussion	70

Bax organelle occupancy coordinates cell death cascades after HI	70
Conclusion	73
CHAPTER III	
DIFFERENTIAL DOSE EFFECTS OF ROTENONE ON BAX SUBCELLULAR LOCALIZATION AND CELL DEATH PHENOTYPE	75
Introduction	76
Materials and Methods	78
Results	90
25µM and 100µM rotenone treatments produce two biochemically and phenotypically distinct forms of cell death.	90
25µM rotenone insult shifts Bax to nuclei at 1h and to mitochondria at 6h.	92
100µM rotenone insult shifts Bax to nuclei at 1h and to ER at 6h.	95
25µM rotenone insult increases nuclear Bax at 1h insult and mitochondrial Bax at 6h insult.	99
100µM rotenone insult increases nuclear Bax at 1h insult and ER Bax at 6h insult.	99
25µM rotenone insult increases caspase-mediated cleavage of the cytoskeletal protein α-fodrin.	100
100µM rotenone insult increases calpain-mediated cleavage of the cytoskeletal protein α-fodrin.	101
Discussion	102
Oxidative stress, energy depletion and cell death phenotype	102
25µM rotenone insult induces mitochondrial Bax localization to activate the intrinsic mitochondrial cell death pathway.	103
100µM rotenone insult induces ER Bax localization to activate ER cell death signaling.	104

25μM and 100μM rotenone insult induces nuclear Bax localization.	105
Conclusion	106
CHAPTER IV	
EFFECTS OF FK506 AND 100% O₂ THERAPY ON BAX-MEDIATED ACTIVATION OF CELL DEATH SIGNALING CASCADES AND RESULTING CELL DEATH PHENOTYPE	108
Introduction	109
Materials and Methods	112
Results	129
FK506 reduces both 25μM and 100μM rotenone-induced cell death	129
FK506-pretreatment reduces 25μM rotenone-induced increases in nuclear Bax at 1h insult and mitochondrial Bax at 6h insult.	132
FK506-pretreatment reduces 100μM rotenone-induced increases in nuclear Bax at 1h insult and ER Bax at 6h insult.	132
FK506-pretreatment reduces 25μM rotenone-mediated increases in caspase-mediated cleavage of the cytoskeletal protein α-fodrin.	135
FK506-pretreatment reduces 100μM rotenone-mediated increases in calpain-mediated cleavage of the cytoskeletal protein α-fodrin.	138
At 24h post HI, hyperoxia therapy Increases HI-induced lesion volume size	140
Hyperoxia therapy does not decrease apoptotic cell death signaling, but does increase inflammatory signaling after HI	142
Hyperoxia therapy increases calpain-mediated but not caspase-mediated cleavage of cytosolic α-fodrin	145
Hyperoxia therapy increases ER Bax levels but not nuclear and mitochondrial Bax levels	148
Discussion	150

Inhibitory effects of FK506 on rotenone-induced Bax localization and activation of cognate cell death signaling cascades	150
Hyperoxia treatment increases HI-induced lesion volume via ER stimulation of necrosis and inflammation	153
Conclusion	155
CHAPTER V	
CONCLUSIONS AND FUTURE DIRECTIONS	157
REFERENCES	162
VITA	179

Figures

Figure 1. Schematic of ROS scavenging systems	8
Figure 2. Representative images of different cell death phenotypes	12
Figure 3. Schematic illustrating portions of the nuclear cell death signaling cascade	18
Figure 4. Schematic illustrating portions of both extrinsic (receptor-mediated) and intrinsic mitochondrial cell death signaling cascades	21
Figure 5. Schematic illustrating normal and UPR-overwhelmed ER states leading to activation of ER cell death signaling cascades	23
Figure 6. Bcl-2 family of proteins and the current disinhibition model for the regulation of the Bcl-2 family	28
Figure 7. Schematic representation of an adult rat to illustrate the location of the electrocauterization site used in the modified protocol of the Rice-Vannucci model used in this dissertation on neonates.	33
Figure 8. Schematic representation of the dissertation central hypothesis	37
Figure 9. HI induces contralateral cortical injury to a lesser extent than ipsilateral cortical injury.	55
Figure 10. Subcellular enrichment of different organelle fractions illustrates the majority of Bax in sham cortices resides in the cytosol.	57
Figure 11. Hypoxic-ischemia (HI) induces cell death in the injured ipsilateral cortex via caspase 3 and caspase12 activation and mitochondrial extrusion of AIF.	59
Figure 12. HI shifts Bax to the nucleus followed by Bax redistribution to the mitochondrial and ER.	61
Figure 13. HI induces maximal colocalization of Bax with mitochondria at 3h post HI	63
Figure 14. When compared to sham, more cells at 3h post HI show Bax colocalization with the mitochondria.	64
Figure 15. HI induces maximal colocalization of Bax with ER at 6h post HI.	66
Figure 16. When compared to sham, more cells at 6h post HI show Bax colocalization with the ER.	67

Figure 17. HI induces Bax translocation into nuclei, coincident with maximal nuclear p53 phosphorylation.	69
Figure 18. Assessment of cellular homogeneity of primary P5 Wistar rat cortical cultures illustrates minimal non-neuronal contamination (~8-10% GFAP+ cells).	82
Figure 19. 25μM and 100μM rotenone treatments produce two biochemically and phenotypically distinct forms of cell death.	91
Figure 20. 25μM rotenone treatment shifts Bax to nuclei at 1h and to mitochondria at 6h insult.	93
Figure 21. 100μM rotenone treatment shifts Bax to nuclei at 1h.	94
Figure 22. 25μM rotenone treatment shifts Bax to nuclei at 1h.	96
Figure 23. 100μM rotenone treatment shifts Bax to nuclei at 1h and to ER at 6h.	97
Figure 24. Supplementary data	98
Figure 25. FK506 reduces both 25μM and 100μM rotenone-induced cell death.	131
Figure 26. FK506-pretreatment reduces 25μM rotenone-induced increases in nuclear Bax at 1h insult.	133
Figure 27. FK506-pretreatment reduces 25μM rotenone-induced increase in mitochondrial Bax at 6h insult.	134
Figure 28. FK506-pretreatment reduces 100μM rotenone-induced increases in nuclear Bax at 1h insult.	136
Figure 29. FK506-pretreatment reduces 100μM rotenone-induced increase in ER Bax at 6h insult.	137
Figure 30. FK506 treatment inhibits 100μM rotenone-induced increases in calpain- and caspase-mediated cleavage of α-fodrin, and inhibits 25μM rotenone-induced increases in caspase-mediated cleavage of α-fodrin. (Preliminary data)	139
Figure 31. At 24h post HI, hyperoxia therapy increases HI-induced lesion volume size.	141
Figure 32. Hyperoxia therapy does not decrease apoptotic cell death signaling, but does increase inflammatory signaling.	143

Figure 33. Hyperoxia therapy increases calpain-mediated but has no effect caspase-mediated cleavage of cytosolic α -fodrin.	147
Figure 34. Hyperoxia therapy increases ER but has no effect on nuclear and mitochondrial Bax levels.	149
Figure 35. Supplementary data II	151
Figure 36. Schematic representations for Bax localization in sham, HI-injured and 100% O ₂ -treated HI-injured cortices.	158

CHAPTER I

Introduction

The examination of Bcl-2 antagonist X (Bax) protein's role in the activation of cognate nuclear, mitochondrial and ER cell death signaling cascades and the resulting effects on cell death phenotype in the brain after neonatal hypoxia-ischemia (HI) requires an understanding of neonatal HI insult and progression, as well as, its dysfunctional outcomes. In addition, knowledge of key concepts of oxidative stress, a major injurious component of HI, and the different cell death phenotypes (i.e. apoptosis and necrosis) will aid in understanding the rationale for the experimental designs used for this study. Furthermore, a review of the organelle cell death signaling cascades, which contribute to the different cell death phenotypes, as well as a review of the B cell lymphoma 2 (Bcl-2) protein family, will contribute to general understanding of the relationship between Bax localization and its coordination of cell death signaling within the injured brain. Lastly, a brief review of the *in vivo* neonatal HI models will provide essential background to the study of cell death progression after neonatal HI.

Neonatal HI and its dysfunctional consequences in childhood development

Epidemiology of neonatal HI

Neonatal hypoxic-ischemic encephalopathy (HIE) occurs in 2 to 4 out of 1000 live births each year in the US (Bissinger and Ohning, 2006; Raju,

2006c) with periventricular hemorrhage-intraventricular hemorrhages (PVH-IVH) occurring in 40-60% of low birth weight babies (<1500g) (Bissinger and Ohning, 2006; Raju, 2006c). In developing countries, the incidence of HIE can range as high as 0.5-1% of all live births. In the past, mortality rates for HIE ranged from 50-75%, but due to advances in obstetric care, this rate has dropped to 27%-50% (Raju, 2006c). Resulting from this increased survival of infants who had previously died from HIE, there is consequently an increased rate of children with developmental neurological disorders resulting from HIE. 80% of the children who survive severe HIEs develop serious complications, while 10-20% develop moderate complications and <10% are normal. Of those children who suffered a moderate HIE, ~30-50% develop serious complications and 10-20% develop minor complications (Raju, 2006c). Thus, understanding the pathogenesis of HIE is crucial to development of novel therapeutics for halting neurodegeneration after HI.

Causes of neonatal HIE

Two major contributing factors to the onset of HIE are the loss of cerebral blood flow autoregulation and a disruption in the normal cerebral blood flow (CBF) (Raju, 2006c), with placental detachment / rupture, umbilical strangulation of the fetus and complications during delivery as major triggers (Raju, 2006c). Unlike the perinatal and adult CBF blood pressure (BP), which has a large dynamic range (40 mm Hg), the CBF BP range for term and preterm

infants is markedly narrow (10-20 mm Hg) (Raju, 2006c). Due to this narrow range, the neonatal brain is highly susceptible to changes in systemic BP and its autoregulation can be rapidly compromised (Raju, 2006c). The hypothesized sequelae leading to HIE are 1) a rise in systemic BP as a response to hypoxemia, 2) followed by a rise in CBF BP outside of its normal dynamic range, 3) thereby disrupting CBF autoregulation 4) and leading to a pressure-passive cerebral circulation, in which the CBF BP is set by the systemic BP. 5) As the systemic BP drops, the CBF BP, also falls, resulting in cerebral ischemia and HIE (Raju, 2006c). Furthermore, several brain regions are vascularized by extremely fragile capillary networks (i.e. subependymal germinal matrix), which may rupture due to the rapid changes in pressure-passive CBF BP, leading to PVH-IVH (Raju, 2006c).

On the tissue level, HIE produces necrotic cysts within the brain parenchyma, which if near the ventricles can become fluid-filled forming PVH-IVHs (Raju, 2006c). After this burst of tissue necrosis, a delayed phase of tissue injury occurs characterized by apoptotic cell death (Raju, 2006c). In addition to these primary tissue insults, a secondary insult can arise from the cerebral edema due to rupture of the blood brain barrier (BBB) and dysfunction of the water homeostasis mechanisms with the brain after HIE, as well as an over-activation of the brain inflammatory response, exacerbating the primary neuronal injury (Raju, 2006c).

Detrimental outcomes after HIE

HIE produces a spectrum of dysfunctional phenotypes, which correlate with the severity of the hypoxic-ischemic insult. The most severe insults result in severe mental retardation, the development of seizures and cerebral palsy (Annibale, 2006), with the location of the infarct dictating the dysfunctional outcome. In the case of PVH-IVH, the most common neurological disorder after insult is cerebral palsy (Annibale, 2006). Cerebral palsy encompasses a broad group of disorders, which negatively affects motor control very early in development and persists into adulthood (Annibale, 2006). Because the cortico-spinal tracts essential to muscle movement run proximal to the lateral ventricles, they are the most susceptible to injury resulting from PVH-IVH (Annibale, 2006). Pertaining to seizure development, HIE injury to the subependymal germinal matrix, which is the primary source of the glial precursors in the developing brain, has been hypothesized to contribute significantly to brain seizure development, although definitive proof has yet to be published (Annibale, 2006).

At the other end of the dysfunctional spectrum, mild HIE often produces subtle insults, which do not manifest themselves immediately. Indeed, many infants suspected to have sustained a mild HIE insult develop “normally” until they reach school age (Smith et al., 2007). It is at this time when higher order brain processing is required for engagement in school learning activities and social interactions. Recent reports have linked mild HIE insults with poor

performance in school, poor social skills and the development of learning disabilities, which further broaden the learning gap between “normal” and “developmentally-delayed” children (Smith et al., 2007). Thus, in both severe and mild cases of HIE, brain trauma sustained in a neonatal / perinatal time frame manifests, or in the case of cerebral palsy, maintains, dysfunctional phenotypic expression into adolescence and adulthood.

Neonatal inflammation and adult injury

Neonatal HIE and the resulting dysfunctional phenotypic outcomes is not an isolated case in illustrating how early developmental brain trauma produces injury and inflammation which manifests itself behaviorally later in adulthood. Recently, Babulas et al. (2006) have demonstrated a positive association between prenatal exposure to maternal genital and reproductive infections with increased risk of adult schizophrenia, rationalizing that the close proximity of the fetus to the infectious microbe may allow easier access to the fetal bloodstream and, the developing CNS (Babulas et al., 2006). These results are in concordance with a previous study linking prenatal influenza infection to adult schizophrenia (Babulas et al., 2006). Furthermore, a 2005 study using human influenza virus-infected, pregnant BALB/c mice have proposed the development of an animal model for autism and schizophrenia, based on the data gathered from the pups of these infected dams (Babulas et al., 2006), citing previous associations of increased prenatal and perinatal cytokine levels with the

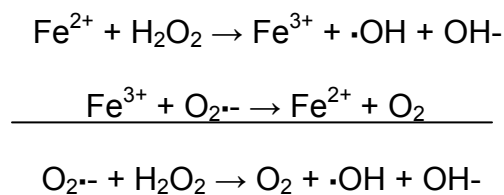
development of autism and schizophrenia (Babulas et al., 2006). Lastly, Bager et al. (2004), despite finding no link between multiple sclerosis (MS) and common childhood infections (measles, mumps, rubella), did uncover a potential correlation between MS and mononucleosis, agreeing with previous reports (Bager et al., 2004). Thus, these studies support recent evidence on neonatal HIE, which suggest prenatal / perinatal trauma and inflammation can produce adult neurological disorders in spite of the appearance of a “normal” development.

Oxidative stress in the neonatal CNS

Sources and Consequences of Reactive Species (RS) in the CNS

Reactive species, a major injurious component of HIE, encompasses reactive oxygen (ROS) and reactive nitrogen species (RNS), which are small oxygen / nitrogen containing molecules, which are highly reactive due to an unpaired electron in their outer electron valence shell. The mitochondrial oxidative phosphorylation chain complexes, monoamine oxidases, reduced nicotinamide adenine dinucleotide phosphate (NADPH) oxidase, cyclooxygenases and nitric oxide synthases (NOS) comprise the five major sources of ROS within the CNS (Perez-Polo lecture notes, 2004). While in low abundance, many of these RS are used as signaling molecules (i.e. nitric oxide, NO \cdot), overproduction of RS can promote cellular dysfunction and cell death through increased lipid peroxidation, protein oxidation and DNA damage (Perez-Polo

lecture notes, 2004). A primary substrate in these RS-mediated reactions is superoxide ($O_2^{\bullet-}$), which results from a one electron reduction of molecular oxygen (Perez-Polo lecture notes, 2004). Together with hydrogen peroxide (H_2O_2), $O_2^{\bullet-}$ can react with ferric and ferrous iron present within the CNS to form the highly reactive hydroxyl radical ($\cdot OH$) via the Fenton and Haber-Weiss reactions:



In addition, $\cdot OH$ can react with $NO\cdot$ to form a powerful oxidant and nitrosylating agent in the CNS, peroxynitrite ($ONOO^-$) (Perez-Polo lecture notes, 2004). To counteract the debilitating effects of RS, the CNS possesses three main antioxidant enzyme mechanisms: 1) catalase, which catalyzes the formation of molecular oxygen and water from H_2O_2 , 2) superoxide dismutase (SOD), which catalyzes the formation of H_2O_2 from $O_2^{\bullet-}$ and 3) glutathione (GSH) peroxidase, which catalyzes the formation of water from H_2O_2 using the reducing equivalents of GSH, which, in turn, can be re-established via GSH reductase (Fig. 1) (Jackson, 1991). Thus, maintenance of the delicate balance of RS in the CNS is crucial to its proper function and survival, especially within the neonatal brain.

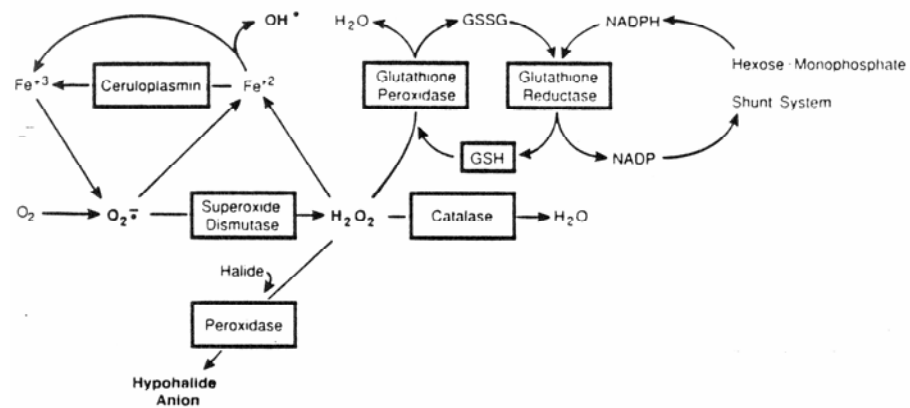


Figure 1. Schematic of ROS scavenging systems

Modified from Jackson, GR (1991).

Susceptibility of the neonatal brain to oxidative stress

In general, the CNS is highly susceptible to oxidative damage due to its high levels of polyunsaturated lipids (from extensive neurite branching and myelination), relatively low levels, when compared to systemic tissues, of cellular antioxidants and high levels of iron, a key substrate for ROS generation (Rassin lecture notes, 2004). Furthermore, the CNS, especially the brain, requires very high protein levels and protein turnover for signal transduction, ionic electrochemical gradient homeostasis, receptor maintenance and neurite remodeling, making the CNS prone to protein oxidation and nitrosylation (Perez-Polo lecture notes, 2004). Plus, the CNS derives the majority of its energy from the mitochondrial oxidative phosphorylation chain, thereby making O₂ a vital necessity and an oxidative risk to the CNS.

In particular, the neonatal brain is even more susceptible than the adult brain, as the perinatal / neonatal period demarks a key neurodevelopmental period for synaptic remodeling and differentiation of oligodendroglial precursors into mature, myelinating oligodendrocytes (Back et al., 2007a; Back et al., 2007b; Back et al., 2002). Furthermore, oxidative damage to key components involved in cytoarchitecture development can have drastic long-lasting consequences beyond the neonatal period (Hu et al., 2006). In addition, the neonatal brain possesses lower levels of the GPH peroxidase and catalase antioxidant enzymes (Rassin lecture notes, 2004). Taken together, the CNS, especially the neonatal

brain, is highly susceptible to insults (i.e. HIE), which generate large amounts of reactive species.

In vitro oxidative stress and energy depletion models mimic in vivo HI

In vitro oxidative stress / energy depletion models have provided tremendous insight into the mechanisms of HI-induced cerebral injury, *in vivo* (Basso et al., 2005; Cole and Perez-Polo, 2004; Jackson et al., 1991; Manakova et al., 2005). In particular, three models dominate oxidative stress / energy depletion / HI literature, each with inherent benefits and flaws: 1) oxygen-glucose deprivation (OGD), 2) application of RS generators and 3) mitochondrial oxidative complex inhibitors. In theory, *in vitro* OGD most resembles clinical HI insult, with reduction in glucose as the ischemic component and replacement of O₂ with N₂ as the hypoxia component (Koubi et al., 2005; Tabakman et al., 2005). Indeed, numerous reports clearly demonstrate strong similarities in signaling pathways between clinical HI and OGD (Koubi et al., 2005; Tabakman et al., 2005). The major drawback to OGD remains proper model application and defining parameters for the model, as OGD requires strict adherence to protocol and lab-to-lab insult variability can be large (Hillion et al., 2005; Tabakman et al., 2005; Tanaka et al., 2005). Application of specific RS generating agents permits determination of the injurious contribution of selective RS. For instance, models using the NO[•] generator, SIN-1, allows, in principle, for determination of the

detrimental molecular action of NO \cdot on various tissue culture systems. In practice though, most RS generators are not truly selective, like SIN-1 with its generation of O $_2^{\cdot-}$, in addition to NO \cdot . Furthermore, application of RS-generating agents does not truly model neonatal HI, as it lacks a true energy depletion component. Like RS-generating agents, mitochondrial complex inhibitors promote excess production of ROS, particularly O $_2^{\cdot-}$, to induce oxidative damage in various *in vitro* CNS injury models (Almeida et al., 2004; Casarejos et al., 2006; Fiskum et al., 2003; Hartley et al., 1994). Unlike RS-generating agents though, mitochondrial complex inhibitors selectively inhibit ATP formation through uncoupling the oxidative phosphorylation chain (Almeida et al., 2004; Casarejos et al., 2006; Fiskum et al., 2003; Hartley et al., 1994), thus providing an alternative (to OGD) *in vitro* model to neonatal HI. Additionally, reports using the mitochondrial complex I inhibitor, rotenone, demonstrate, through simple dose modulation, rotenone-induced differences in cell death phenotype, with increased rotenone concentration promoting necrosis (Bal-Price and Brown, 2000; Leist et al., 1999). Therefore, the use of *in vitro* oxidative stress / energy depletion models, which mimic the clinical HI-injury signaling mechanisms, can provide a reductionist approach for ascertaining HI-induced cell death signaling progression and therapeutic efficacy testing prior to *in vivo* application.

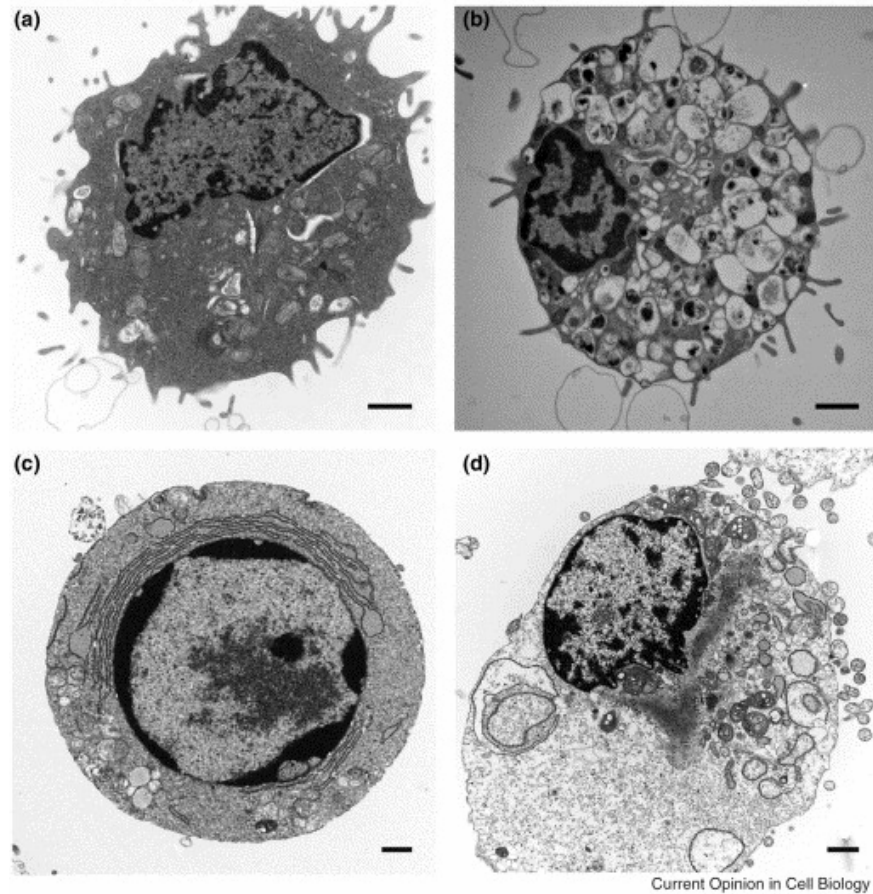


Figure 2. Representative images of different cell death phenotypes

a) Normal, b) autophagic c) apoptotic d) necrotic. Scale bars = 1 μm. Modified with permission from Elsevier (Edinger et al., 2004).

Apoptosis, necrosis and points in between

Apoptosis: non-inflammatory, cell death by design (Fig. 2A-D)

Apoptosis, first characterized by Kerr et al. (1972) (Kerr et al., 1972), is a programmed cell death defined by the nuclear and cellular morphological changes resulting from activation of its signaling cascades (Kerr et al., 1972). Phenotypically, apoptotic nuclei display DNA fragmentation and chromatin condensation (pyknosis and karyorrhexis, respectively), while the dying cells become shrunken with plasma membrane blebbing (Edinger and Thompson, 2004). Furthermore, the cytosolic organelles retain their physiological size, and, in the later stages of apoptosis, the cell breaks down into plasma membrane-bound apoptotic bodies with their cellular contents inside, thus preventing an inflammatory response due to cytosolic enzymes spilling into the extracellular milieu (Edinger and Thompson, 2004).

Previous reports have shown apoptosis to be an ATP-requiring process that involves two main, generalized pathways (the extrinsic and intrinsic pathways) ultimately leading to the activation of aspartate residue-cleaving cysteine proteases (caspases) (Stefanis, 2005; Aggarwal et al., 1999; Bender et al., 2005). The extrinsic apoptotic pathway, or receptor-mediated apoptosis, commonly involves Fas ligand and TNF- α receptor-mediated organization of the death-inducing signaling complex (DISC), which involves the recruitment of cell death domain carrying scaffolding proteins, such as FADD, and TNF-R1 associated TRADD (Aggarwal et al., 1999; Bender et al., 2005). These

associated proteins, then, recruit pro-caspase 8, an initiator caspase, to promote its activation and, then, caspase 8 activates downstream, effector caspases (i.e. caspases 3, 7) which activate the enzymes responsible for chromatin cleavage and shut down of the cell's functional machinery (Aggarwal et al., 1999; Bender et al., 2005). The intrinsic, or mitochondrial, apoptotic pathway involves trauma-induced release of cytochrome c from the mitochondrial matrix to the cytosol where it interacts with dATP, Apaf-1 and pro-caspase 9 (an initiator caspase) to form the apoptosome (Rao et al., 2002; Stefanis, 2005). This association promotes the cleavage and activation of caspase 9, which, like caspase 8, activates downstream effector caspases to carry out the organized disintegration of cell constituents (Rao et al., 2002; Stefanis, 2005).

Necrosis: unregulated, explosive cell death triggering inflammation

Unlike the organized signaling of apoptosis, necrosis has been classically defined as a passive event commonly characterized in a negative manner, in that necrosis does not possess characteristics of apoptosis (Edinger and Thompson, 2004). For example, necrotic nuclei do not undergo either pyknosis or karyorrhexis, and necrotic cells do not shrink in cell volume. Typical necrotic phenotype markers include early rupture of the plasma membrane, swelling of the intracellular organelles and inflammation resulting from the cytosolic contents spilling into the extracellular matrix (Edinger and Thompson, 2004).

As a passive event, past reports have demonstrated that necrosis does not require ATP (Edinger and Thompson, 2004) and is the result of acute, highly injurious trauma to tissues (Edinger and Thompson, 2004). In the CNS, acute trauma models, via shut down of ionic homeostatic mechanisms, promote a water influx due to the electrochemical gradient run-down (Bredesen et al., 2006; Yuan et al., 2003; Bredesen et al., 2006; Yuan et al., 2003). This water surge surpasses the cell volume regulatory machinery and causes cell rupture triggering microglial-mediated inflammation (Bhat et al., 1996; Hailer et al., 2005). Furthermore, because necrosis does not involve signaling cascades, no definitive cellular markers for passive necrosis exist, limiting its examination in *in vivo* trauma models.

Aponecrosis and necroptosis: cell death phenotypes in between

Recent reports have demonstrated that CNS trauma-induced cell death does not always fall into either the apoptotic or necrotic phenotype (Degterev et al., 2005; Formigli et al., 2000; Pretorius and Bornman, 2005; Yakovlev and Faden, 2004). Rather, close examination of tissue injury reveals CNS trauma results in a spectrum of cell death phenotypes, with true apoptosis and passive necrosis at either end of the spectrum and cells possessing various combinations of molecular / phenotypic features of apoptosis or necrosis, named aponecrotic (Formigli et al., 2000; Pretorius and Bornman, 2005) or necroptotic (Degterev et al., 2005; Yakovlev and Faden, 2004), sandwiched in between (from

here, aponecrosis will be used to signify these in-between cell death phenotypes) (Degterev et al., 2005; Hu et al., 2007; Mehta et al., 2007; Papucci et al., 2004; Yakovlev and Faden, 2004). Moreover, initial reports have linked insult models of high oxidative stress and energy depletion with more necrotic-like cell death and insult models, which produce moderate oxidative stress and energy depletion, with more apoptotic-like cell death (Formigli et al., 2000). Illustrating this concept, Formigli et al. (2000) could model apoptotic, necrotic and aponecrotic cell death just by varying doses of mitochondrial complex III and I inhibitors, such as antimycin and rotenone, respectively, thereby varying the state of oxidative stress and energy depletion (Formigli et al., 2000). In addition, recent reports have suggested a developmental role for programmed necrosis, and, thus, have added a new avenue for investigation into the purpose of aponecrotic cell death.

With this new insight into cell death, multiple areas of research, including cancer and neurodegenerative research, have begun to unravel the mechanisms involved in determining the cell death phenotype after insult (Edinger and Thompson, 2004; Hu et al., 2007; Moubarak et al., 2007). Although there have been numerous reports on specific models inducing specific pathways, such as DNA methylating agents applied to primary cortical neurons (Degterev et al., 2005; Edinger and Thompson, 2004; Hu et al., 2007; Mehta et al., 2007; Moubarak et al., 2007), very few common themes have emerged to date. One theme, which has emerged, addresses the role of organelle cell death

signaling in determining the cell death phenotype, with activation of ER cell death signaling cascades linked to necrotic-like cell death and activation of mitochondrial cell death signaling linked to apoptotic-like cell death (Moubarak et al., 2007). This theme prompted our current investigation into the cell death mechanisms after neonatal HI. However, in order to fully comprehend our experimental rationale, a brief review of nuclear, mitochondrial and ER cell death signaling is required.

Cognate organelle cell death signaling

Nuclear cell death signaling cascades (Fig. 3)

Three primary cell death markers signal activation of nuclear cell death signaling: 1) upregulation of p53-mediated transcription, 2) cleavage and inactivation of PARP-1 and 3) nuclear translocation of mitochondrial AIF. p53 is a “DNA damage-sensing” transcription factor which can regulate cell cycle progression, DNA repair mechanisms and initiate cell death signaling based on the degree of the genotoxic insult (Culmsee and Mattson, 2005; Xiang et al., 1998). In addition to sumoylation and acetylation, differential phosphorylation can not only activate p53-mediated transcription, but also dictate what genes p53 will transcribe (Appella and Anderson, 2001; Morris et al., 2001). Regarding induction of cell death, phosphorylation and activation of p53 on serine 15 promotes transcription of pro-cell death genes, including PUMA, NOXA and BAX (Appella and Anderson, 2001; Morris et al., 2001). Poly-ADP ribose polymerase

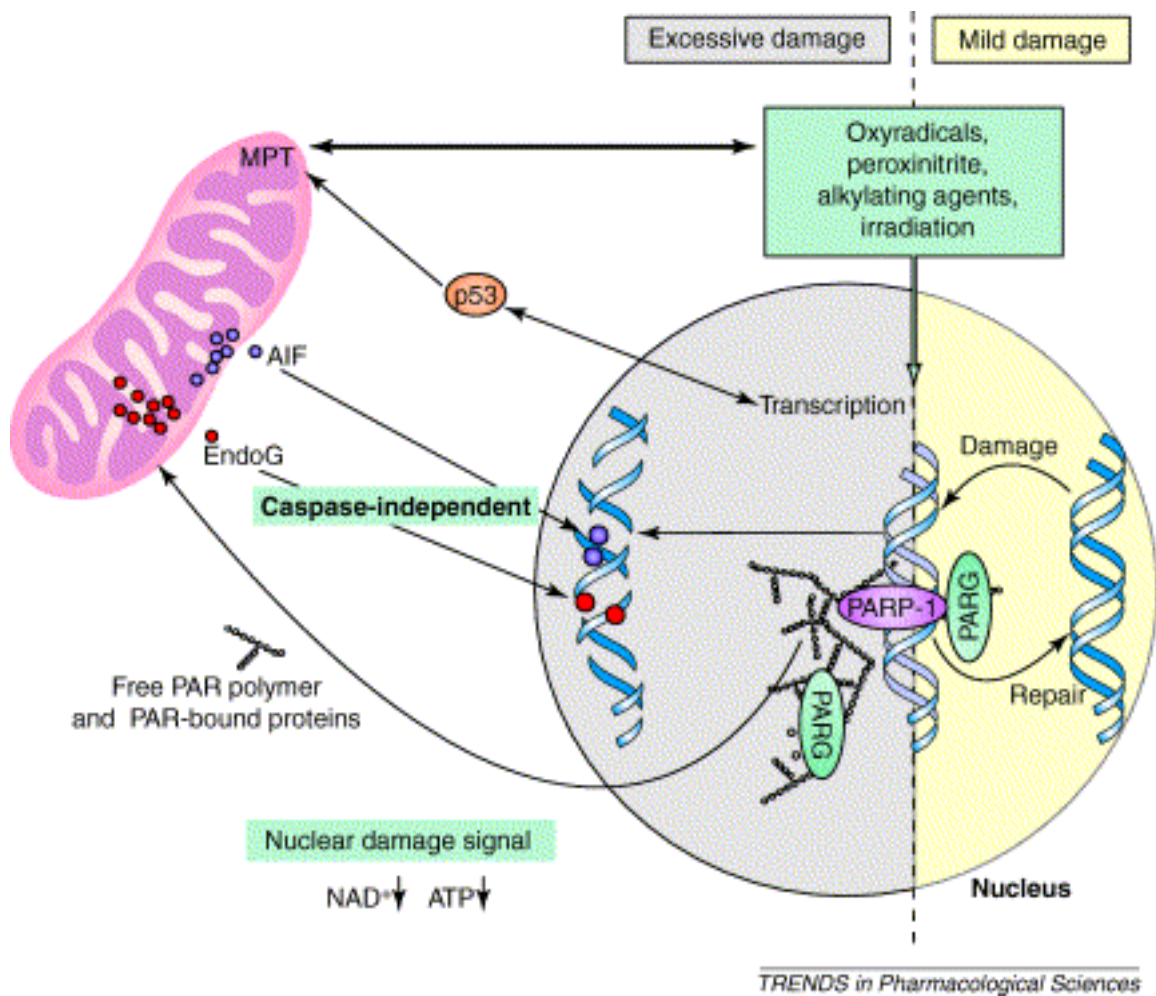


Figure 3. Schematic illustrating portions of the nuclear cell death signaling cascade.

Modified with permission from Elsevier (Hong et al, 2004).

1 (PARP-1) is a key DNA repair protein, which requires NAD⁺, cofactor for ATP generation, for its actions. DNA damage triggers the activation of PARP-1, which catalyzes the addition of 50-200 ADP ribose moieties to multiple protein targets, including histones and DNA polymerases (Goto et al., 2002; Ha et al., 2002; Martin et al., 2005). This ADP ribose addition effectively reduces the affinity of these proteins for DNA allowing the DNA repair machinery access to the damaged site (Goto et al., 2002; Ha et al., 2002; Martin et al., 2005). Because it requires NAD⁺ as a cofactor, excessive PARP-1 activity can drain the cellular NAD⁺ pool and increase energy depletion (D'Amours et al., 2001; Martin et al., 2005; Tentori et al., 2002). To prevent this drain and save energy for apoptotic signaling, PARP-1 is cleaved and inactivated by caspase 3, yielding a characteristic apoptotic 85kD fragment (D'Amours et al., 2001; Martin et al., 2005; Tentori et al., 2002). Furthermore, recent reports have shown PARP-1 to be differentially cleaved during programmed necrosis by lysosomal cathepsins, yielding a characteristic necrotic 55kD fragment (Ditsworth et al., 2007; Gobeil et al., 2001; Moubarak et al., 2007). In addition to p53 and PARP-1, apoptosis inducing factor (AIF) is 67kD, mitochondrial oxidoreductase, which, upon cleavage and activation, translocates to the nucleus and induces large scale DNA fragmentation (>50kb) in a caspase-independent manner (Cheung et al., 2005; Culmsee et al., 2005; Plesnila et al., 2004; Zhu et al., 2007). The exact mechanism of nuclear AIF action is still unknown, but activation of AIF has been shown recently to involve cleavage mediated by calpain, and ER cell death

associated cysteine protease (Polster et al., 2005). Moreover, calpain-mediated nuclear AIF translocation has been shown to be involved in apoptotic cell death (Moubarak et al., 2007).

Caspase-dependent and –independent mitochondrial cell death signaling (Fig. 4)

Mitochondria, in addition to acting as the main source of cellular energy, acts as the central hub in intrinsic apoptotic cell death (Dejean et al., 2005; Precht et al., 2005). Mitochondria, also, act as a temporary Ca^{2+} reservoir, minimizing the cytosolic Ca^{2+} concentration. Oxidative stress-induced disruption of the oxidative phosphorylation chain, excessive mitochondrial uptake of Ca^{2+} due to trauma-induced ER dumping of its Ca^{2+} stores and damage to mitochondrial DNA triggers the activation of cell death signaling. Classical caspase-dependent cell death signaling is mediated by the Bcl-2 family of proteins (discussed in more detail later). Although the exact mechanism is still under intense investigation, pro-apoptotic Bcl-2 family members, Bax and Bak trigger the formation of the permeability transition pore (PTP) (Dejean et al., 2005; Precht et al., 2005). Consisting of voltage-dependent anion channel and / or adenosine nucleotide translocator (still a contentious topic), formation of PTP allows release of cytochrome c from the inner mitochondrial matrix into the cytosol, thereby activating initiator, which amplify the cell death signal via activation of effector caspases (Precht et al., 2005). Effector caspases, in turn, carry out the activation of protein machinery involved in apoptotic cell death, such

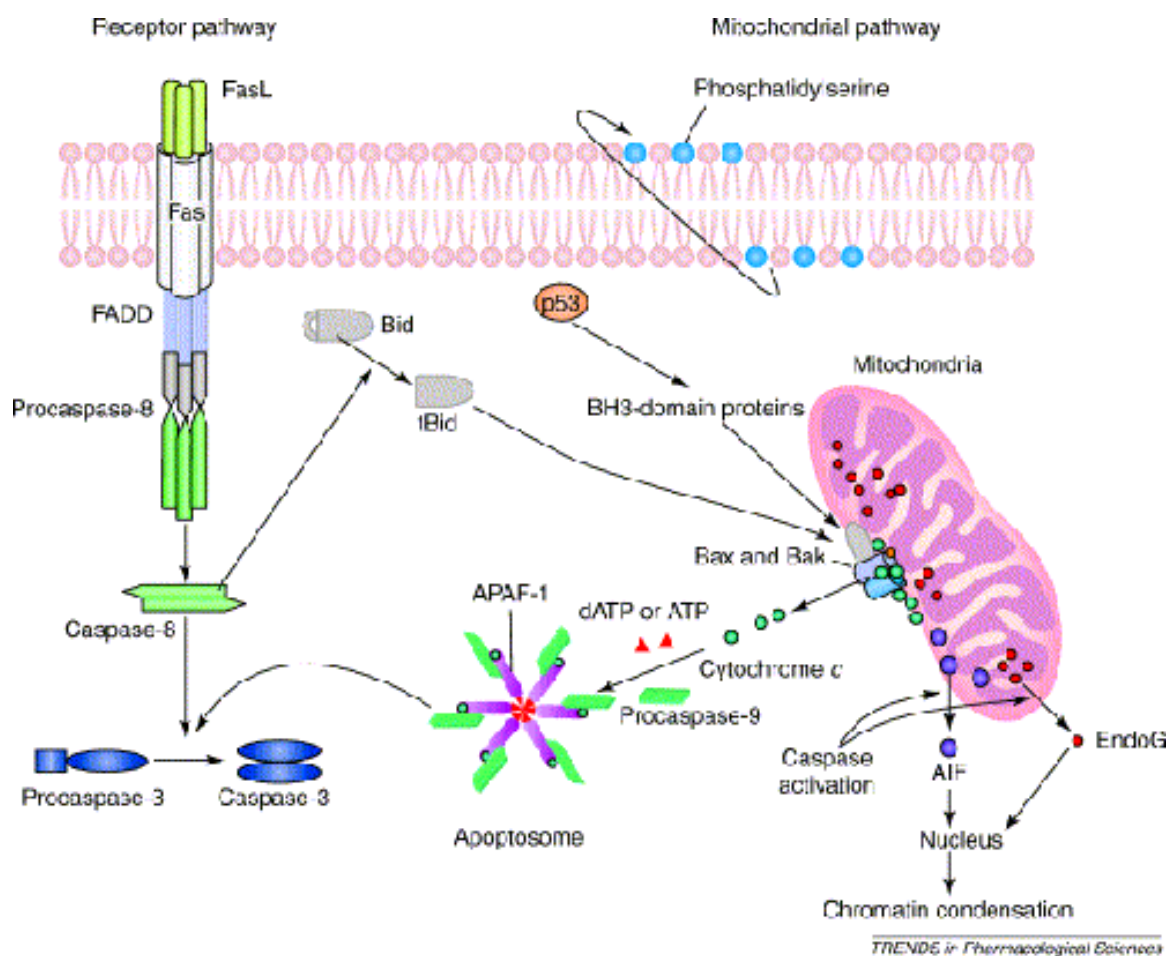


Figure 4. Schematic illustrating portions of both extrinsic (receptor-mediated) and intrinsic mitochondrial cell death signaling cascade.

Modified with permission from Elsevier (Hong et al., 2004).

as caspase-activated DNase (CAD), which promotes 180bp DNA fragmentation, as well as inactivate repair proteins (i.e. PARP-1), which would function in vain to return the cell to homeostasis (Precht et al., 2005). In addition to caspase-dependent mechanisms, mitochondria possess caspase-independent mechanisms to carry out cellular demise, which is not always apoptotic. Smac / DIABLO and OMI / HtrA2 have been linked to caspase-dependent cell death through their inhibition of the inhibitors of apoptosis (IAP) protein family, which prevent cytochrome c from being released into the cytosol (Wang et al., 2004). However, recent reports demonstrate OMI / HtrA2 possesses a protease activity to initiate cell death independent of its inhibitory actions on IAPs (Hegde et al., 2002; Suzuki et al., 2004). Beyond Smac / DIABLO and OMI /HtrA2, endonuclease G (Endo G), also, plays a role in caspase-independent cell death as Endo G acts in coordination with other DNases to cleave cellular DNA, as well as mitochondrial DNA (Saelens et al., 2004; Tanaka et al., 2005). Perhaps, the most-reported protein associated with mitochondrial caspase-independent cell death is AIF. Through its large scale DNA fragmentation, AIF has been reported to independently induce cell death (Hong et al., 2004; Saelens et al., 2004), as well as in coordination with caspase-dependent mechanisms, acting as an additional mechanism to facilitate cell death execution (Hong et al., 2004; Saelens et al., 2004).

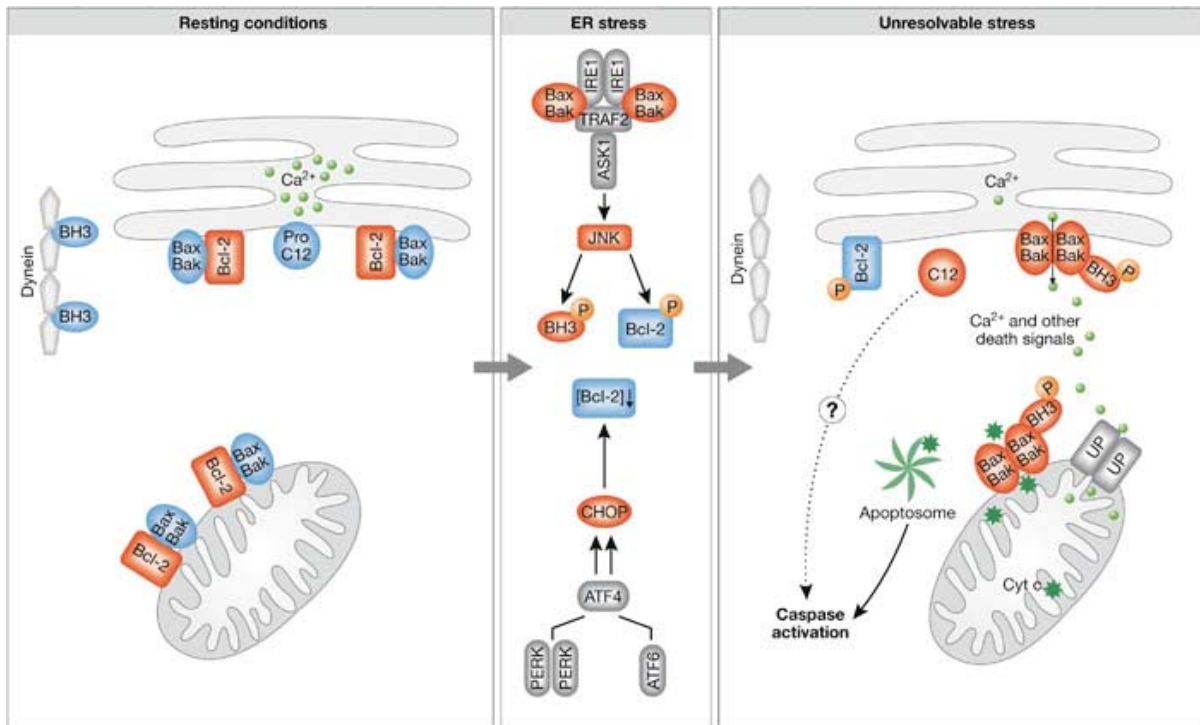


Figure 5. Schematic illustrating normal and UPR-overwhelmed ER states leading to activation of ER cell death signaling cascades

Modified with permission from Macmillan Publishers Ltd. (Szegezdi et al., 2006).

Overwhelming the UPR promotes ER cell death signaling (Fig. 5)

The ER, in particular the rough ER, receives newly translated protein from ribosomes and properly folds proteins into their correct conformers via the actions of ER resident chaperones, such as calnexin and calregulin (Terrinoni et al., 2004). In addition, the ER acts as the main intracellular Ca^{2+} store, with the IP_3 receptors and the SERCA pump regulating ER and cytosolic Ca^{2+} homeostasis. Due to its function as the protein folding hub, the ER acts, also, as a sensor for oxidative stress-induced increases in protein misfolding (Jakob et al., 1999; Sitia and Molteni, 2004). In response to increases in protein misfolding, the ER activates the unfolded protein response (UPR), which acts in 3 capacities to curb protein misfolding: 1) inhibits protein translation through PERK-mediated phosphorylation of $\text{eIF2}\alpha$, 2) increases protein folding capacity through IRE1- and ATF6-mediated transcription of chaperones, such as GRP78 and GRP94, and 3) eliminates misfolded proteins through activation of Sec61 / proteosome ER-associated degradation pathway (ERAD) (DeGracia and Montie, 2004; Kaneko and Nomura, 2003; Larner et al., 2006). If oxidative stress produces dramatic increases in protein misfolding, which surpass the UPR's corrective capacity, then, the ER initiates its cognate cell death signaling cascade.

The ER cell death signaling pathway has previously been reported to have three main components: 1) IRE1-mediated activation of JNK signaling and subsequent cell death, 2) CHOP / GADD-153 transcription of pro-cell death

genes and 3) cleavage and activation of ER caspase 12, which can activate the effector caspase, caspase 7 (Nakagawa et al., 2000; Yoneda et al., 2001). Recent reports have, also, linked ER stress with activation of the family of Ca^{2+} -activated cysteine proteases (calpain) (Golstein and Kroemer, 2007; Moubarak et al., 2007). CNS trauma induces not only oxidative stress to promote misfolded proteins, but also triggers release of ER Ca^{2+} into the cytosol promoting activation of calpains (Camins et al., 2006; Larner et al., 2006; Polster et al., 2005). Calpains, in turn, through cleavage of AIF have been reported to trigger a necrotic-like caspase-independent cell death (Polster et al., 2005; Zhu et al., 2007). Exacerbating the insult, recent publications have shown uptake of dumped Ca^{2+} into the mitochondria, also, disrupts oxidative phosphorylation and triggers mitochondrial cell death signaling (Boehning et al., 2003; Chinopoulos and dam-Vizi, 2006; Nutt et al., 2002b; Rao et al., 2002). Thus, evolving from these previous studies of individual organelle cell death signaling is a common theme, which involves cross-talk between the different organelle cognate cell death signaling cascades.

Cross-talk between cognate organelle cell death signaling cascades

Recently, focus in cell death literature has shifted from the study of individual cell death signaling cascade to the holistic approach of studying the cross-talk / interplay between the signaling cascades (Moubarak et al., 2007; Sanges et al., 2006; Sanges and Marigo, 2006). Reports have linked nuclear

and mitochondrial cell signaling: AIF nuclear translocation (Cheung et al., 2005; Hong et al., 2004), caspase 3-mediated cleavage of PARP-1 (D'Amours et al., 2001; Martin et al., 2005) and Puma and p53-mediated Bax mitochondrial translocation (Akhtar et al., 2006; Chipuk et al., 2005). In addition, reports have associated ER and nuclear cell death cascades: calpain-mediated PARP-1 cleavage (Moubarak et al., 2007), p53-mediated activation of ER scotin (Bourdon et al., 2002) and p73 α -mediated activation of scotin and ER stress (Terrinoni et al., 2004). Furthermore, reports have connected ER and mitochondrial cell death signaling: calpain-mediated AIF cleavage and activation (Moubarak et al., 2007; Polster et al., 2005), IRE1-mediated JNK activation to trigger intrinsic mitochondrial cell death (Lee et al., 2007; Yoneda et al., 2001) and Bax and Bak localization to the ER to promote release of ER Ca²⁺ (Nutt et al., 2002a; Nutt et al., 2002b; Oakes et al., 2005; Oakes et al., 2003; Scorrano et al., 2003). Despite this recent focus, few studies exist, which actually link a phenotypic or functional outcome to this crosstalk.

Bcl-2 family of proteins: regulators of cell death

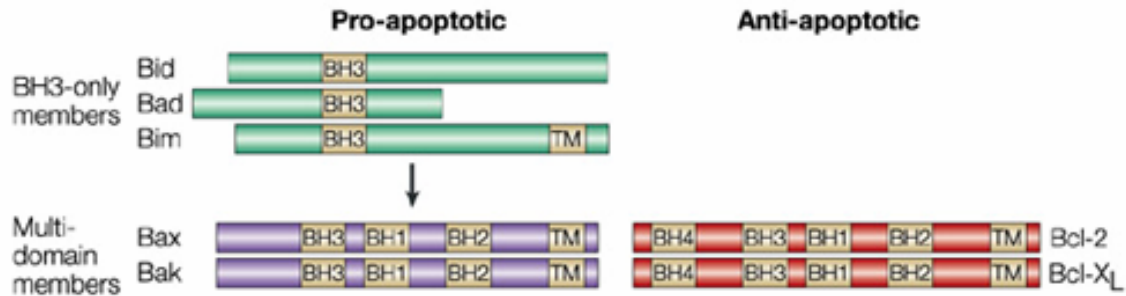
General review of the Bcl-2 family of proteins

The B cell lymphoma 2 (Bcl-2) family of proteins remains, still, at the center of cancer, cell death and neurodegeneration research, 19 years after David Vaux et al. (1988) linked anti-apoptotic Bcl-2 with tumorigenesis (Vaux et al., 1988). The Bcl-2 family consists of two main functional classes of proteins:

pro-apoptotic and anti-apoptotic members (Jesenberger and Jentsch, 2002), with the pro-apoptotic group further sub-divided into multi-domain (i.e. Bax, Bak) and BH3-only proteins (i.e. Bid, Puma). B cell homology (BH1-4) domains are characteristic stretches of conserved amino acid sequences, with each member of Bcl-2 family protein possessing at least one BH domain (Fig. 6A) (Jesenberger and Jentsch, 2002). Via the BH3 domain, pro-apoptotic protein can interact with other pro-apoptotic members to initiate cell death signaling or with anti-apoptotic Bcl-2 family proteins to inhibit cell death signaling (Jesenberger and Jentsch, 2002). Anti-apoptotic Bcl-2 proteins (i.e. Bcl-2, Bcl-X_L) possess all four BH domains with the BH4 domain necessary to their anti-apoptotic function (Cao et al., 2002). Furthermore, reports have demonstrated that the BH4 domain is sufficient for an anti-apoptotic effect (Cittelly et al., 2007). Beyond structural composition, previous reports have shown Bcl-2 family proteins to be developmentally and anatomic-spatially regulated (Yuan et al., 2003). For example, Bcl-2 expressed in the neonatal brain and Bcl-X_L highly expressed in the adult spinal cord.

Classically, the Bcl-2 family has been described as regulators of the intrinsic mitochondrial cell death pathway (Koubi et al., 2005; Shimizu et al., 1999; Spierings et al., 2005). Previously, the rheostat hypothesis proposed a cellular balance in the expression of pro- and anti-apoptotic Bcl-2 proteins (Korsmeyer et al., 1993). If this balance were tipped towards increased cellular pro-apoptotic protein levels, then cell death via the intrinsic apoptotic pathway

A)



B)

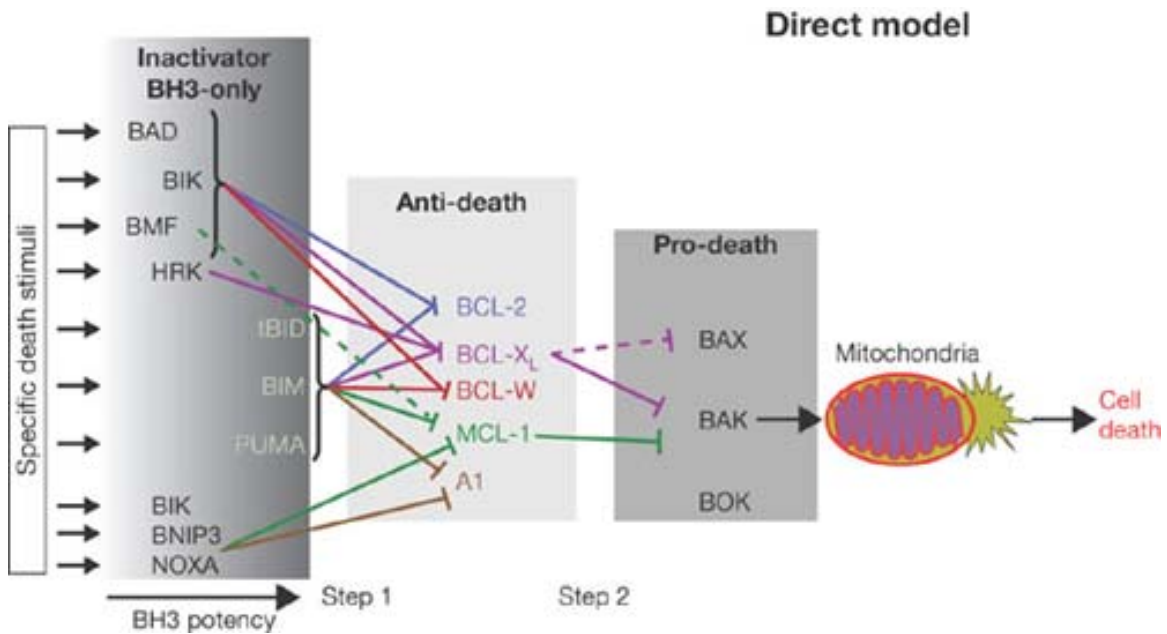


Figure 6. Bcl-2 family of proteins and the current disinhibition model for the regulation of the Bcl-2 family

A) Schematic of the 2 main functional groups within the Bcl-2 family. Modified with permission from Macmillan Publishers Ltd. (Jesenerger and Jentsch, 2002). B) Current disinhibition model for the regulation of the Bcl-2 family of proteins. Modified with permission from Macmillan Publishers Ltd. (Kim et al., 2006a).

would occur. On the other hand, if the balance were tipped towards increased cellular anti-apoptotic protein levels, then unchecked cellular proliferation would result in tumorigenesis. This rheostat model relied on the proposed direct interaction of multi-domain pro- and anti-apoptotic Bcl-2 family members, which proved elusive to demonstrate. Recently, this rheostat model has given way to a disinhibition hierarchy model of activation (Kim et al., 2006a) (Fig. 6B). Unlike the rheostat model, the hierarchical model does not suggest a direct interaction between multi-domain pro- and anti-apoptotic Bcl-2 family members, but rather an interaction between anti-apoptotic and BH3-only proteins, which serve as activators of Bax and Bak (Kim et al., 2006a). Therefore, initiation of cell death requires inhibition of the inhibitory anti-apoptotic members (disinhibition) to allow BH3-only protein mediated activation of multi-domain pro-apoptotic Bax and Bak and thereby activation of cell death machinery (Kim et al., 2006a).

Bax and activation of mitochondrial cell death signaling

In 1993, Stanley Korsmeyer and his research team reported on the first pro-apoptotic member of the Bcl-2 family, named Bcl-2 antagonist X protein (Bax) (Oltvai et al., 1993). Since then, debate still remains over how Bax initiates cell death at the mitochondria. Previous reports have proposed: Bax interacts and modulates channels already present within the mitochondria (i.e. VDAC) allowing release of cytochrome c (Shimizu et al., 1999; Shimizu et al., 2000), Bax self-oligomerizes to form a channel allowing the release of mitochondrial

cytochrome c (Dejean et al., 2005; Wei et al., 2001) and, lastly Bax oligomerizes through Bid-mediated activation to disrupt the mitochondrial electrochemical gradient, thereby promoting PTP formation and release of cytochrome c (Korsmeyer et al., 2000). Despite this on-going debate, Bax translocation to the mitochondria and subsequent release of cytochrome c release into the cytosol remains a canon in cell death literature (Gould et al., 2006; Hetz et al., 2006; Karbowski et al., 2006; Mishra et al., 2006).

Bcl-2 family proteins localize to organelles other than mitochondria

Recently, reports have been published in cancer cell lines, which demonstrate Bcl-2 family members localize to organelles other than their canonical mitochondrial site in response to chemotherapeutic agents (Cho et al., 2006; Godlewski et al., 2001; Mandal et al., 2001; Salah-eldin et al., 2000; Zong et al., 2003). Specifically, in the MCF-7 human breast cancer cell line, Bax and Bcl-2 localize to the nucleus, ER and mitochondria in response to camptothecin treatment (Godlewski et al., 2001). Regarding a functional role for ER Bax, research published by Scorrano et al. (2003) and Oakes et al. (2003, 2005) have suggested that both Bax and Bcl-2 play a role in ER Ca^{2+} homeostasis. Though ER targeting of Bcl-2 and Bax, they demonstrated that targeting anti-apoptotic Bcl-2 to the ER reduces resting ER Ca^{2+} levels, such that adding ER stressors decreases ER Ca^{2+} mobilization and cell death, while ER targeting of Bax had the opposite effect, increasing a cell death, which could not be inhibited by

apoptotic antagonists (Oakes et al., 2005; Oakes et al., 2003; Scorrano et al., 2003). This ER Ca^{2+} would promote cell death through caspase 12 and calpain activation.

Nuclear Bax localization has been shown in colon cancer cell lines (Mandal et al., 1998) and neuroblastoma cell lines (Karlsson et al., 2007) after chemotherapeutic treatment. Unlike its ER counterpart, the functional role for nuclear Bax has not yet been resolved. Several recent reports suggest a role for Bax in p53-mediated cell death signaling as Bax co-immunoprecipitates with p53 (Raffo et al., 2000). Furthermore, porcine models of global fetal hypoxia suggest nuclear envelope-associated Bax regulates nuclear Ca^{2+} . However, definitive evidence is lacking. Regarding the mechanism of how Bax localizes to the nucleus, Karlsson et al. (2007) have shown that Bax overexpression in SY5Y cells localizes full-length Bax to both the nuclear envelope and the inside of the nucleus, with N-terminal Bax cleavage locking it in the nucleus (Karlsson et al., 2007). Thus, the localization of Bax and Bcl-2 to organelles other than the mitochondria suggests that the Bcl-2 family may regulate cell death on a multi-organelle level. In order to properly investigate this hypothesis, an appropriate model must be chosen which can activate nuclear, mitochondrial and ER cell death signaling cascades.

Neonatal models of HI

Neonatal HI very adequately can be mimicked in the post-natal rodent. Post natal day 10 (P10) in mice and P7 in rats is equivalent to a third trimester human fetus in regards to brain maturation (Dobbing et al., 1979). As such, most current models of neonatal HI use pups from these time points in various combinations of hypoxic and ischemic insult. The most clinically relevant models of HI are those which involve transient occlusion of either the middle cerebral artery (MCA) or the common carotid artery (CCA) followed by reperfusion, which in neonates is a daunting task. A model of reversible focal ischemia has been developed, which has been shown to generate a non-hemorrhagic focal lesion in the P7 neonatal rat pup brain (Derugin et al., 1998).

Despite this recent model development, for over 20 years, the stalwart animal model used to investigate neonatal HI has been the Rice-Vannucci P7 rat pup model (Vannucci et al., 1988). The Rice-Vannucci model of neonatal HI involves a permanent, unilateral ligation of the common carotid (Fig. 7) (www.biologycorner.com) followed by a global, 2h hypoxic period (nitrogen balanced 8.0% O₂) in a P7 rat pup (Vannucci et al., 1988). This model results in injury due to energy failure and increased oxidative stress (Northington et al., 2005) with the parietal cortex of the ipsilateral hemisphere at greatest risk, due to its vascularization by small diameter branches of the middle cerebral artery (Back et al., 2007b). Furthermore, the aforementioned high dependence on glucose metabolism and high levels of polyunsaturated fatty acids present predispose the

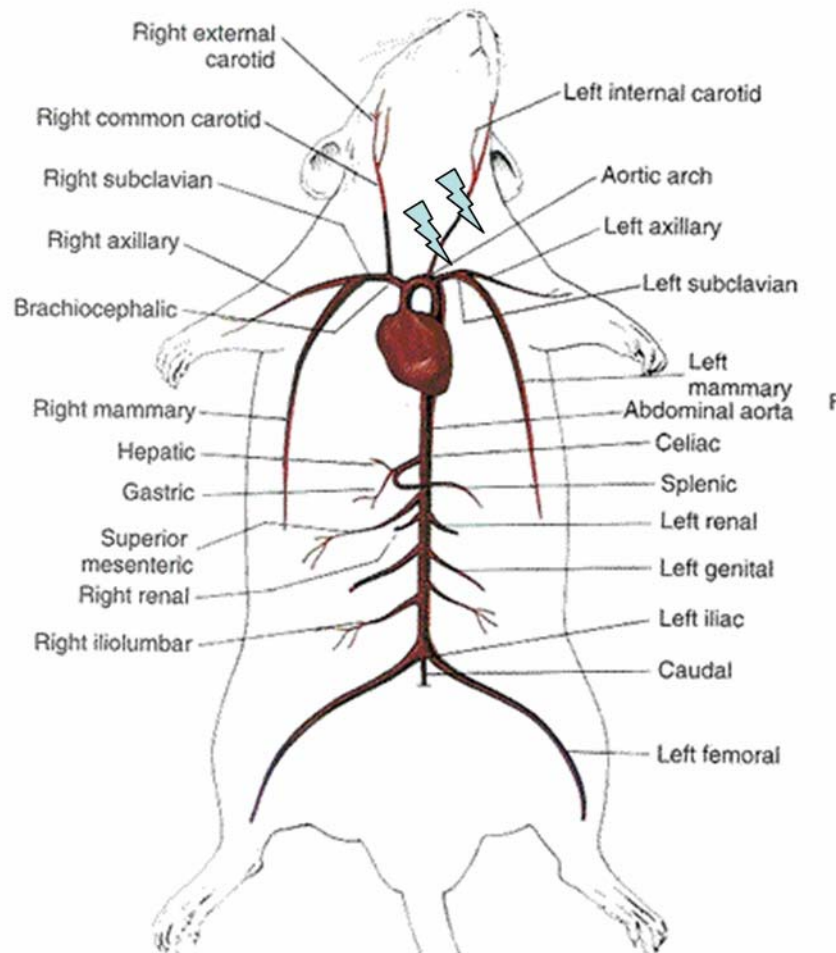


Figure 7. Schematic representation of an adult rat to illustrate the location of the electrocauterization site used in the modified protocol of the Rice-Vannucci model used in this dissertation on neonates.

Modified from (Muskopf S, 2006).

CNS to oxidative stress insults, but even more so for the neonatal rat pup brain because of its immature free radical scavenging system (decreased glutathione peroxidase and catalase relative to the adult) (Rassin lecture notes, 2004). The increased oxidative stress promotes the formation of DNA adducts, lipid peroxidation and protein misfolding, as well as, the depletion of glucose and O₂, which triggers further disruption of oxidative phosphorylation. Reports using the Rice-Vannucci model have demonstrated increases in cell death signaling at the nucleus, mitochondria and ER (Ikeda et al., 2006; Jatana et al., 2006; Nakajima et al., 2000; Northington et al., 2005). Thus, the Rice-Vannucci model of neonatal HI possesses the essential injurious components involved in clinical HIE to allow investigation into the coordinating role for Bax in multi-organelle cell death signaling cascades, as well as to allow extrapolation into the clinical setting.

Project Aims

The purpose of this dissertation was to evaluate the novel hypothesis that Bax coordinates the activation of multiple cognate organelle cell death signaling cascades after neonatal HI. Furthermore, this dissertation sought to correlate Bax-mediated activation of particular organelle cell death signaling with a particular phenotypic outcome. This dissertation combined both *in vivo* and *in vitro* experimental designs, as well as therapeutic manipulation of

these experimental treatments, to critically evaluate this hypothesis. Specifically, the main aims of this dissertation were as follows:

Aim 1. HI induces Bax localization to the mitochondria, ER and nucleus resulting in the activation of organelle-specific cell death mechanisms that increase cell death.

Rationale. In vivo, we will demonstrate Bax localization to the mitochondria, ER and nucleus correlates with increased protein levels of cleaved-caspase 3, cleaved-caspase 12 and the phosphorylation of p53 (Ser15), respectively, and these events result in increased cell death. In addition, we will demonstrate HI-induced changes in organelle-specific pro-cell death protein levels, which contribute to cell death signaling.

Aim 2. Differential Bax localization to the mitochondria, ER and / or nucleus, and differential activation of cell death signaling cascades will correlate with different cell death phenotypes.

Rationale. In vitro, certain cell death stimuli will produce specific cell death phenotypes in P5 rat primary cortical neurons. Using a necrotic and an apoptotic stimulus, we will demonstrate whether the differential localization of Bax to the mitochondria, ER and nucleus, as well as differential activation of respective organelle-specific cell death signaling cascades, correlate with specific cell death phenotypes.

Aim 3. Decreasing Bax localization to the nucleus, mitochondria and / or ER will decrease cell death and modulate the cell death phenotype based on which organelle cell death signaling cascades were down-regulated, i.e. on the differential sensitivity of these signaling cascades.

Rationale. Using hyperoxia therapy (the clinically approved therapy for children suspected to have suffered HIE) *in vivo* and FK506 (a clinically approved immunosuppressant with anti-cell death activity) *in vitro*, we will demonstrate that these therapeutic interventions decrease cell death through inhibition of Bax localization and activation of cognate organelle cell death signaling. Furthermore, we will elucidate whether differential down-regulation of particular organelle cell death signaling cascades induces a change in the resulting cell death phenotype (Fig. 8).

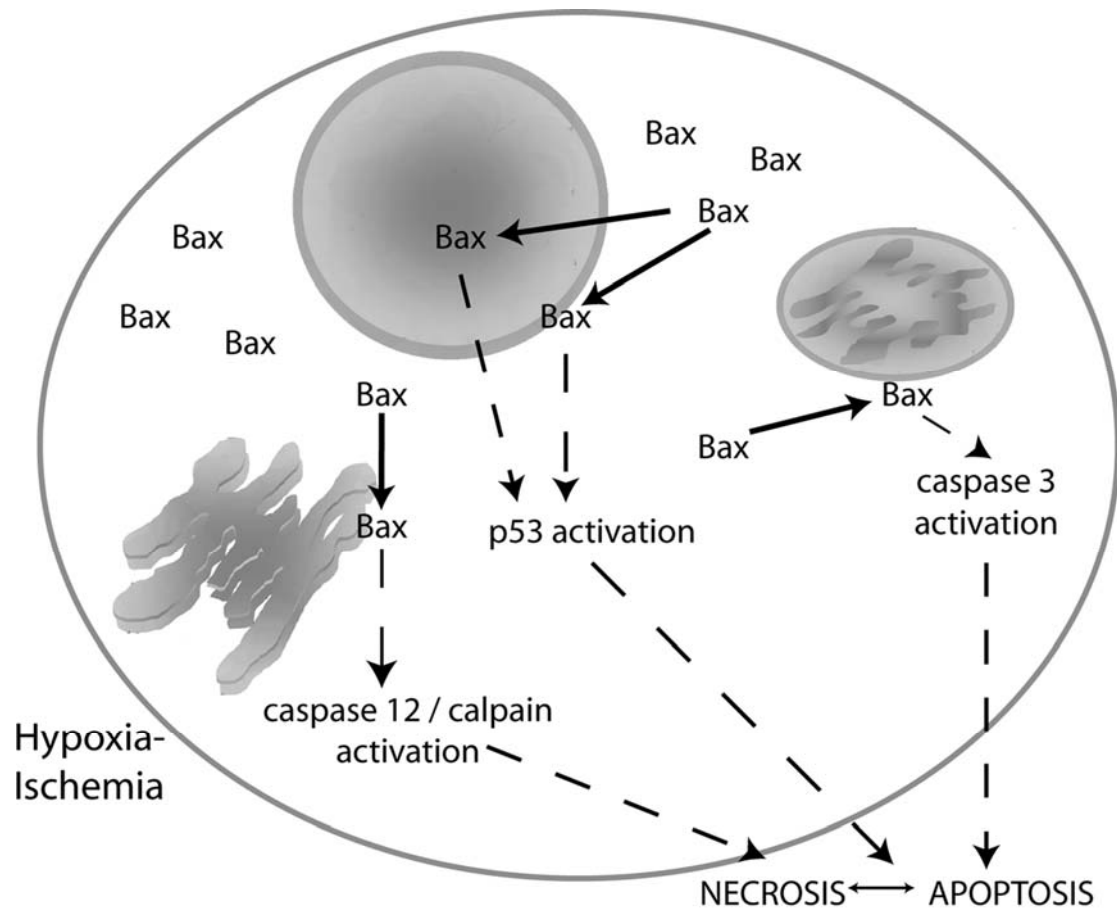


Figure 8. Schematic representation of the dissertation central hypothesis

HI induces Bax localization to the nucleus, mitochondria and ER where Bax coordinates the activation of cognate organelle cell death signaling cascades, which through differential activation modulates resulting cell death phenotype.

CHAPTER II

HI induces nuclear, mitochondrial and ER Bax localization to activate cognate organelle cell death signaling cascades

Perinatal hypoxic-ischemia (HI) occurs in 0.2-0.4% of all live births. HI produces a necroptotic cell death phenotype spectrum associated with a spectrum of dysfunctional outcomes. However, mechanisms to explain this phenotypic spectrum are not fully understood. Here, we provide evidence that Bcl-2-antagonist X protein (Bax) coordinates multi-subcellular cell death signaling cascade activation after neonatal HI to promote cell death phenotype diversity. Using the Rice-Vannucci model, we demonstrate a novel organelle-specific time course for increased Bax protein levels, with an early increase in intranuclear and total nuclear Bax levels followed by a later Bax redistribution to the mitochondria and ER. Correlating with this organelle-specific Bax time course, we observed cognate organelle cell death signaling mechanism activation (increased nuclear phospho-p53, cytosolic cleaved caspase 3 and cleaved caspase 12). These data provide the first evidence in support of the proposed role for Bax in coordinating the cell death signaling at multiple subcellular organelles.

Introduction

Perinatal hypoxic-ischemia (HI) occurs in 0.2-0.4% of all live births (Odding et al., 2006; Platt et al., 2007; Raju, 2006b; de Menezes and Shaw, 2006; Raju, 2006c), with 100% O₂ remaining the standard clinical treatment

(Raju, 2006a). HI produces a necroptotic cell death phenotype spectrum (Colbourne et al., 1999; Edinger and Thompson, 2004; Formigli et al., 2000; Nakajima et al., 2000; Proskuryakov et al., 2003) associated with a spectrum of dysfunctional outcomes (Chu et al., 2002; Northington et al., 2005; Cole and Perez-Polo, 2004). However, mechanisms to explain this phenotypic spectrum are not fully understood.

In vivo injury models have been shown to induce cell loss through initiation of cell death signaling cascades at multiple subcellular sites (Northington et al., 2001; Sanges and Marigo, 2006; Tan et al., 2002), including the nucleus, mitochondria, and /or endoplasmic reticulum (ER) via: p53-mediated transcription (Appella and Anderson, 2001; She et al., 2000), differential necrotic and apoptotic cleavage of poly-ADP-ribose 1 (PARP-1) (D'Amours et al., 2001; Gobeil et al., 2001; Mandir et al., 2000) and the necrosis-induced release of nuclear high mobility group box 1 (HMGB1) triggering inflammation (Bell et al., 2006; Ditsworth et al., 2007; Kim et al., 2006b; Scaffidi et al., 2002); activation of downstream effector caspases (Dejean et al., 2005; Krajewski et al., 1999; Reed, 2006) and AIF-mediated caspase-independent mechanisms (Culmsee et al., 2005; Plesnila et al., 2004; Zhu et al., 2007); as well as, caspase 12 / calpain activation promoting necrotic-like cell death (Kalai et al., 2003; Larner et al., 2006; Yoneda et al., 2001; Nakagawa et al., 2000; Hu et al., 2005a). Despite the ongoing in vivo research, there are few accounts of how individual organelle cell death signaling cascades act in concert to modulate cell death.

As the precise mechanism of pro-apoptotic Bax activation is still under intense investigation (Kim et al., 2006a), Bax-mediated initiation of mitochondrial apoptosis remains a canon in the programmed cell death literature (Goping et al., 1998; Korsmeyer et al., 1999; Shimizu et al., 1999; Wei et al., 2001; Wolter et al., 1997). However, recent cancer cell biology studies have shown chemotherapeutics to promote Bax localization to other organelles in addition to mitochondria, such as the nucleus and ER (Gajkowska et al., 2004; Godlewski et al., 2001; Salah-eldin et al., 2000), where Bax promotes cell death via manipulation of Ca^{2+} homeostasis (Nutt et al., 2002a; Nutt et al., 2002b; Oakes et al., 2005; Oakes et al., 2003). Therefore, we sought to characterize the coordinating role of Bax in neonatal HI cell death signaling and cell death phenotype diversity.

We used the Rice-Vannucci model of neonatal HI, which increases cell death signaling at the nucleus (DeGracia and Montie, 2004; Larner et al., 2006; Walton et al., 1999; Zhu et al., 2003), mitochondria (Zhu et al., 2000) and ER (DeGracia and Montie, 2004; Larner et al., 2006; Walton et al., 1999; Zhu et al., 2003), to ascertain if Bax mediates the activation of cell death signaling at the nucleus, mitochondria and ER in the HI-injured cortex and what role the activation of these cascades plays in the determination of cell death phenotype. We showed a distinct multi-subcellular time course for Bax relocation in the HI-injured cortex, with Bax localizing first to the nucleus as early as 30min post HI, then to mitochondria and, finally, to the ER. In addition, we confirmed the

presence of Bax both in the nuclei and nuclear envelope, a novel in vivo observation. We also showed that Bax localization to the different organelles correlates with the initiation of each organelle's respective cell death signaling cascade. Together, these data provide the first evidence in support of the proposed role for Bax in coordinating the cell death signaling at multiple subcellular organelles.

Materials and Methods

Materials. All chemicals were purchased from Sigma-Aldrich (Saint Louis, MO). N, N-bisacrylamide was purchased from Bio-rad Laboratories (Hercules, CA). Surgical instruments were purchased from Roboz Surgical Instrument Company (Gaithersburg, MD) and 5-0 P3 surgical silk was purchased from Ethicon (Somerville, NJ).

Animal Care. E15 pregnant Wistar rat dams (Charles Rivers Laboratories, Wilmington, MA) were housed upon arrival in 12h light-dark cycle with access to food and water *ad libitum*. The day of birth was designated P0. On P1, litters were culled to ten pups. On P7, the day of HI insult, all pups were removed from the dam, sexed, weighed and randomly assigned to HI-injured groups of variable survival duration or sham groups of variable survival duration. In lieu of using the contralateral hemisphere as the control group, sham groups were utilized because the model of hypoxia-ischemia insult described below produced injury to both the contralateral and ipsilateral cortices, as measured by increased cytosolic

cleaved caspase 3 expression and increased cytosolic oligonucleosome formation at 3h post hypoxia-ischemia (Figure 9 A-C). For survival time course analyses at multiple time points after HI insult, multiple dams were ordered and housed as described above, except that on P1 after culling to ten pups, the pups were mixed among the dams to minimize potential, confounding litter effects among the multiple groups.

Surgical protocols (Hypoxia-ischemia). Hypoxia-ischemia (HI) insult involving a unilateral, permanent ligation of the common carotid was performed as described elsewhere (Hu et al., 2005b; Vannucci et al., 1988) with minor modifications. Briefly, anesthesia was induced in P7 rat pups by 7-minute incubation in 5% isoflurane, balanced with blood-gas grade 100% O₂, in a 37°C E-Z anesthesia chamber (Euthanex Corp., Palmer, PA) with maintenance of anesthesia at 2.0% isoflurane. As prolonged neuroprotective effects have been observed with isoflurane incubations of greater than 1h (Loepke et al., 2006), care was taken to ensure that no pup was anesthetized for longer than 0.75h. After a mid-neckline incision, the left common carotid was isolated and ischemia was induced by electrocauterization at two points, one rostral and one caudal, along the isolated artery using a ball-end cauterizer. Double electrocauterization cut the left common carotid in the majority of surgeries (>95%). In those cases in which the blood vessel did not sever, the artery was cut between the two cauterization points using micro-spring scissors to prevent reperfusion across cauterization points. Furthermore, care was taken not to damage the vagal

nerve which runs parallel and dorsal (underneath) the common carotid artery. After cauterization, the mid-neckline incision was sutured with 5-0 P3 surgical silk and the pup was returned to a normoxic (20.8% O₂) 37°C chamber until the effects of the anesthesia dissipated (5-10 min). Sham pups were anesthetized, given the mid-neckline incision and, then, sutured. Isolation of the left common carotid was not performed on sham pups as isolation of the artery can produce minor (<1-2s) ischemia-reperfusion events (unreported observational finding). The total time for performing ischemia surgery on a litter of pups was approximately 1h. After the last pup recovered from anesthesia, the pups were returned to the dam for a 2.5h recovery period to prevent any potential isoflurane-mediated respiratory complications during the hypoxia component of the HI injury.

After the 2.5h recovery period, all pups were removed from the dam and placed either in a normoxic 37°C chamber (sham) or hypoxic (8.0% O₂ balanced with blood-gas grade nitrogen) 37°C chamber for 1.5h. A small pet intensive care unit (ICU) (Harvard Apparatus, Boston, MA) was used for the hypoxia chamber as its larger volume promoted greater inertia of oxygen levels and its heated internal water bath reduced temperature variations commonly observed with small chambers wrapped in heated water pads (unreported observational finding). After the 1.5h period, designated 0h survival, pups were returned to the dam until their randomly assigned survival time point. Cortices were collected

from sham (0h) and HI-injured pups at 0.5, 1, 2, 3, 6, 12, 24, 48 and 72h survival times after HI (n=3 / time point).

Subcellular Fractionation of P7 Wistar rat pup cortices. At the designated survival time point after HI or HHI, pups were deeply anesthetized in an isoflurane-filled gas chamber and then decapitated. Whole brains were removed and both contralateral and ipsilateral cortices, from the anterior tuber cinereum to anterior of the occipital cortex (encompassing the parietal cortex), were isolated and flash frozen in liquid nitrogen. Cortical tissue was stored at -80°C until processed. All of the following fractionation steps were carried out in ice or a 4°C cold room.

Each isolated cortex was suspended in ice-cold fractionation buffer (FB) (in mM: 10 HEPES, 0.5 EGTA, 2 EDTA, 10 DTT, 250 sucrose) containing 1 Roche Complete Protease Inhibitor Tablet (Roche Applied Sciences, Indianapolis, IN) and 100µl Phosphatase Inhibitor Cocktail II (Sigma-Aldrich, Saint Louis) per every 10mL of FB. Cortices were disrupted by 30 strokes in a tight-fitting dounce homogenizer (Wheaton Science, Millville, NJ). Homogenates were centrifuged for 20min at 1000g to pellet nuclei and unbroken cells. To aid in the enrichment of the fractionation procedure, we employed a 50-80 supernatant removal process. Briefly, 50% of the supernatant was removed to a new chilled tube [labeled supernatant 1 (S1)] and FB roughly equivalent to half of the supernatant volume taken off was added to the pellet. The nuclear pellet was resuspended, and, again, the homogenate was centrifuged for 20min at 1000g to

repellet nuclei and any remaining unbroken cells. Now 80% of the supernatant was removed and placed in the S1 tube. The remaining supernatant was discarded and the nuclear pellet was resuspended in pellet buffer (PB) (in mM: 20 HEPES, 400 NaCl, 1 EDTA, 1 EGTA, 1 DTT, 1 PMSF) containing 1 Roche Complete Protease Inhibitor Tablet and 100µl Phosphatase Inhibitor Cocktail II per every 10mL of PB. The suspended nuclear pellet was shaken at 1400rpm on an orbital shaker for 30min and then centrifuged at 14000rpm for 10 min. To minimize repetitive freeze-thaw cycles, the supernatant (nuclear fraction) was stored in aliquots at -80°C until further analysis.

While processing the nuclear fraction, the supernatant in the S1 tube was centrifuged at 3300g for 10min to pellet any remaining nuclei and unbroken cells. The supernatant was removed to a new chilled tube (M) and the pellet was discarded. The supernatant in the M tube was centrifuged at 10000g for 20min to pellet heavy and light mitochondria. As with the original 1000g step, which used the 50-80 supernatant removal steps, 50% of the supernatant was removed to a new chilled tube (S2), the pellet was resuspended and centrifuged again at 10000g for 20min. 80% of the supernatant was removed to the S2 tube and the remaining supernatant was discarded. The mitochondrial pellet was resuspended in PB and then was briefly pulse-sonicated (30kHz, <2s). After sonication, the sonicated resuspension (mitochondrial fraction) was stored in aliquots at -80°C until further analysis.

While processing the mitochondrial fraction, the supernatant in the S2 tube was centrifuged at 15000g for 10min to pellet any remaining light mitochondria. The supernatant was then removed to a new chilled tube (E) and the pellet was discarded. The supernatant in the E tube was centrifuged at 100000g for 1h to pellet rough and smooth endoplasmic reticulum (ER). The supernatant (cytosolic fraction) was removed and stored in aliquots at -80°C until further analysis. The ER pellet was resuspended in PB and, then, was briefly pulse-sonicated (30kHz, <2s). After sonication, the sonicated resuspension (ER fraction) was stored in aliquots at -80°C until further analysis. Using Lamin-B₁, IκB-α, cytochrome c oxidase IV (COXIV) and protein disulfide isomerase (PDI) as respective nuclear, cytosolic, mitochondrial and ER markers, we observed that this subcellular fractionation protocol yielded highly enriched nuclear, cytosolic, mitochondrial and ER fractions (Figure 2A).

Western Blot Analysis. Protein concentration of subcellular fractions was determined via the bicinchoninic acid (BCA) assay (Pierce, Rockford, IL). 50μg of protein were separated via electrophoresis on a 10% or 12% SDS-polyacrylamide gel, depending upon the main protein of interest for analysis. Protein was transferred overnight at 4°C in transfer buffer [in mM: 25 Tris base, 192 glycine, 10% (v/v) methanol] to a PDVF membrane (Millipore, Billerica, MA). Protein-containing PDVF membranes were blocked for 1h at room temperature in blocking buffer (BB) [4% bovine serum albumin (BSA), 0.2% Tween-20 in Tris-buffered saline (TBS, pH 7.4)]. Following blocking, membranes were washed 2X

in wash buffer (WB) [0.2% Tween-20 in Tris-buffered saline (TBS, pH 7.4)]. Next, membranes were incubated overnight (or 1h at room temperature) with primary antibody diluted in primary antibody buffer (PAB) [1% bovine serum albumin (BSA), 0.2% Tween-20 in Tris-buffered saline (TBS, pH 7.4)]. The following primary antibodies [with their dilution used] were examined: mouse anti-Bax (6A7 clone) [1:1000], rabbit anti-IL-1 β [1:500], mouse anti-Lamin B₁ [1:1000] (Invitrogen, Carlsbad, CA), rabbit anti-I κ B- α [1:1000] (Santa Cruz Biotechnology, Santa Cruz, CA), mouse anti-COXIV [1:4000] (Abcam, Cambridge, MA), rabbit anti-high mobility group protein 1 (HMG1/HMGB1) [1:1000], rabbit anti-caspase 12 (C-terminus) [1:1000] (Millipore, Billerica, MA), mouse anti-PDI [1:1000] (Assay Designs, Inc., Ann Arbor, MI), rabbit anti-phospho-p53 (Ser15) [1:1000], rabbit anti-cleaved caspase 3 [1:1000], rabbit anti-apoptosis inducing factor (AIF) [1:500] (Cell Signaling Technologies, Inc., Danvers, MA) and mouse anti- β -actin [1:50000] (Sigma-Aldrich, Saint Louis, MO). After incubation with the primary antibody, membranes were washed 6X 10min in WB. Following these washes, the membranes were incubated 1h at room temperature with the appropriate secondary antibody diluted in secondary antibody buffer (SAB) [0.5% bovine serum albumin (BSA), 0.2% Tween-20 in Tris-buffered saline (TBS, pH 7.4)]. The following secondary antibodies were employed: goat anti-mouse-POD, rat adsorbed, and goat anti-rabbit F(ab')₂-POD, human and mouse adsorbed (Southern Biotech, Birmingham, AL). All secondary antibodies were diluted 1:3000, except for mouse anti- β -actin for which the secondary antibody was

diluted 1:15000. Following incubation with the secondary antibody, membranes were washed 6X 10min in WB and, then, developed using the enhanced chemiluminescence (ECL) system (GE Healthcare, Piscataway, NJ). Films were scanned and densitometric analyses were performed using AlphaEase software (Alpha Innotech, San Leandro, CA). Samples were normalized first to β -actin values and then represented as fold values relative to sham.

ELISA detection of cytosolic oligonucleosome formation. As a measure of apoptotic cell death, the presence of cytosolic oligonucleosomes (DNA+histone complexes resulting from cleavage at the interlinker regions between histones on DNA) was detected using the Cell Death Detection ELISA® (Roche Applied Sciences, Indianapolis, IN), by following the manufacturer's protocol. All steps were carried out at room temperature. Briefly, a 96-well microplate was coated for 1.5h with a mouse monoclonal antibody, diluted in supplied coating buffer (clone H11-4 to the histones H2A, H2B, H3 and H4). The plate was then incubated in the supplied incubation buffer for 0.5h. 50 μ g of cytosolic protein from each sample loaded in triplicate wells was diluted in incubation buffer. The cytosolic samples were incubated for 1.5h. After incubation, the microplate was washed 3X with supplied wash buffer and then incubated for 1.5h in a peroxidase conjugated antibody to DNA, diluted in incubation buffer. The microplate, again, was washed 3X in wash buffer and then incubated for 5 min to 1h in 2,2-azino-bis(3-ethylbenzthiazoline-6-sulphonic acid) (ABTS) substrate solution on a rotary shaker (250rpm). During this incubation, multiple readings at 405nm were

recorded using a Dynex MRX™ microplate reader (Dynex Technologies, Chantilly, VA). Absorbance values at 405nm were represented as fold change relative to sham absorbance values at 405nm.

Tissue preparation for immunofluorescent staining. Survival time points after HI, which showed maximal Bax protein levels in each fraction, were selected for confocal immunohistochemical analysis. At these time points, pups were given an overdose of Nembutal (120mg/kg, i.p.) and perfused transcardially with 0.22µm-filtered 0.9% (w/v) saline. Pups were, then, fixed with 0.22µm-filtered 4% (w/v) paraformaldehyde / phosphate-buffered saline (PBS). Whole brains were removed and fixed for an additional 24h in 0.22µm-filtered 4% (w/v) paraformaldehyde / PBS at 4°C. Fixed, whole brains were trimmed from the anterior tuber cinereum to anterior of the occipital cortex (encompassing the parietal cortex), and incubated in 30% (w/v) sucrose / PBS at 4°C until the sections sank (roughly 72h). Trimmed brains were given a nick on the ipsilateral hemisphere (for distinguishing the hemispheres), encased in O.C.T. compound (Sakura Finetek, Torrance, CA) on dry ice and, then, stored at -20°C until frozen solid. Trimmed brains were sectioned using a frozen microtome into 20µm slices onto poly-L-lysine coated glass slides and stored at -20°C until immunohistochemical staining.

For immunofluorescence staining, sections were post-fixed with ice cold acetone for 5min and then allowed to air dry for 30min. Sections were washed 3X for 7min in immunohistochemistry wash buffer (IWB) (50mM Tris base, 0.9%

(w/v) NaCl, 0.45 μ m filter-sterilized, pH 7.6). Then, sections were permeabilized 3X for 7min with IWB + 0.1% Triton X-100. Following permeabilization, sections were blocked for 45min with IWB+ 5%(v/v) normal goat serum (NGS)+ 0.3% (w/v) BSA + 0.1% Triton X-100. After removal of the blocking solution, sections were incubated overnight in a humidified chamber with the primary antibodies diluted in IWB+ 1%(v/v) normal goat serum (NGS)+ 0.3% (w/v) BSA + 0.1% Triton X-100. The following primary antibodies [with their dilutions used] were examined: rabbit anti-Bax (N-terminus) [1:200] (Millipore, Billerica, MA), mouse anti-PDI [1:100] (Assay Designs, Inc., Ann Arbor, MI) and mouse anti-ATP synthase β [1:100] (Abcam, Cambridge, MA). Following overnight incubation, the sections were washed 3X for 7min in IWB + 0.05% (v/v) Tween-20. Then, the sections were incubated for 1h with appropriate fluorescent secondary antibodies diluted in IWB. The following secondary antibodies [and their dilutions] were employed: AlexaFluor 568 goat anti-rabbit [1:1000] and AlexaFluor 488 goat anti-mouse [1:1000] (Invitrogen, Carlsbad, CA). Again, sections were washed 3X for 7min in IWB + 0.05% (v/v) Tween-20. Following these wash steps, the sections were incubated with Hoechst 33258 (0.5 μ g/mL) for 5 min to stain nuclei. Vectashield mounting medium (Vector Labs, Burlingame, CA) was applied to the sections and Assistant glass cover slips (No. 1.5 thickness) (Harvard Apparatus, Holliston, MA) were placed on top and sealed with clear nail polish. Fluorescent stained slides were stored in the dark at -20°C until viewing. Sets of slides to be

used for comparison studies using the same primary antibodies were performed on the same day to eliminate inter-experimental variance.

Confocal microscopy. Fluorescent stained slides were viewed using the Biorad Radiance 2100 laser scanning system (Carl Zeiss, Thornwood, NY) fitted onto a Nikon Eclipse E800 microscope (Nikon, Melville, NY). Images were collected using LaserSharp 2000 software (Carl Zeiss, Thornwood, NY). Fluorescence was detected using the following laser and emission filter sets: for cyan fluorophores, a 405nm laser with an HQ442/45 emission filter, for green fluorophores, a 488nm laser with an HQ515/30 emission filter, and for red fluorophores, a 568nm laser with an E600LP emission filter. Two dichroic mirrors were placed along the optical path to prevent fluorescence bleed-through- a 500DCLPXR mirror for the cyan and green fluorophores and a 560DCLPXR for the green and red fluorophores. A third 100% deflection mirror was used when imaging the cyan fluorophore.

Sham animals were used to set the baseline parameters for laser intensity, gain and offset for slides stained with the same primary antibodies. Using the SETCOL lookup table (LUT), the three parameters were chosen which maximized the width of the gray scale with few red (high intensity) pixels and few green (low intensity) pixels. Optimal pinhole size was computer generated for each laser at each objective. For the Fluor 40X oil (NA 1.3), the pinhole settings were as follows: for 405nm, 0.9mm, for 488nm, 1.1mm and for 568, 1.3mm. For the Plan Apo 60X oil (NA 1.4), the pinhole settings were as follows: for 405nm,

1.3mm, for 488nm, 1.5mm and for 568nm, 1.8mm. After the parameters had been selected, the settings were maintained for all images taken involving the same primary antibodies and the entire image set was collected on the same day.

Images were scanned using the sequential scan setting for the three lasers, set at a scan rate of 50 lines per second (lps), and using a Kalman averaging (N=6) to minimize background signal. A 60X oil objective (NA 1.4) with a computer-driven 2.6X zoom was used to acquire images for analyzing the presence of Bax colocalization with particular subcellular organelles, and a Fluor 40X oil objective (NA 1.3) was used to acquire images for the blind counting of the cells within regions of interests (ROIs) which exhibited Bax colocalization with a particular subcellular organelle. Sets of 40X confocal images for each primary antibody combination were counted by the same blind reviewers to minimize reviewer-to-reviewer variability. Prior to analysis, collected images were deconvolved using a 2D iterative deconvolution plug-in based on the DAMAS algorithm (Brooks and Humphreys, 2004; Dougherty, 2005) for NIH ImageJ shareware (<http://rsb.info.nih.gov/ij/>).

Detecting Intranuclear Bax and Nuclear Bax Fluorescence Intensity Using LineProfile Analysis. To analyze if Bax translocated into the nucleus and the changes in nuclear Bax fluorescence as a result of HI, LineProfile analyses of z-stacks of cells from sham and HI-injured cortices were performed. Briefly, random ROIs within the ipsilateral cortex from both sham and HI-injured stained

slides were used to generate z-stack images. Having established the baseline parameters as described above, multiple scans at 0.7 μ m steps in the z-direction of a ROI were taken. Then, using the LineProfile program within LaserSharp 2000 software, a hemisecting line of 1 pixel diameter was drawn across the nuclei of cells within the ROI (Figure 9A). Using the Hoechst 33258 (blue) pixel intensity values along the hemisecting line to define the boundary of the nucleus, we defined intranuclear Bax as the presence of ascending and descending peaks in Bax (red) pixel intensity along the same hemisecting line within the boundaries set by the Hoechst 33258 pixel intensity (Figure 9B). Using this same hemisecting line but increasing its diameter to equal the size of the nucleus at a particular 0.7 μ m step, we measured the average nuclear Bax pixel intensity at this z-step. Then, we defined the average nuclear Bax pixel intensity of a cell within the ROI as the average of the individual 0.7 μ m step averages of Bax nuclear pixel intensity. We performed these measurements on multiple cells from multiple ROI for comparison of nuclear Bax fluorescence intensities from within sham and injured cortices (Figure 9C)(3 ROIs / hemisphere, n = 15 cells / hemisphere, three sham hemispheres and three 1h survival post HI hemispheres analyzed) .

Statistical Analysis. Statistical analyses were performed using GraphPad Prism 5 software (GraphPad Software, San Diego, CA). For analyses involving two groups, a student's t-test was performed and a p-value less of than 0.05 was considered significant. If variances for the two groups were deemed

significantly different, a Welsh correction was added to the student's t-test. For analyses involving two or more groups, a one-way analysis of variance (ANOVA) was performed with a Tukey-Kramer post-hoc test to compare groups. A p-value of less than 0.05 was deemed significant.

Results

HI induces contralateral cortical injury to a lesser extent than ipsilateral cortical injury

The Rice-Vannucci model of HI with its global hypoxia component can result in bilateral hemispheric injury (Ashwal et al., 2007; Meng et al., 2006), although there is less injury in the contralateral hemisphere. In order to assess the extent to which our modified Rice-Vannucci model resulted in both contralateral and ipsilateral changes in the experimental outcomes measured here, we subjected a litter of pups to HI with 1.5h of 8% hypoxia. We sacrificed the pups at 3h post HI, a time at which there is a significant increase in caspase 3 cleavage in the ipsilateral cortex (Hu et al., 2005b; Hu et al., 2003) and, compared the ipsilateral and contralateral cortices for cytosolic oligonucleosome levels and caspase 3 cleavage. When compared to the 3h sham-injured ipsilateral cortices, there was a significant increase in both the ipsilateral (2.087 ± 0.34 ; $p < 0.001$) and contralateral (1.382 ± 0.12 ; $p < 0.05$) cytosolic oligonucleosome values (Fig. 9C) and the catalytically active p17 and p15 cleaved caspase 3 fragments [(ipsilateral, 2.732 ± 0.71 ; $p < 0.001$) (contralateral,

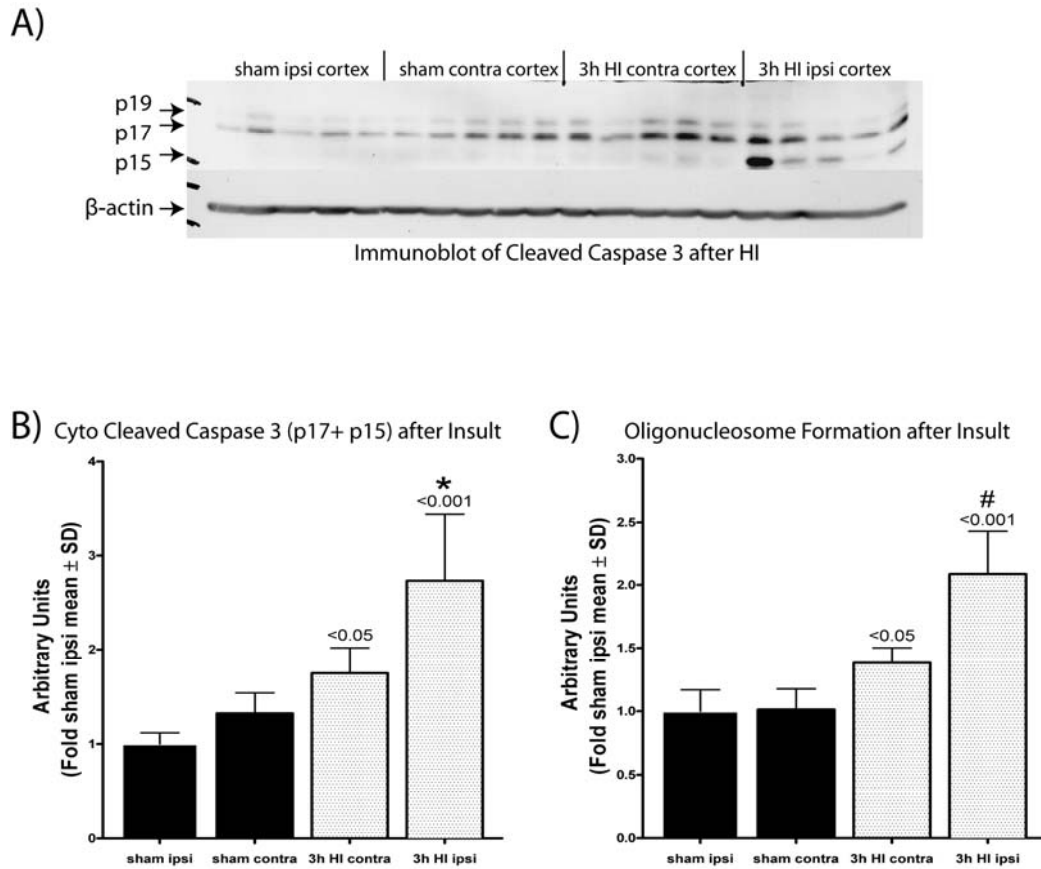


Figure 9. HI induces contralateral cortical injury to a lesser extent than ipsilateral cortical injury.

A) HI increases cytosolic cleaved caspase 3 levels in both the ipsi- and contralateral cortices of 3h post HI-injured animals. Western blot of cytosolic cleaved caspase 3 levels in 3h sham ipsilateral, 3h sham contralateral, 3h post HI contralateral and 3h post HI ipsilateral cortices. β -actin was used as a loading control. B) HI increases cytosolic cleaved caspase 3 levels in both the ipsi- and contralateral cortices of 3h post HI-injured animals [2.732 ± 0.71 ($p < 0.001$) and $1.748 \pm .27$ ($p < 0.05$), respectively, vs. sham (1.000 ± 0.12)]. Densitometric values for cytosolic cleaved caspase 3 (p17 + p15) levels in 3h sham and 3h post HI-injured contralateral and ipsilateral cortices. Data were normalized to β -actin and expressed as fold change of sham value \pm S.D. C) HI increases cytosolic oligonucleosome levels in both the ipsi- and contralateral cortices of 3h post HI-injured animals [2.087 ± 0.34 ($p < 0.001$) and 1.382 ± 0.12 ($p < 0.05$), respectively, vs. sham (1.000 ± 0.17)]. Data are represented as fold change of sham \pm S.D. Numerical value above column bars denotes p-value when compared to sham ipsilateral cortex. *, $p < 0.05$ when compared to 3h post HI contralateral cortex, #, $p < 0.001$ when compared to 3h post HI contralateral cortex.

1.748 \pm .27; $p < 0.05$)] (Fig. 9A, 9B). For both injury markers (cytosolic oligonucleosomes and cleaved caspase 3 fragments), the ipsilateral cortex contained higher levels compared to the contralateral cortex ($p < 0.001$ and $p < 0.05$, respectively) (Fig. 9B, 9C). Based on these findings, we used a separate group of animals for sham-injured ipsilateral cortex measurements throughout our study.

Bax in sham-treated animals is mostly in cytosol

In order to determine the levels of Bax in the cytosol, mitochondria, ER and nucleus after HI, we carried out subcellular fractionation of P7 Wistar rat pup cortices in order to obtain highly-enriched cytosolic, mitochondrial, ER and nuclear fractions. We modified the centrifugation and the supernatant removal steps in a commonly used sucrose fractionation protocol as a means to optimize the conditions for organelle enrichment (Boehning et al., 2003). Using Lamin-B₁, protein disulfide isomerase (PDI), cytochrome c oxidase subunit IV (COXIV) and I κ B- α as respective nuclear, ER, mitochondrial and cytosolic markers in Western blots, we confirmed that the P7 rat pup cortex fractionation protocol used gave highly-enriched nuclear, ER, mitochondrial and cytosolic fractions (Fig. 10A). As I κ B- α has been shown to translocate into the nucleus after cellular perturbations, we also confirmed the level of our cytosolic enrichment using another cytosolic marker, β -tubulin (data not shown).

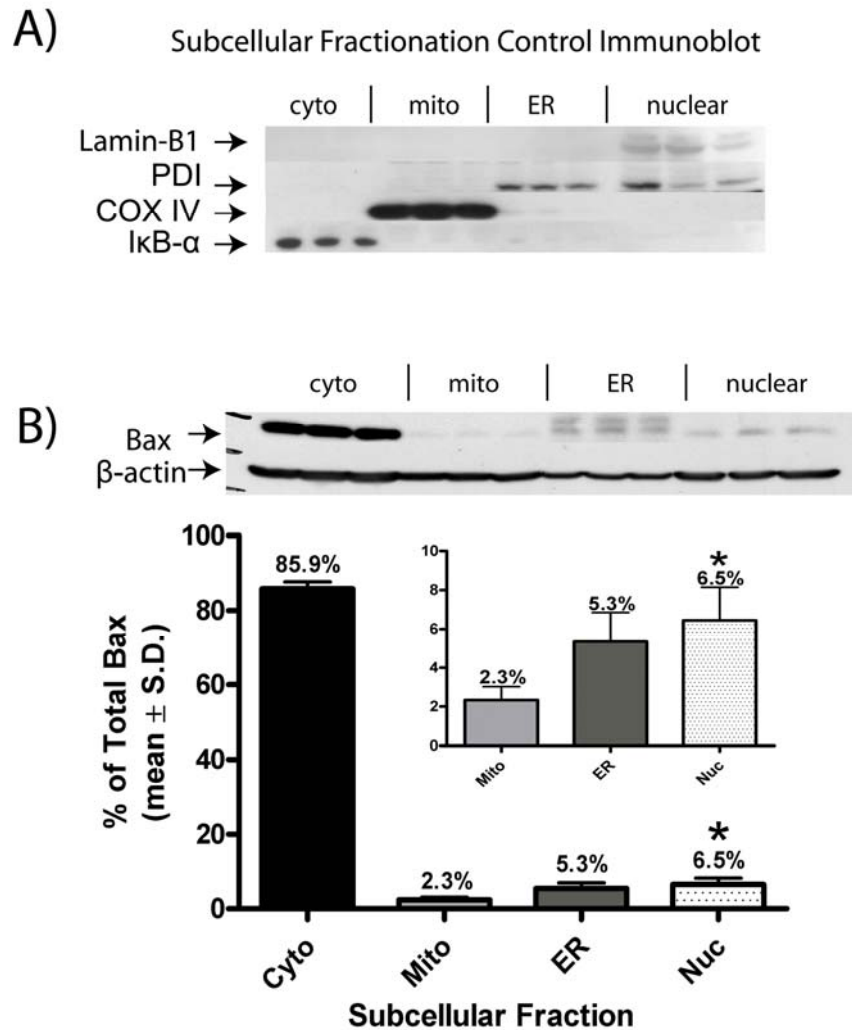


Figure 10. Subcellular enrichment of different organelle fractions illustrates the majority of Bax in sham cortices resides in the cytosol.

A) Fractionation protocol described in Materials and Methods yields highly-enriched nuclear, ER, mitochondrial and cytosolic fractions. Western blots for Lamin-B₁, PDI, COXIV and IκB-α illustrate high enrichment of the nuclear, ER, mitochondrial and ER fractions obtained by using the fractionation protocol described in methods. B) The majority of Bax protein resides within the cytosolic fraction of sham-injured P7 pups. Western blot for Bax distribution amongst the four fractions in sham ipsilateral cortices. Graph represents densitometric values for Bax levels in the four fractions isolated from sham cortices. Graph inset contains an enlargement of the mitochondrial, ER and nuclear Bax column bars. Densitometric data were normalized to β-actin and are represented as percentage of total Bax ± S.D. *, p<0.05 when compared to mitochondrial Bax levels in sham ipsilateral cortices.

In order to determine the distribution of Bax among the four cell fractions in sham animals as a frame of reference, we measured Bax levels in each cell fraction by Western blot analysis. While the major portion of Bax was in the cytosolic fraction ($85.8 \pm 1.8\%$), the remaining Bax was mostly in the nuclear ($6.45 \pm 1.7\%$) and ER ($5.35 \pm 1.5\%$) fractions and a lesser amount in the mitochondrial fraction ($2.34 \pm 0.68\%$; $p < 0.05$ compared to nuclear; Fig. 10B).

HI induces cell death in the ipsilateral cortex via activation of mitochondrial- and ER- mediated cell death

We asked whether HI induces apoptotic cell death in the ipsilateral cortex via activation of mitochondrial and/or ER cell death. We assessed the extent of apoptosis over time by measuring cytosolic oligonucleosome levels and caspase 3 cleavage as measures of mitochondria-dependent cell death and caspase 12 cleavage in the ER fraction as a measure of ER-dependent cell death over time. We also measured mitochondrial apoptosis-inducing factor (AIF) levels indicative of caspase-independent mitochondrial cell death over time. HI increased cytosolic oligonucleosome [(3h, 2.36 ± 0.19 ; $p < 0.05$) (24h, 3.02 ± 0.54 ; $p < 0.05$) (48h, 3.50 ± 0.53 ; $p < 0.05$)] at all times measured (Fig. 11A). HI also increased cytosolic caspase 3 cleavage [(3h, 2.85 ± 0.35 ; $p < 0.001$) (6h, 3.15 ± 0.4 ; $p < 0.001$) (12h, 2.66 ± 0.49 ; $p < 0.01$) (24h, 2.23 ± 0.33 ; $p < 0.05$)] (Fig. 11B). HI also increased caspase 12 cleavage in the ER after 6h (3.25 ± 0.43 ; $p < 0.001$) (Fig. 11C) but decreased mitochondrial AIF levels over time [(6h, 0.694 ± 0.036 ;

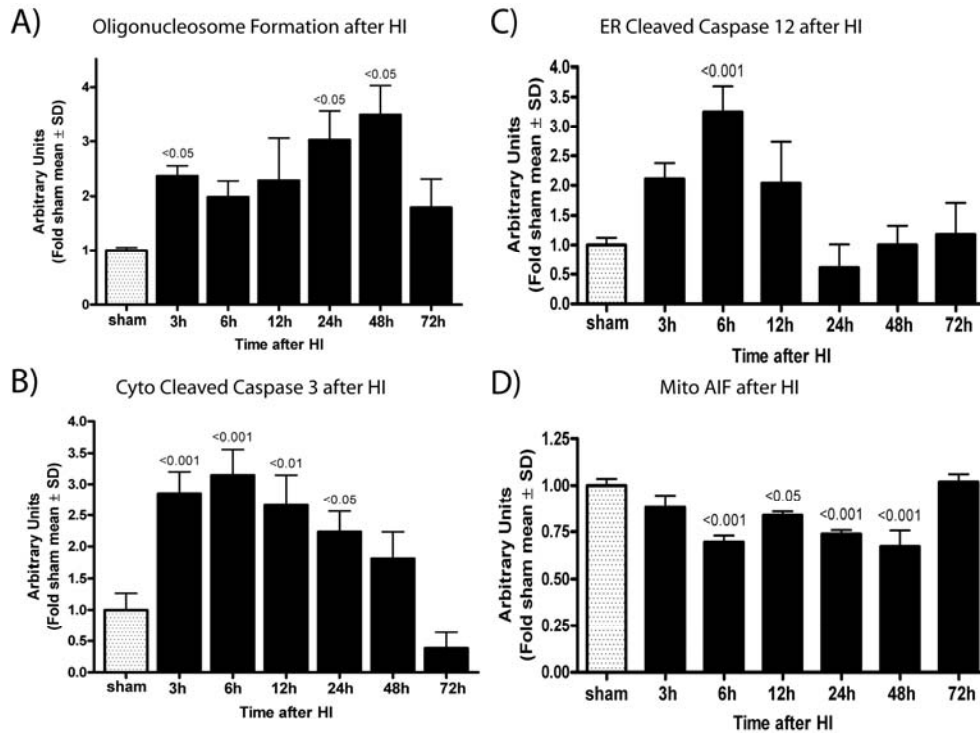


Figure 11. Hypoxic-ischemia (HI) induces cell death in the injured ipsilateral cortex via caspase 3 and caspase12 activation and mitochondrial extrusion of AIF.

A) HI increases cytosolic oligonucleosome levels in the ipsilateral cortex of HI-injured animals reaching significance at 3, 24 and 48h post HI [2.360 ± 0.19 ($p < 0.05$), 3.023 ± 0.54 ($p < 0.05$) and 3.496 ± 0.53 ($p < 0.05$), respectively, vs. sham (1.000 ± 0.05)]. Cytosolic oligonucleosomes levels in sham and HI-injured cortices at various survival times post HI. Data are represented as fold change of sham \pm S.D. B) HI increases cleaved caspase 3 levels in the ipsilateral cortex of 3, 6, 12 and 24h post HI-injured animals [2.851 ± 0.35 ($p < 0.001$), 3.149 ± 0.41 ($p < 0.001$), 2.660 ± 0.49 ($p < 0.01$) and 2.234 ± 0.33 ($p < 0.05$), respectively, vs. sham (1.000 ± 0.2657)]. Densitometric values for cytosolic cleaved caspase 3 (p17 + p15) levels in sham and HI-injured cortices at various survival times post HI. C) HI increases ER cleaved caspase 12 levels in the ipsilateral cortex of 6h post HI-injured animals [3.250 ± 0.43 ($p < 0.001$) vs. sham (1.000 ± 0.12)]. Densitometric values for ER cleaved caspase 12 (p42) levels in sham and HI-injured cortices at various survival times post HI. D) HI decreases mitochondrial apoptosis inducing factor (AIF) levels in the ipsilateral cortex of 6, 12, 24 and 48h post HI-injured animals [0.6938 ± 0.036 ($p < 0.001$), 0.8373 ± 0.022 ($p < 0.05$), 0.7368 ± 0.022 ($p < 0.001$) and 0.6699 ± 0.087 ($p < 0.001$), respectively, vs. sham (1.000 ± 0.04)]. Densitometric values for mitochondrial AIF levels in sham and HI-injured cortices at various survival times post HI. Densitometric data were normalized to β -actin and are represented as fold change of sham \pm S.D. Numerical value above column bars denotes p-value when compared to sham.

p<0.001) (12h, 0.837 ± 0.022 ; p<0.05) (24h, 0.737 ± 0.022 ; p<0.001) (48h, 0.670 ± 0.087 ; p<0.001)] (Fig. 11D).

HI shifts Bax sequentially to the nucleus and then to mitochondria and ER

Having established that HI increased apoptotic cell death in the ipsilateral cortex in part through activation of mitochondrial and ER cell death cascades, we asked if the times of the HI-induced cell death cascades correlated with the HI-induced shifts of Bax to the different organelles. Thus, we did a time course analysis of Bax levels in cytosolic, mitochondrial, ER and nuclear fractions after HI. Cytosolic Bax levels (0.554 ± 0.0042 ; p<0.05) decreased steadily and returned to sham levels 3h after HI (Fig. 12A). Mitochondrial Bax levels increased at 3h (1.99 ± 0.24 ; p<0.001) and 6h (1.71 ± 0.13 ; p<0.01) but returned to sham levels after that and actually were lower than sham levels by 72h after HI (0.415 ± 0.12 ; p<0.05) (Fig. 12B). HI also increased ER Bax levels after 6h [(6h, 2.37 ± 0.094 ; p<0.01) (12h, 2.04 ± 0.10 (p<0.05) (48h, 2.16 ± 0.26 (p<0.01))] (Fig. 12C). Interestingly, there was an HI-induced increase in nuclear Bax levels as early as 0.5h after HI that persisted for at least 3h [(0.5h, 2.54 ± 0.11 ; p<0.05) (1h, 3.86 ± 0.70 ; p<0.001) (2h, 3.54 ± 0.49 ; p<0.001) (3h, 1.72 ± 0.074 ; p<0.05)] (Fig. 12D). Thus, there was an organelle-specific Bax localization time course after HI, consisting of an early, abrupt increase in nuclear Bax levels fraction, followed by a transient increase in mitochondrial Bax and a later steady increase in ER Bax levels. Furthermore, the increases in mitochondrial and ER Bax levels

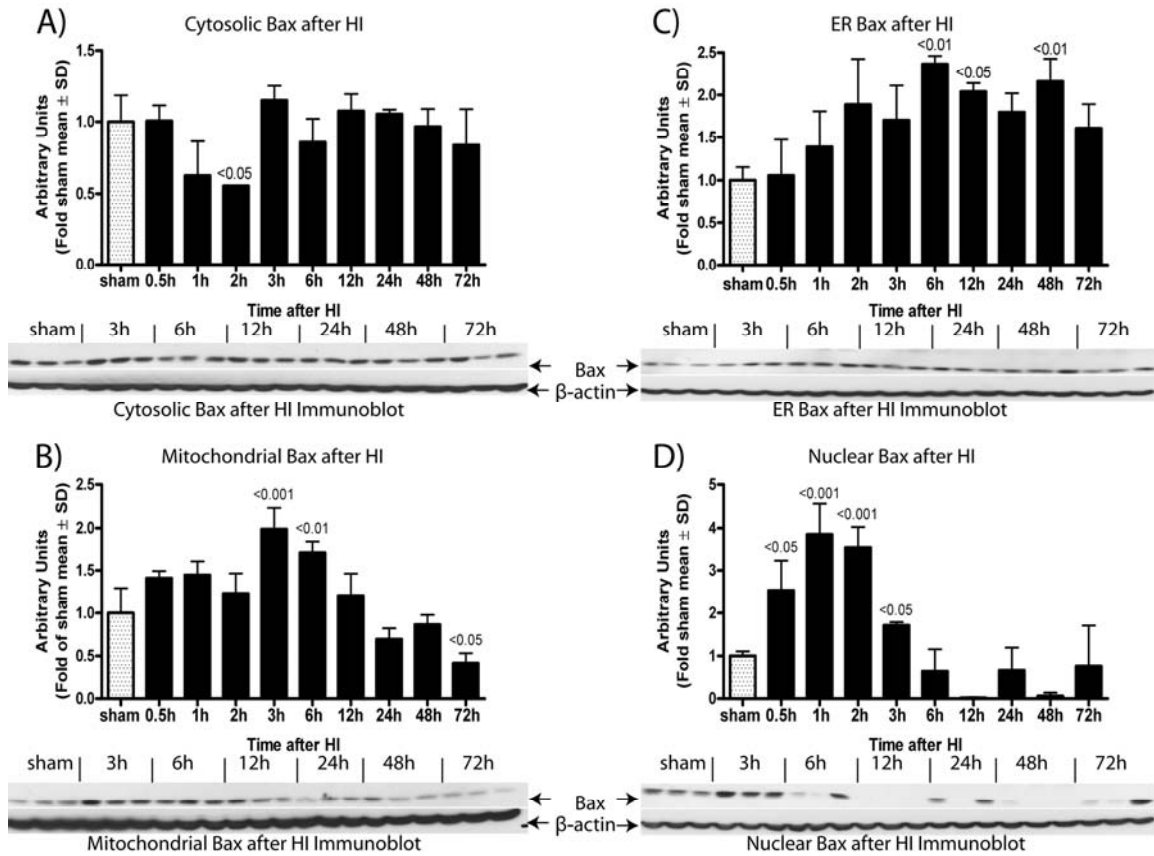


Figure 12. HI shifts Bax to the nucleus followed by Bax redistribution to the mitochondrial and ER.

A) HI decreases cytosolic Bax levels in the ipsilateral cortex of 2h post HI-injured animals [0.5539 ± 0.004 ($p < 0.05$) vs. sham (1.000 ± 0.19)]. Densitometric values for cytosolic Bax levels in sham and HI-injured cortices at various survival times post HI. Below, representative Western blot for cytosolic Bax and β -actin levels at various survival time points after HI. B) HI increases mitochondrial Bax levels in the ipsilateral cortex of 3 and 6h post HI-injured animals [1.988 ± 0.24 ($p < 0.001$) and 1.707 ± 0.13 ($p < 0.01$), respectively, vs. sham (1.000 ± 0.29)] and decreases mitochondrial Bax levels in the ipsilateral cortex of 72h post HI-injured animals [0.4146 ± 0.118 ($p < 0.05$)]. Densitometric values for mitochondrial Bax levels in sham and HI-injured cortices at various survival times post HI. Below, representative Western blot for mitochondrial Bax and β -actin levels at various survival time points after HI. C) HI increases ER Bax levels in the ipsilateral cortex of 6, 12 and 48h post HI-injured animals [2.365 ± 0.09 ($p < 0.01$), 2.041 ± 0.10 ($p < 0.05$) and 2.162 ± 0.26 ($p < 0.01$), respectively, vs. sham (1.000 ± 0.15)]. Densitometric values for ER Bax levels in sham and HI-injured cortices at various survival times post HI. Below, representative Western blot for ER Bax and β -actin levels at various survival time points after HI. D) HI increases nuclear Bax levels in

the ipsilateral cortex of 0.5, 1, 2 and 3h post HI-injured animals [2.536 ± 0.11 ($p < 0.05$), 3.857 ± 0.70 ($p < 0.001$), 3.536 ± 0.49 ($p < 0.001$) and 1.716 ± 0.074 ($p < 0.05$), respectively, vs. sham (1.000 ± 0.11)]. Densitometric values for nuclear Bax levels in sham and HI-injured cortices at various survival times post HI. Below, representative Western blot for nuclear Bax and β -actin levels at various survival time points after HI. Densitometric data were normalized to β -actin and are represented as fold change of sham \pm S.D. Numerical value above column bars denotes p-value when compared to sham.

correlated temporally with the initiation of mitochondrial and ER cell death cascades.

HI-induced mitochondrial Bax

To confirm the HI-induced increases in mitochondrial Bax levels determined by Western blot analyses of mitochondrial fractions, we performed confocal immunofluorescence analysis on sham and HI-treated cortices using ATP-synthase β as a mitochondrial marker. There were maximal levels of Bax in mitochondria as assessed by colocalization of Bax with ATP-synthase β at 3 and 6h after HI in the parietal cortex (Fig. 13A-D; 14C).

In order to quantitate the extent of colocalization, we conducted blind cell counts of randomly selected confocal images (Fig. 14A, B) from within the selected parietal cortical region (Fig. 14C) for both sham- and HI-treated animals at 3h for colocalization of Bax and ATP-synthase β . There were significantly more cells labeled with both Bax and ATP-synthase β 3h after HI ($23.9 \pm 4.5\%$; $p = 0.001$) in the parietal cortex compared to sham-treated parietal, in agreement with the mitochondrial fraction Western blot data (Fig. 14C).

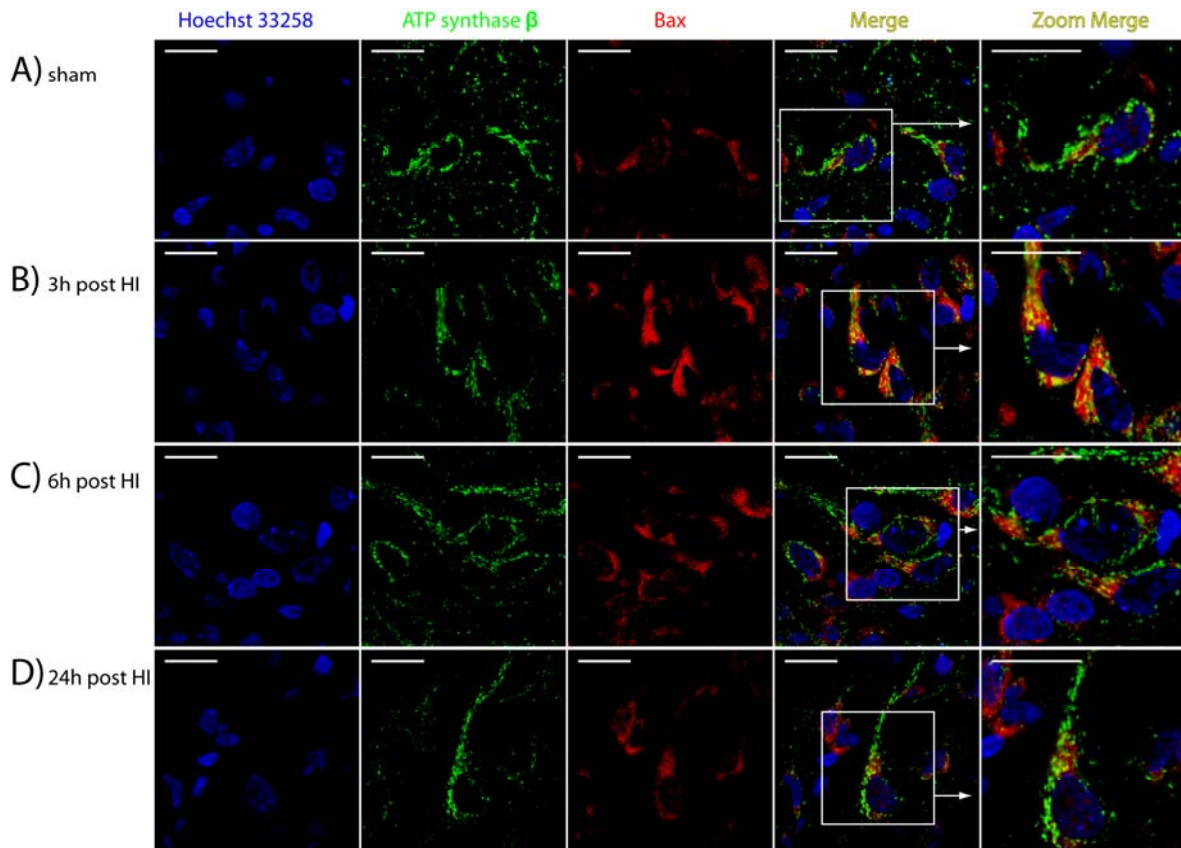


Figure 13. HI induces maximal colocalization of Bax with mitochondria at 3h post HI.

60X (2.6X zoom) confocal florescent images from sham and HI-injured ipsilateral cortices at survival time points post HI, which showed peak Bax levels in the isolated fractions via Western blot analysis. Zoom Merge is a digital zoom of the boxed portion of the Merge frame. Hoechst 33258 = nuclear fluorescent dye, ATP-synthase β = mitochondrial marker. A) Sham ipsilateral cortices exhibit little Bax colocalization with mitochondrial ATP-synthase β . Representative 60X (2.6X zoom) confocal florescent micrograph from a sham ipsilateral cortex. B) 3h post HI-injured ipsilateral cortices exhibit maximal Bax colocalization with mitochondrial ATP-synthase β . Representative 60X (2.6X zoom) confocal florescent micrograph from a 3h post HI ipsilateral cortex. C) 6h post HI-injured ipsilateral cortices exhibit minor Bax colocalization with mitochondrial ATP-synthase β . Representative 60X (2.6X zoom) confocal florescent micrograph from a 6h post HI ipsilateral cortex. D) 24h post-HI injured ipsilateral cortices exhibit little Bax colocalization with mitochondrial ATP-synthase β . Representative 60X (2.6X zoom) confocal florescent micrograph from a 24h post HI ipsilateral cortex. Scales bars = 20 μ m.

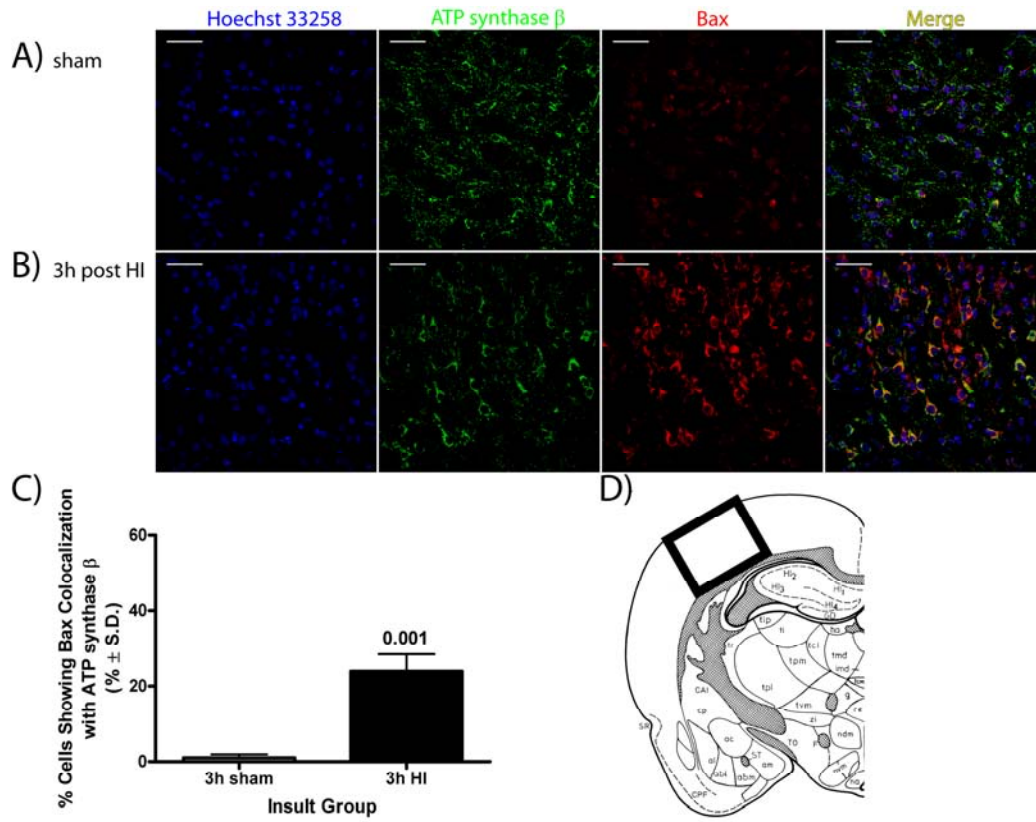


Figure 14. When compared to sham, more cells at 3h post HI show Bax colocalization with the mitochondria.

40X confocal florescent images from sham and HI-injured ipsilateral cortices at survival time points post HI, which showed peak Bax levels in the isolated fractions via Western blot analysis. Hoechst 33258 = nuclear fluorescent dye, ATP-synthase β = mitochondrial marker. A) Sham ipsilateral cortices contain few cells possessing Bax colocalization with mitochondrial ATP-synthase β . Representative 40X confocal florescent micrograph of a region of interest (ROI) in a sham ipsilateral cortex. B) 3h post HI-injured ipsilateral cortices contain more cells possessing Bax colocalization with mitochondrial ATP-synthase β when compared to sham ipsilateral cortices. Representative 40X confocal florescent micrograph of a region of interest (ROI) in a 3h post HI ipsilateral cortex. C) 3h post HI-injured ipsilateral cortices contain significantly more cells possessing Bax colocalization with mitochondrial ATP-synthase β when compared to sham ipsilateral cortices [$23.93 \pm 4.5\%$ ($p=0.001$) vs. sham ($1.026 \pm 0.88\%$)]. Blinded cell counts of representative ROIs from sham and HI-injured ipsilateral cortices at 3h post HI. Values represent percentage of cells demonstrating colocalization of Bax with the mitochondrial marker, ATP-synthase β . Data are presented as mean percentage of cells expressing colocalization \pm S.D. D) Depiction of the region of the ipsilateral cortex from where the all ROIs were selected. Scale bars = 50 μ m

HI-induced ER Bax

To confirm the HI-induced increases in ER Bax levels determined by Western blot analyses of ER fractions, we performed confocal immunofluorescence analysis on sham and HI-treated cortices using protein disulfide isomerase (PDI) as an ER marker. There were maximal levels of Bax in ER as assessed by colocalization of Bax with PDI at 6h after HI in the parietal cortex (Fig. 15A-D; 16C).

In order to quantitate the extent of colocalization, we conducted blind cell counts of randomly selected confocal images (Fig. 16A, B) from within the selected parietal cortical region (Fig. 16C) for both sham- and HI-treated animals at 6h for colocalization of Bax and PDI. There were significantly more cells labeled with both Bax and PDI 6h after HI ($39.9 \pm 8.5\%$; $p=0.024$) in the parietal cortex compared to sham-treated parietal, in agreement with the ER fraction western blot data (Fig. 16B).

HI induces Bax translocation into nuclei, coincident with maximal nuclear p53 phosphorylation

To our knowledge, this is the first report to show an increase in nuclear Bax levels using the Rice-Vannucci model of neonatal HI. In order to confirm the observation of HI-induced increases in Bax in nuclear fractions by Western blot assays, we performed multiple z-series confocal immunofluorescence analyses on sham and HI-injured cortices for both Bax and the nuclear stain, Hoechst

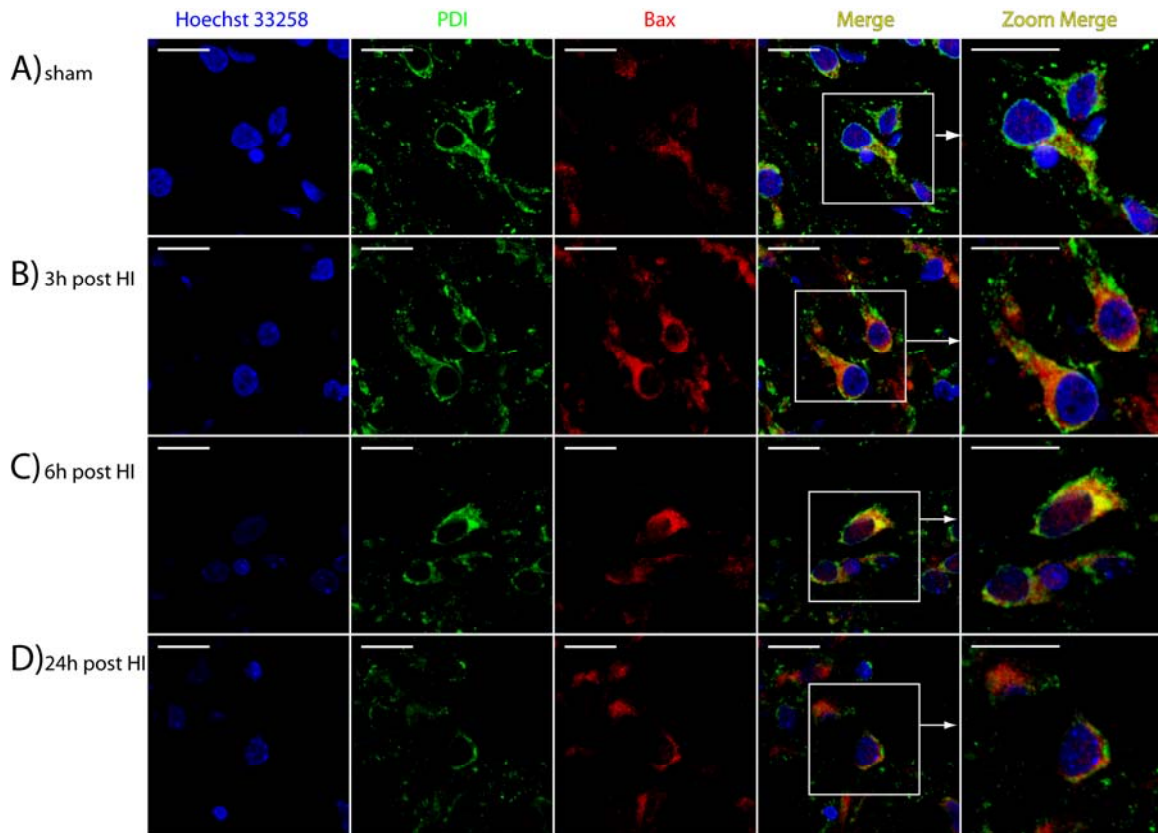


Figure 15. HI induces maximal colocalization of Bax with ER at 6h post HI.

60X (2.6X zoom) confocal florescent images from sham and HI-injured ipsilateral cortices at survival time points post HI, which showed peak Bax levels in the isolated fractions via Western blot analysis. Zoom Merge is a digital zoom of the boxed portion of the Merge frame. Hoechst 33258 = nuclear fluorescent dye, protein disulfide isomerase (PDI) = ER marker. A) Sham ipsilateral cortices exhibit little Bax colocalization with ER PDI. Representative 60X (2.6X zoom) confocal florescent micrograph from a sham ipsilateral cortex. B) 3h post HI-injured ipsilateral cortices exhibit minor Bax colocalization with ER PDI. Representative 60X (2.6X zoom) confocal florescent micrograph from a 3h post HI ipsilateral cortex. C) 6h post HI-injured ipsilateral cortices exhibit maximal Bax colocalization with ER PDI. Representative 60X (2.6X zoom) confocal florescent micrograph from a 6h post HI ipsilateral cortex. D) 24h post HI-injured ipsilateral cortices exhibit little Bax colocalization with ER PDI. Representative 60X (2.6X zoom) confocal florescent micrograph from a 24h post HI ipsilateral cortex. Scales bars = 20µm.

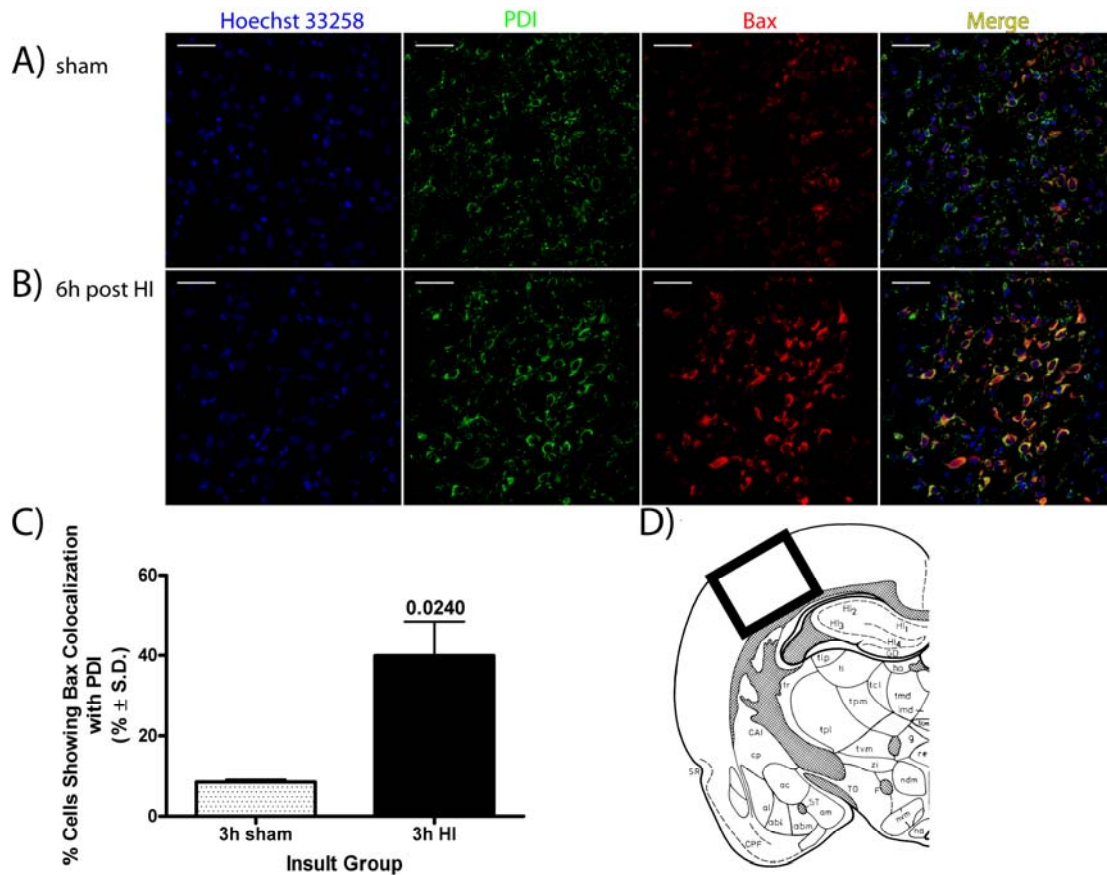


Figure 16. When compared to sham, more cells at 6h post HI show Bax colocalization with the ER.

40X confocal florescent images from sham and HI-injured ipsilateral cortices at survival time points post HI, which showed peak Bax levels in the isolated fractions via Western blot analysis. Hoechst 33258 = nuclear fluorescent dye, protein disulfide isomerase (PDI) = ER marker. A) Sham ipsilateral cortices contain few cells possessing Bax colocalization with ER PDI. Representative 40X confocal florescent micrograph of a region of interest (ROI) in a sham ipsilateral cortex. B) 6h post HI-injured ipsilateral cortices contain more cells possessing Bax colocalization with ER PDI when compared to sham ipsilateral cortices. Representative 40X confocal florescent micrograph of a region of interest (ROI) in a 6h post HI ipsilateral cortex. C) 6h post HI-injured ipsilateral cortices contain significantly more cells possessing Bax colocalization with ER PDI when compared to sham ipsilateral cortices [$39.93 \pm 8.5\%$ ($p=0.024$) vs. sham ($8.591 \pm 0.60\%$)]. Blinded cell counts of representative ROIs from sham and HI-injured ipsilateral cortices at 6h post HI. Values represent percentage of cells demonstrating colocalization of Bax with the ER marker, PDI. Data are presented as mean percentage of cells expressing colocalization \pm S.D. D) Depiction of the region of the ipsilateral cortex from where the all ROIs were selected. Scale bars = $50\mu\text{m}$.

33258. There was maximal Bax colocalization with Hoechst 33258 1h after HI (Fig. 17A). In order to determine if the colocalized nuclear Bax was intranuclear or perinuclear, i.e. associated with the nuclear envelope, we performed LineProfile analyses (see Methods) to determine if increasing and decreasing peaks of Bax fluorescence were present within the Hoechst 33258-defined nuclear boundaries moving through the z-series of 60X ROI images. There were peaks of high intensity Bax fluorescence within the Hoechst 33258-defined nuclear boundaries present in the ipsilateral cortex of 1h post HI-injured pups (Fig. 17B). In order to quantify this finding, we calculated the intranuclear Bax fluorescence average for cells within the parietal cortex at every step of the z-series. There was a significantly increased intranuclear Bax fluorescence intensity in the ipsilateral cortex 1h after HI (1.75 ± 0.50 ; $p=0.031$) (Fig. 17C), consistent with the Western blot data and confirming that HI triggers intranuclear Bax translocation.

As with ER- and mitochondria-mediated cell death, we hypothesized that HI-induced increases in nuclear Bax would correlate with the activation of nuclear cell death signaling cascades. To test this hypothesis, we measured nuclear phospho-p53 (Ser15) levels after HI by Western blot analysis, as phosphorylation of p53 at serine 15 activates p53-mediated pro-apoptotic transcription. There was a significant HI-induced increase in nuclear phospho-p53 (Ser15) levels in the ipsilateral cortices of the HI-treated pups after 3h (1.94 ± 0.25 ; $p<0.05$) (Fig. 17D). Thus, as was the case for the mitochondria and ER,

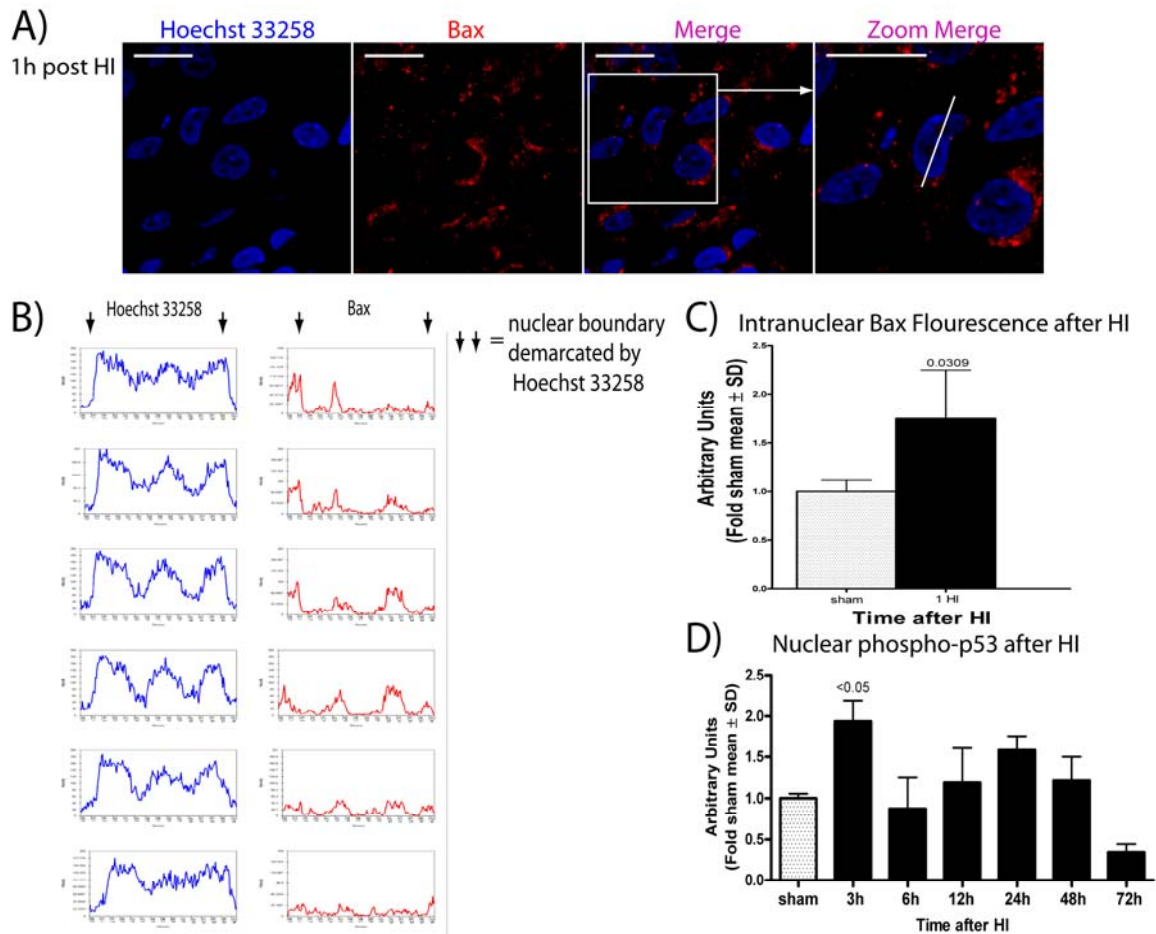


Figure 17. HI induces Bax translocation into nuclei, coincident with maximal nuclear p53 phosphorylation.

A) 1h post HI-injured ipsilateral cortices contain cells possessing intranuclear Bax colocalization with the nuclear stain, Hoechst 33258. Representative 60X (2.6X zoom) confocal fluorescent micrograph from a 1h post HI ipsilateral cortex. Zoom Merge is a digital zoom of the boxed portion of the Merge frame. Hoechst 33258 = nuclear fluorescent dye. Line in the Zoom Merge frame represents the location of the hemisecting line used in B) for LineProfile analysis of the fluorescence pixel intensity of Bax and Hoechst 33258. Scale bars = 20µm. B) HI induces increasing and decreasing peaks of Bax fluorescence within the Hoechst 33258-defined nuclear boundary. Representative fluorescence pixel intensity (FPI) data gathered using the LineProfile analysis (see Materials and Methods) to determine the presence of intranuclear Bax in cells of 1h post HI ipsilateral cortices. For each 0.7µm step (top-to-bottom), a FPI plot for Hoechst 33258 (left) and a FPI plot for Bax (right) was gathered using the same one pixel-diameter hemisecting line across a nucleus. On the xy graph of FPI data generated, the abscissa is the pixel location along the hemisecting line for which the ordinate

contains the fluorescence intensity at the pixel. Increasing and decreasing peaks of fluorescence intensity within the Hoechst 33258-defined nuclear boundary were considered evidence for the presence of intranuclear Bax. C) At 1h post insult, HI increases intranuclear Bax fluorescence [1.748 ± 0.50 ($p=0.0309$) vs. sham (1.000 ± 0.12)]. Average intranuclear Bax fluorescence intensity quantified as described in Methods. Data are represented as fold change of average sham intranuclear Bax fluorescence \pm S.D. D) HI increases nuclear phospho-p53 (Ser15) levels in the ipsilateral cortex of 3h post HI-injured animals [1.937 ± 0.25 ($p<0.05$) vs. sham (1.000 ± 0.06)]. Densitometric values for nuclear phospho-p53 (Ser15) levels in sham and HI-injured cortices at various survival times post HI. Densitometric data were normalized to β -actin and are represented as fold change of sham \pm S.D. Numerical value above column bars denotes p-value when compared to sham.

nuclear Bax localization correlates with an increase in nuclear cell death signaling.

Discussion

Bax organelle occupancy coordinates cell death cascades after HI

We used the Rice-Vannucci neonatal HI model to demonstrate, for the first time, shifts in cortical Bax organelle occupancy, with Bax localizing first to the nucleus, as early as 30 minutes after HI, then to the mitochondria and, finally, to the ER (Fig. 12-17). Together with the appearance of Bax at the different organelles, there were increases in each organelle's cognate cell death cascade (Fig. 11). This is the first evidence that Bax acts in a sequential manner in the coordination of the nuclear, mitochondrial and ER cell death signaling cascades in the cortex after HI.

In agreement with previous reports (Hu et al., 2005b; Hu et al., 2003; Martin et al., 2005; Nakajima et al., 2000), we observed a significant

increase in cortical HI-induced apoptosis, as cytosolic oligonucleosome levels were increased at all time points. In addition, there was a significant increase in mitochondrial Bax levels correlating with the cleavage of caspase 3 (Fig. 11, 12). Interestingly, the mitochondrial apoptotic signaling pathway cannot account for the increased oligonucleosome cytosolic presence at later time points, suggesting that other cell death mechanisms were also involved, i.e. caspase-independent mechanisms. As cleaved-caspase 3 levels decreased, we observed mitochondrial extrusion of AIF, a DNase capable of large scale DNA fragmentation, concurrent with the later increases in cytosolic oligonucleosome levels (Fig. 11). Therefore, AIF could account for the late increases in cytosolic oligonucleosomes, as both parameters returned to sham values by 72h post HI.

Gajkowska et al. (2004) have reported chemotherapeutic treatment of MCF-7 cells shifts Bcl-2 family proteins to locales outside of their canonical mitochondrial site. Also, Scorrano et al. (2003) have shown that targeting anti-apoptotic Bcl-2 to the ER reduces resting ER Ca^{2+} levels, such that adding ER stressors decreases ER Ca^{2+} mobilization and cell death, while ER targeting of Bax had the opposite effect, increasing a cell death, which could not be inhibited by apoptotic antagonists (Oakes et al., 2005; Oakes et al., 2003; Scorrano et al., 2003).

Supporting the evidence for Bax-mediated ER cell death signaling, we observed a delayed, relative to the nucleus and mitochondria, increase in ER Bax levels beginning 6h post HI (Fig. 12), and, in parallel with increased

cleavage of ER caspase 12 (Fig. 11). Consistent with these findings, 100% O₂ promoted earlier HI-induced increases (3h post HI) in ER Bax levels and calpain activity, a Ca²⁺-activated protease linked to ER cell death signaling (Fig. 33, 34).

In agreement with reports suggesting crosstalk between ER and caspase-independent mitochondrial cell death signaling cascades (Polster et al., 2005; Sanges and Marigo, 2006), we observed, after HI, mitochondrial extrusion of AIF concurrent with observed increases in caspase 12 cleavage (Fig. 11). A recent report states calpain activation occurs prior to mitochondrial Bax translocation suggesting Bax activation is downstream of calpain activation (Moubarak et al., 2007). However, this report did not determine whether Bax localizes to the ER concurrently with calpain activation. In addition, whether mitochondrial-mediated cell death precedes its ER-mediated counterpart or the reverse is likely to depend on the specific cell death stimulus given and sensitivity to the stimulus (Chinopoulos and Zam-Vizi, 2006; Hong et al., 2004; Lin and Beal, 2006; Polster et al., 2005; Rao et al., 2002; Sanges and Marigo, 2006; Yu et al., 2002).

Cancer literature has reported nuclear Bax localization (Godlewski et al., 2001; Mandal et al., 1998; Nishita et al., 1998; Salah-eldin et al., 2000) and suggest a role for Bax in p53 nuclear activity (Raffo et al., 2000). In addition, Bax overexpression in SY5Y cells localizes full-length Bax to both the nuclear envelope and the inside of the nucleus, with N-terminal Bax cleavage locking it in the nucleus (Karlsson et al., 2007). Furthermore, porcine models of global fetal hypoxia suggest nuclear envelope-associated Bax regulates nuclear Ca²⁺

(Ashraf et al., 2001), hinting at Bax regulation of Ca^{2+} homeostasis in all organelles in response to oxidative stress.

Using the Rice-Vannucci HI model, we observed Bax localization to the perinuclear envelope and intra-nuclear space prior to shifts to the ER and mitochondria (Fig. 12, 17). Furthermore, this nuclear Bax shift correlated with the serine 15 phosphorylation of nuclear p53, an activating event (Fig. 17), agreeing with cancer research linking Bax to p53. While current experiments are underway to further characterize the nuclear role of Bax in this neonatal HI model, in a P5 cortical neuronal culture model, we, also, observed early increases in nuclear Bax after exposure to both apoptotic and necrotic stimuli, suggesting nuclear Bax localization as a general early cell death event across many paradigms (Gill et al., unpublished observations). Interestingly, unlike previous reports, we did not observe the presence of cleaved Bax in our *in vivo* or *in vitro* experiments. However, the Bax antibody used for the Western blots in these studies was raised against the N-terminal sequence, the portion of Bax reported to be cleaved (Karlsson et al., 2007). Therefore, it remains to be resolved if nuclear Bax cleavage occurs *in vivo* after HI.

Conclusion

In conclusion, we report here for the first time *in vivo*, a distinct subcellular time course for Bax in the HI-injured cortex, with Bax localizing first to the nucleus as early as 30 minutes after HI, then to mitochondria and, finally, to the

ER. Furthermore, we report that Bax localization to these organelles coordinates with activation of each organelle's cognate cell death cascade, suggesting a new role for Bax, thus providing the first evidence in support of the proposed role for Bax in coordinating the cell death signaling at multiple subcellular organelles.

CHAPTER III

Differential dose effects of rotenone on Bax subcellular localization and cell death phenotype

Recently, we have demonstrated neonatal hypoxic-ischemic (HI) insult induces Bax localization to the nucleus, mitochondria and ER, where it coordinates the activation of cognate cell death signaling cascades. In addition, we demonstrated, when compared to untreated HI-injured rat pups, 100% O₂ intervention increased HI-induced ER Bax localization, ER-mediated cell death signaling and injury and inflammation through increased necrosis. In this report, we sought to further validate our previous data's findings and other reports, which link ER cell death signaling and necrotic-like cell death, by demonstrating a necrotic-like stimulus would promote increased ER Bax localization and increased ER cell death signaling, while an apoptotic stimulus would promote increased mitochondrial Bax localization and increased mitochondrial cell death signaling.

Using P5 primary cortical neurons and rotenone, we used a high (100 μ M) and a low (25 μ M) rotenone dose, as respective necrotic-like and apoptotic stimuli, and measured their effect on Bax localization and subsequent activation of ER / mitochondrial cell death signaling. With the apoptotic stimulus, we observed early increased nuclear Bax followed by later mitochondrial Bax localization, which increased caspase-mediated cleavage of α -fodrin. With the

necrotic-like stimulus, we observed early increased nuclear Bax followed by later ER Bax localization, which increased calpain-mediated cleavage of α -fodrin. Using the immunosuppressive and neuroprotective FK506, we found 1h FK506 pretreatment effectively delayed high and low dose rotenone-mediated Bax localization shifts and subsequent cell death signaling. These results validate reports linking ER Bax, ER cell death signaling and necrotic-like cell death and suggest a common, FK506-inhibited Bax activation step.

Introduction

Recently, we have demonstrated neonatal hypoxic-ischemic (HI) insult induces Bax localization to the nucleus, mitochondria and ER, where it coordinates the activation of cognate cell death signaling cascades (Gill et al. unpublished observations). In addition, we demonstrated, when compared to untreated HI-injured rat pups, 100% O₂ intervention increased HI-induced ER Bax localization, ER-mediated cell death signaling and injury and inflammation through increased necrosis (Gill et al. unpublished observations). Multiple reports have linked Bax activation and subsequent mitochondrial translocation with activation of apoptotic cell death signaling (D'Alessio et al., 2005; Dejean et al., 2005; Ferrer and Planas, 2003). Not until recently, though, have reports been published, which link Bax to ER-associated cell death signaling (Oakes et al., 2003; Scorrano et al., 2003). Despite these recent publications, evidence

linking ER Bax localization, ER cell death signaling and necrotic-like cell death remains elusive.

Apoptosis is a programmed cell death defined by its characteristic, nuclear and cell morphological changes (Edinger and Thompson, 2004). Classically, the Bcl-2 family has been described as regulators of apoptotic cell death (Edinger and Thompson, 2004), with mitochondrial Bax translocation as the trigger to cellular demise (Edinger and Thompson, 2004). Necrosis, on the other hand has been classically defined as a passive, unregulated event commonly characterized in a negative manner, i.e. not possessing apoptotic characteristics (Edinger and Thompson, 2004). However, recent reports have shown, like apoptosis, there exists programmed necrosis, which could play a significant role in tissue-specific development (Festjens et al., 2006; Proskuryakov et al., 2003).

These recent reports on programmed necrosis have appeared concurrently with reports illustrating cell death phenotypes possessing apoptotic and necrotic phenotypic markers, termed aponecrotic and necroptotic (Formigli et al., 2000; Pretorius and Bornman, 2005; Yakovlev and Faden, 2004). Moreover, initial reports have linked insult models of high oxidative stress and energy depletion with more necrotic-like cell death and insult models, which produce moderate oxidative stress and energy depletion, with more apoptotic-like cell death (Formigli et al., 2000; Formigli et al., 2002). Taken together with programmed necrosis, these recent findings have sparked a surge in neurodegeneration and cancer research attempting to uncover common

mechanisms involved in models of programmed necrosis, and the consequences they have on cell death phenotype (Formigli et al., 2000; Formigli et al., 2002). In concordance with this novel avenue in neurodegenerative research, this report focuses on the downstream consequences, regarding Bax subcellular localization, cognate organelle cell death signaling and cell death phenotype, resulting from necrotic and apoptotic stimuli.

To address this question we treated P5 primary cortical neurons with high (100 μ M) and low (25 μ M) doses of rotenone, as respective necrotic-like and apoptotic stimuli. We observed the apoptotic stimulus increased mitochondrial Bax localization and caspase-mediated cleavage of α -fodrin, while the necrotic-like stimulus increased ER Bax localization and calpain-mediated cleavage of α -fodrin. Interestingly, both treatments induced early nuclear Bax localization. Furthermore, we found 1h pretreatment with immunosuppressive and neuroprotective FK506 delayed high and low dose rotenone-mediated Bax relocalization and cell death signaling. This report is the first to link ER Bax, ER cell death signaling and necrotic-like cell death and to suggest a common, FK506-inhibited Bax activation step.

Materials and Methods

Materials. All chemicals were purchased from Sigma-Aldrich (Saint Louis, MO). N, N-bisacrylamide was purchased from Bio-rad Laboratories (Hercules, CA).

Animal Care. E15 pregnant Wistar rat dams (Charles Rivers Laboratories, Wilmington, MA) were housed upon arrival in 12h light-dark cycle with access to food and water *ad libitum*. The day of birth was designated P0. On P5, the day of primary neuron isolation, pups were removed from the dam and kept housed on an electrical warming pad surgery.

Isolation and culture maintenance of P5 primary cortical neurons. Isolation of primary cortical neurons was carried out following Brewer et al. (1997) with modifications in the isolation method. Prior to extraction of brain tissue, papain (40U / mL) was partially activated by incubation at 37°C for 30min in Hibernate A medium (BrainBits, Carbondale, IL) containing 2% **B**-27, 1% penicillin-streptomycin-neomycin (PSN), 50g / mL **g**entamycin and 0.5mM **L**-glutamine (HA-BPGL) (Invitrogen, Carlsbad, CA). After activation, the papain solution was filtered (0.22µm) and pre-sterilized DnaseI (20U / mL) was added. The enzyme solution was stored at 4°C until use, but no longer than 1.5h.

On P5, Wistar rat pups were deeply anesthetized in an isoflurane-filled gas chamber and then decapitated. Quickly, meninges were removed and cortices from the anterior tuber cinereum to anterior of the occipital cortex (encompassing the parietal cortex) were placed in a glass Petri dish in a laminar flow hood (from here sterile technique should be strictly adhered). Cortices were chopped in 1-2mm blocks and then placed in HA-BPGL medium (2 mL / 2 cortices). Then, minced cortices were enzymatically dissociated in an orbitally,

rotating (170rpm) incubator for 30 min at 30°C in the previously made papain / DNaseI solution.

After enzymatic dissociation, the enzyme solution was aspirated and the tissue was incubated for 5min in warmed (30°C) HA-BPGL (4mL). Next, the cortices were triturated 10X and allowed to sediment for 2min. After the tissue has settled, the supernatant was removed and carefully layered Nycoprep 1.077A / HA-BPGL step gradient (1ml each of 22.1%, 29.4%, 36.3% and 51.4% Nycoprep 1.077A) (Accurate Chemical, Westbury, NY). This trituration process was repeated twice more. The layered, cell containing supernatant was centrifuged at 800g for 15min at room temperature, which separates neurons, astrocytes, oligodendroglia and microglia based on cell density. The neuron containing fraction was removed and resuspended in 6mL warmed, HA-BPGL to dilute the Nycoprep 1.077A. Again, the neuron containing solution was centrifuged at 200g for 1min at room temperature. The neuron-containing pellet was resuspended in Neurobasal-A medium (Invitrogen, Carlsbad, CA) containing the same proportions of BPGL (NA-BPGL) + 5ng / mL basic fibroblast growth factor (bFGF). Neurons were plated at 3.2×10^4 neurons / cm² on poly-D-lysine / β -laminin coated tissue culture plates and incubated for 1.5h at 37°C in 5% CO₂. After incubation, the medium was exchanged for fresh FGF-containing NA-BPGL to remove non-attached cells and cultured at 37°C in 5% CO₂. Day of isolation was deemed 0 days *in vitro* (0DIV).

On 3DIV, fresh media was applied to the neuronal cultures. On 4DIV, 3 μ M cytosine arabinofuranoside (AraC) was added for 48h to kill contaminating proliferating glial cells. On 7DIV, AraC-containing medium was removed and fresh media was applied to culture. Observed at 8DIV, this isolation and culture maintenance protocol yielded a very low glial-contaminated culture (~8-10% GFAP+ cells on 8DIV) (Fig. 18A-C).

Rotenone experimental protocols. All primary neuronal culture experiments were carried out at 8DIV. Rotenone and FK506 were made into stock solutions with DMSO and stored at room temperature and -20°C, respectively. Control medium used for 6 and 16h incubations contained 0.66% DMSO, as that was the maximal concentration of DMSO added in any combination of FK506 and rotenone. Neuronal cultures were washed once with experimental medium and were incubated for various times, with either 25 μ M (apoptotic stimulus) or 100 μ M (necrotic-like) rotenone. Unless specified, control 0h cultures were washed once with experimental medium and, then, immediately processed. For experiments involving, confocal microscopy or western blot analyses, we used an n=3 (or 4 for FK506 experiments). For ELISA experiments, we used an n=4 run in triplicate wells.

Cytosolic fractionation of P5 primary cortical neurons. At the designated rotenone insult duration, neurons were washed once with ice cold PBS. Then, primary neurons were suspended in ice-cold fractionation buffer (FB) (in mM: 10 HEPES, 0.5 EGTA, 2 EDTA, 10 DTT, 250 sucrose) containing 1 Roche

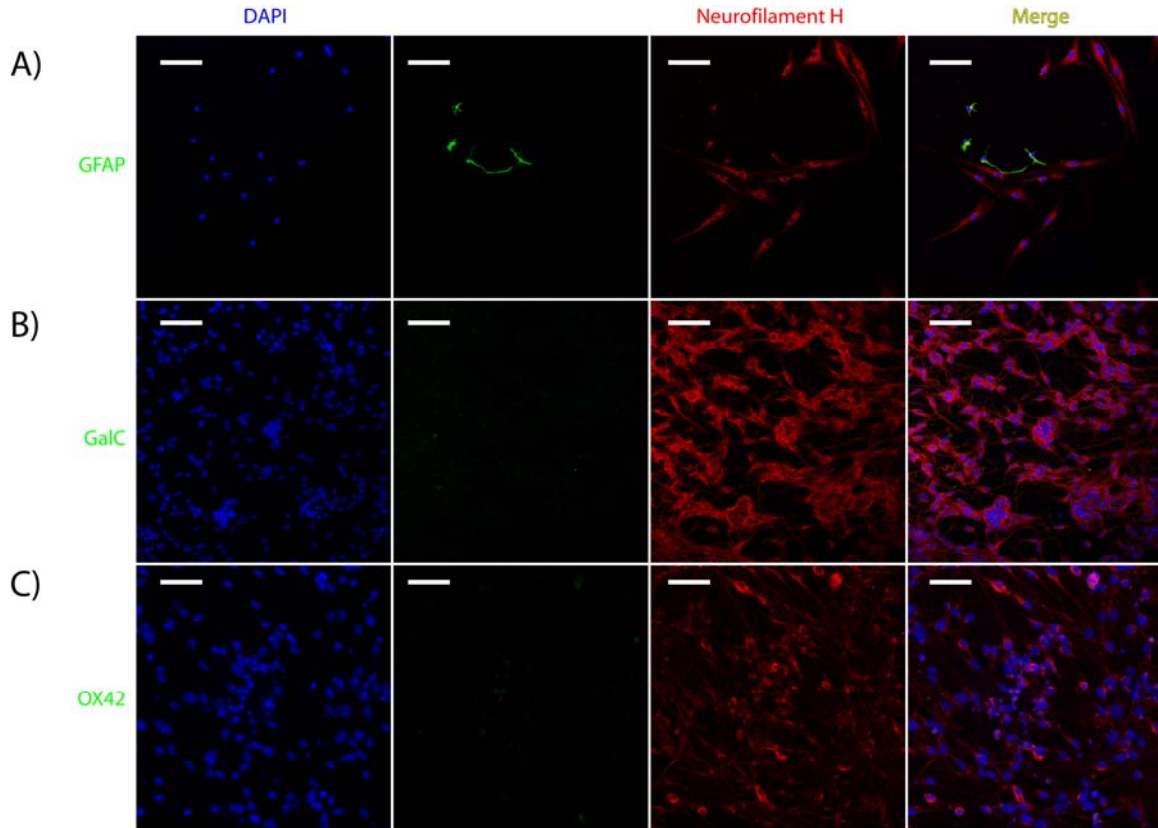


Figure 18. Assessment of cellular homogeneity of primary P5 Wistar rat cortical cultures illustrates minimal non-neuronal contamination (~8-10% GFAP+ cells).

A) Isolation protocol enriches diminishes GFAP+ contaminating cells to ~8-10%. Representative 20X confocal florescent micrograph of a region of interest (ROI) within primary neuronal cultures. B) Isolation protocol shows no GalC+ contaminating cells. Representative 20X confocal florescent micrograph of a region of interest (ROI) within primary neuronal cultures. C) Isolation protocol shows no OX42+ contaminating cells. Representative 20X confocal florescent micrograph of a region of interest (ROI) within primary neuronal cultures.

Complete Protease Inhibitor Tablet (Roche Applied Sciences, Indianapolis, IN) and 100µl Phosphatase Inhibitor Cocktail II (Sigma-Aldrich, Saint Louis) per every 10mL of FB, and were scraped from wells using a plastic policeman into a 1.5mL centrifuge tube. Cells and protein extracts were kept on ice or in a 4°C cold room throughout the duration of the fractionation. Neurons were lysed via three 5s pulses at 15W using the KONTES micro ultrasonic cell disruptor (KONTES, Vineland, NJ). Cells were placed in ice after each 5s pulse to prevent overheating of the sample. After cell disruption, homogenates were incubated on ice for 10min. Then, homogenates were centrifuged for 30min at 14000rpm to pellet any nuclei, mitochondria or unbroken cells. The supernatant (cytosolic fraction) was removed and stored in aliquots at -80°C until further analysis.

Western Blot Analysis. Protein concentration of subcellular fractions was determined via the bicinchoninic acid (BCA) assay (Pierce, Rockford, IL). 30µg of protein were separated via electrophoresis on a 10% or 12% SDS-polyacrylamide gel, depending upon the main protein of interest for analysis. Protein was transferred overnight at 4°C in transfer buffer [in mM: 25 Tris base, 192 glycine, 10% (v/v) methanol] to a PDVF membrane (Millipore, Billerica, MA). Protein-containing PDVF membranes were blocked for 1h at room temperature in blocking buffer (BB) [4% bovine serum albumin (BSA), 0.2% Tween-20 in Tris-buffered saline (TBS, pH 7.4)]. Following blocking, membranes were washed 2X in wash buffer (WB) [0.2% Tween-20 in Tris-buffered saline (TBS, pH 7.4)]. Next, membranes were incubated overnight (or 1h at room temperature) with

primary antibody diluted in primary antibody buffer (PAB) [1% bovine serum albumin (BSA), 0.2% Tween-20 in Tris-buffered saline (TBS, pH 7.4)]. The following primary antibodies [with their dilution used] were examined: mouse anti-alpha fodrin [1:1000] (BIOMOL International, LP, Plymouth Meeting, PA), rabbit anti-cleaved caspase 3 [1:1000] (Cell Signaling Technologies, Inc., Danvers, MA) and mouse anti- β -actin [1:50000] (Sigma-Aldrich, Saint Louis, MO). After incubation with the primary antibody, membranes were washed 6X 10min in WB. Following these washes, the membranes were incubated 1h at room temperature with the appropriate secondary antibody diluted in secondary antibody buffer (SAB) [0.5% bovine serum albumin (BSA), 0.2% Tween-20 in Tris-buffered saline (TBS, pH 7.4)]. The following secondary antibodies were employed: goat anti-mouse-POD, rat adsorbed, and goat anti-rabbit F(ab')₂-POD, human and mouse adsorbed (Southern Biotech, Birmingham, AL). All secondary antibodies were diluted 1:3000, except for mouse anti- β -actin for which the secondary antibody was diluted 1:15000. Following incubation with the secondary antibody, membranes were washed 6X 10min in WB and, then, developed using the enhanced chemiluminescence (ECL) system (GE Healthcare, Piscataway, NJ). Films were scanned and densitometric analyses were performed using AlphaEase software (Alpha Innotech, San Leandro, CA). Samples were normalized first to β -actin values and then represented as fold values relative to sham.

Lactate Dehydrogenase (LDH) release cytotoxicity assay. The release of intracellular LDH can be used as a measure of cell death for insult paradigms >12-24h and can be used as a marker of necrosis-induced plasma membrane rupture for insult paradigms <10-12h (Lee et al., 1998). The release of intracellular LDH was detected using the Cytotoxicity Detection Kit® (Roche Applied Sciences, Indianapolis, IN), by following the manufacturer's protocol. All steps were carried out at room temperature. Briefly, 100µL of LDH-containing medium from control, different dose rotenone-treated, FK506-treated and FK506-pretreated, and different dose rotenone-treated primary neuronal cultures were transferred in triplicate to a 96-well microplate. Then, the samples were incubated in 100µL of the supplied reaction buffer, containing diaphorase / NAD⁺ / iodotetrazolium chloride, from 20min to 1hr on a rotary shaker (250rpm). During this incubation, multiple readings at 405nm were recorded using a Dynex MRX™ microplate reader (Dynex Technologies, Chantilly, VA). High controls (HC) consisted of medium from control cells lysed with 2% Triton X-100 for 10min at 37°C. Low controls (LC) were medium without incubation with cells. Absorbance values (Abs.) at 490nm (630 nm reference) were represented as % of control cell viability ± S.D., determined via the following equation:

$$\% \text{ cell viability} = 100 - [(Abs - LC) / (HC - LC)] * 100$$

ELISA detection of cytosolic oligonucleosome formation. As a measure of apoptotic cell death, the presence of cytosolic oligonucleosomes (DNA+histone complexes resulting from cleavage at the interlinker regions between histones on

DNA) was detected using the Cell Death Detection ELISA® (Roche Applied Sciences, Indianapolis, IN), by following the manufacturer's protocol. All steps were carried out at room temperature. Briefly, a 96-well microplate was coated for 1.5h with a mouse monoclonal antibody, diluted in supplied coating buffer (clone H11-4 to the histones H2A, H2B, H3 and H4). The plate was then incubated in the supplied incubation buffer for 0.5h. 30µg of cytosolic protein from each sample loaded in triplicate wells was diluted in incubation buffer. The cytosolic samples were incubated for 1.5h. After incubation, the microplate was washed 3X with supplied wash buffer and then incubated for 1.5h in a peroxidase conjugated antibody to DNA, diluted in incubation buffer. The microplate, again, was washed 3X in wash buffer and then incubated for 5 min to 1h in 2,2-azino-bis(3-ethylbenzthiazoline-6-sulphonic acid) (ABTS) substrate solution on a rotary shaker (250rpm). During this incubation, multiple readings at 405nm were recorded using a Dynex MRX™ microplate reader (Dynex Technologies, Chantilly, VA). Absorbance values at 405nm were represented as fold change relative to sham absorbance values at 405nm.

Cell preparation for immunofluorescent staining. Rotenone treatment duration was selected based on the time point at which biochemical markers demonstrated a difference between the apoptotic and necrotic-like stimuli (Fig. 2A, B). At these time points, neurons, plated on Assistent glass cover slips (No. 1.5 thickness) (Harvard Apparatus, Holliston, MA), were washed once with ice cold PBS and, then, fixed with 4% paraformaldehyde / 10% sucrose PBS for

15min at room temperature. Fixed cells were washed 3X 5mins in 1XPBS, subsequently post-fixed with ice cold methanol for 5min at -20°C, and then allowed to air dry at room temperature for 30min.

After air drying, neurons were washed 3X for 5min in immunocytochemistry wash buffer (IWB) (1X PBS, 0.45µm filter-sterilized, pH 7.4). Then, neurons were blocked for 1h with IWB+ 5%(v/v) normal goat serum (NGS)+ 0.3% Triton X-100. After removal of the blocking solution, neurons were incubated overnight in a humidified chamber with the primary antibodies diluted in IWB+ 1%(v/v) normal goat serum (NGS) + 0.3% Triton X-100. The following primary antibodies [with their dilutions used] were examined: rabbit anti-Bax (N-terminus) [1:200] (Millipore, Billerica, MA), mouse anti-PDI [1:100] (Assay Designs, Inc., Ann Arbor, MI) and mouse anti-ATP synthase β [1:100] (Abcam, Cambridge, MA). Following overnight incubation, neurons were washed 3X for 5min in IWB. Then, neurons were incubated for 1h with appropriate fluorescent secondary antibodies diluted in IWB. The following secondary antibodies [and their dilutions] were employed: AlexaFluor 568 goat anti-rabbit [1:1000] and AlexaFluor 488 goat anti-mouse [1:1000] (Invitrogen, Carlsbad, CA). Again, neurons were washed 3X for 5min in high salt IWB (IWB + 4.676g NaCl / 200mL of IWB). Following these wash steps, Vectashield mounting medium containing DAPI (Vector Labs, Burlingame, CA) was applied to the neurons and were placed on top of glass slides and sealed with clear nail polish. Fluorescent stained slides were stored in the dark at -20°C until viewing. Sets of slides to be

used for comparison studies using the same primary antibodies were performed on the same day to eliminate inter-experimental variance.

Confocal microscopy. Fluorescent stained slides were viewed using the Biorad Radiance 2100 laser scanning system (Carl Zeiss, Thornwood, NY) fitted onto a Nikon Eclipse E800 microscope (Nikon, Melville, NY). Images were collected using LaserSharp 2000 software (Carl Zeiss, Thornwood, NY). Fluorescence was detected using the following laser and emission filter sets: for cyan fluorophores, a 405nm laser with an HQ442/45 emission filter, for green fluorophores, a 488nm laser with an HQ515/30 emission filter, and for red fluorophores, a 568nm laser with an E600LP emission filter. Two dichroic mirrors were placed along the optical path to prevent fluorescence bleed-through- a 500DCLPXR mirror for the cyan and green fluorophores and a 560DCLPXR for the green and red fluorophores. A third 100% deflection mirror was used when imaging the cyan fluorophore.

Control neurons were used to set the baseline parameters for laser intensity, gain and offset for slides stained with the same primary antibodies. Using the SETCOL lookup table (LUT), the three parameters were chosen which maximized the width of the gray scale with few red (high intensity) pixels and few green (low intensity) pixels. Optimal pinhole size was computer generated for each laser at each objective. For the Fluor 40X oil (NA 1.3), the pinhole settings were as follows: for 405nm, 0.9mm, for 488nm, 1.1mm and for 568, 1.3mm. For the Plan Apo 60X oil (NA 1.4), the pinhole settings were as follows: for 405nm,

1.3mm, for 488nm, 1.5mm and for 568nm, 1.8mm. After the parameters had been selected, the settings were maintained for all images taken involving the same primary antibodies and the entire image set was collected on the same day.

Images were scanned using the sequential scan setting for the three lasers, set at a scan rate of 50 lines per second (lps), and using a Kalman averaging (N=6) to minimize background signal. A 60X oil PlanAPO objective (NA 1.4) was used to acquire images for analyzing the presence of Bax colocalization with particular subcellular organelles, a 20X Plan APO (NA 0.75) for characterizing cell types after primary isolation and a Fluor 40X oil objective (NA 1.3) was used to acquire images for the blind counting of the cells within regions of interests (ROIs) which exhibited Bax colocalization with a particular subcellular organelle. Sets of 40X confocal images for each primary antibody combination were counted by the same blind reviewers to minimize reviewer-to-reviewer variability. Prior to analysis, collected images were deconvolved using a 2D iterative deconvolution plug-in based on the DAMAS algorithm (Brooks and Humphreys, 2004; Dougherty, 2005) for NIH ImageJ shareware (<http://rsb.info.nih.gov/ij/>).

Statistical Analysis. Statistical analyses were performed using GraphPad Prism 5 software (GraphPad Software, San Diego, CA). For analyses involving two groups, a student's t-test was performed and a p-value less of than 0.05 was considered significant. If variances for the two groups were deemed significantly

different, a Welsh correction was added to the student's t-test. For analyses involving two or more groups, a one-way analysis of variance (ANOVA) was performed with a Tukey-Kramer post-hoc test to compare groups. A p-value of less than 0.05 was deemed significant.

Results

25 μ M and 100 μ M rotenone treatments produce two biochemically and phenotypically distinct forms of cell death.

Cytotoxicity time course analysis for 25 μ M and 100 μ M rotenone insults in primary neuronal culture revealed the two insults displayed similar cell death time courses, each reducing cell viability to 50% at ~16h insult (Fig. 24A). We looked at plasma membrane integrity and cleavage and activation of caspase 3 at early insult to ascertain whether the two treatments produce necrotic-like or apoptotic-like cell death, respectively. We found 100 μ M rotenone insult produced a significant decrease ($83.4 \pm 3.2\%$; $p < 0.01$) in plasma membrane integrity at 6h insult, the same time at which 25 μ M rotenone produced no decrease (Fig. 19A). Furthermore at 6h insult, 25 μ M rotenone insult increased caspase 3 cleavage (1.67 ± 0.36 ; $p < 0.05$), while 100 μ M rotenone did not (Fig. 19A). Assessment of cell death morphology time course revealed that 100 μ M rotenone increased neuron soma size, promoted intracellular vacuolization and cell rupture / axonal disintegration, while 25 μ M rotenone decreased neuron soma size, promoted peripheral nuclear localization and smooth retraction of neurites (Fig. 19B, C).

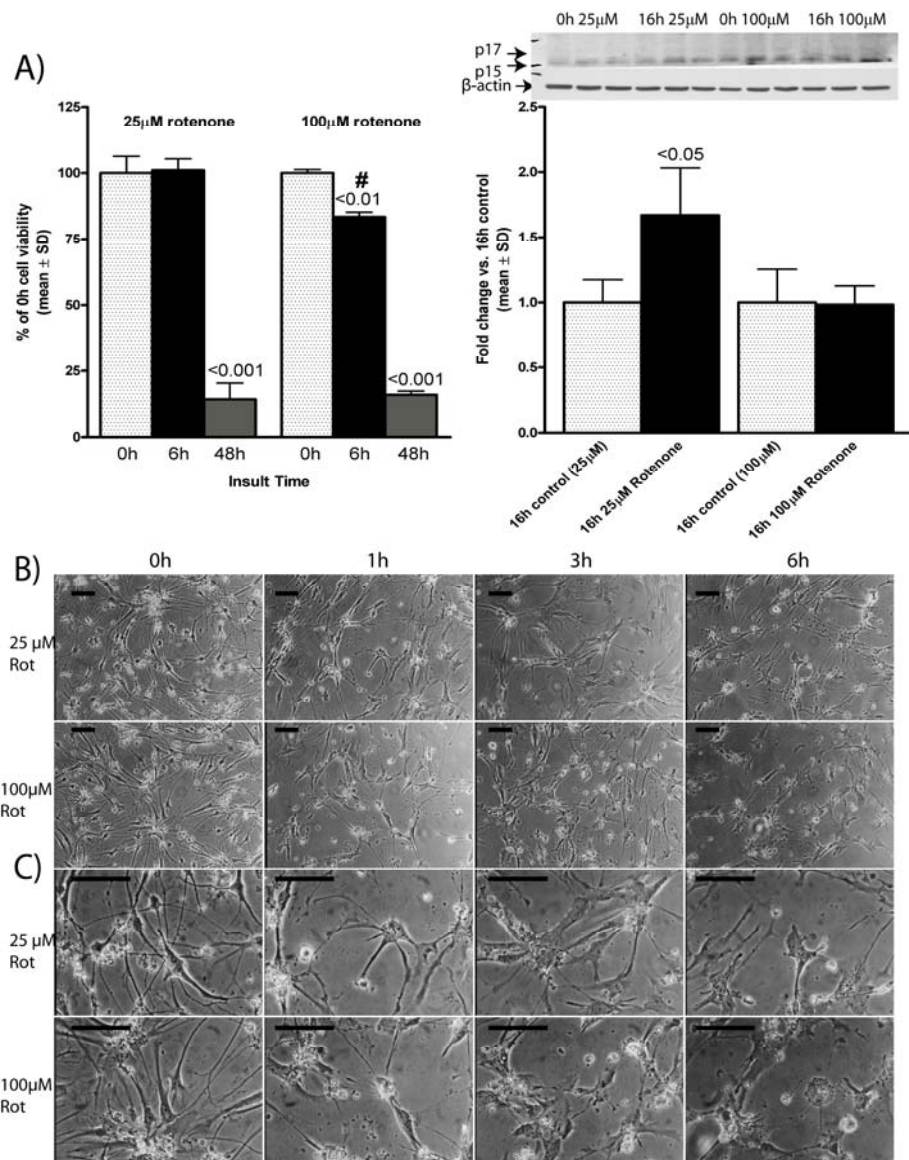


Figure 19. 25μM and 100μM rotenone treatments produce two biochemically and phenotypically distinct forms of cell death.

A) 100μM rotenone insult promotes earlier plasma membrane rupture when compared to 25μM rotenone insult ($83.4 \pm 3.2\%$; $p < 0.01$), and 25μM but not 100μM rotenone increases cytosolic cleaved caspase 3 expression at 16h insult (1.67 ± 0.36 ; $p < 0.05$). LDH cytotoxicity data (top left) gathered at various time points of 25μM and 100μM rotenone insults. Data are represented as % cell viability of 0h control cultures \pm S.D. Above right, representative western blot for cytosolic cleaved caspase 3 after 25μM and 100μM rotenone insults. Graph represents densitometric values for cytosolic cleaved

caspase 3. Densitometric data were normalized to β -actin and are represented as fold 0h control cultures \pm S.D. p-values above columns denote significance relative to 0h control cultures. B) 25 μ M rotenone insult produces a phenotypically apoptotic like cell death. Representative 10X (top) and 25X (bottom) phase contrast images taken at various time points of 100 μ M rotenone insult. C) 100 μ M insult produces a phenotypically necrotic-like cell death. Representative 10X (top) and 25X (bottom) phase contrast images taken at various time points of 100 μ M rotenone insult. Scale bars = 100 μ m.

Taken together, these data reveal that despite possessing similar cell death time courses, 25 μ M rotenone insult produces an apoptotic-like, while 100 μ M rotenone insult produces a necrotic-like cell death phenotype.

25 μ M rotenone insult shifts Bax to nuclei at 1h and to mitochondria at 6h.

Low doses of rotenone have been shown previously to activate the intrinsic, mitochondrial apoptotic cell death pathway, triggered via mitochondrial Bax translocation (Hartley et al., 1994; Segura and Kostrzewa, 2004). In order to determine if the cleaved caspase 3 increases we observed (Fig. 19A) were mediated by mitochondrial Bax translocation, we performed confocal immunocytochemical analyses of 6h 25 μ M rotenone-treated primary neuronal cultures. We observed increases of Bax in mitochondria as assessed by colocalization of Bax with the mitochondrial marker, cytochrome c oxidase IV (COXIV), at 6h after 25 μ M rotenone insult when compared to 0h control cultures (Fig. 20D). Interestingly, we, also, observed a dramatic increase in nuclear Bax after 1h 25 μ M rotenone insult when compared to 0h control cultures (Fig. 20B), which agrees with our recent *in vivo* findings investigating Bax localization after

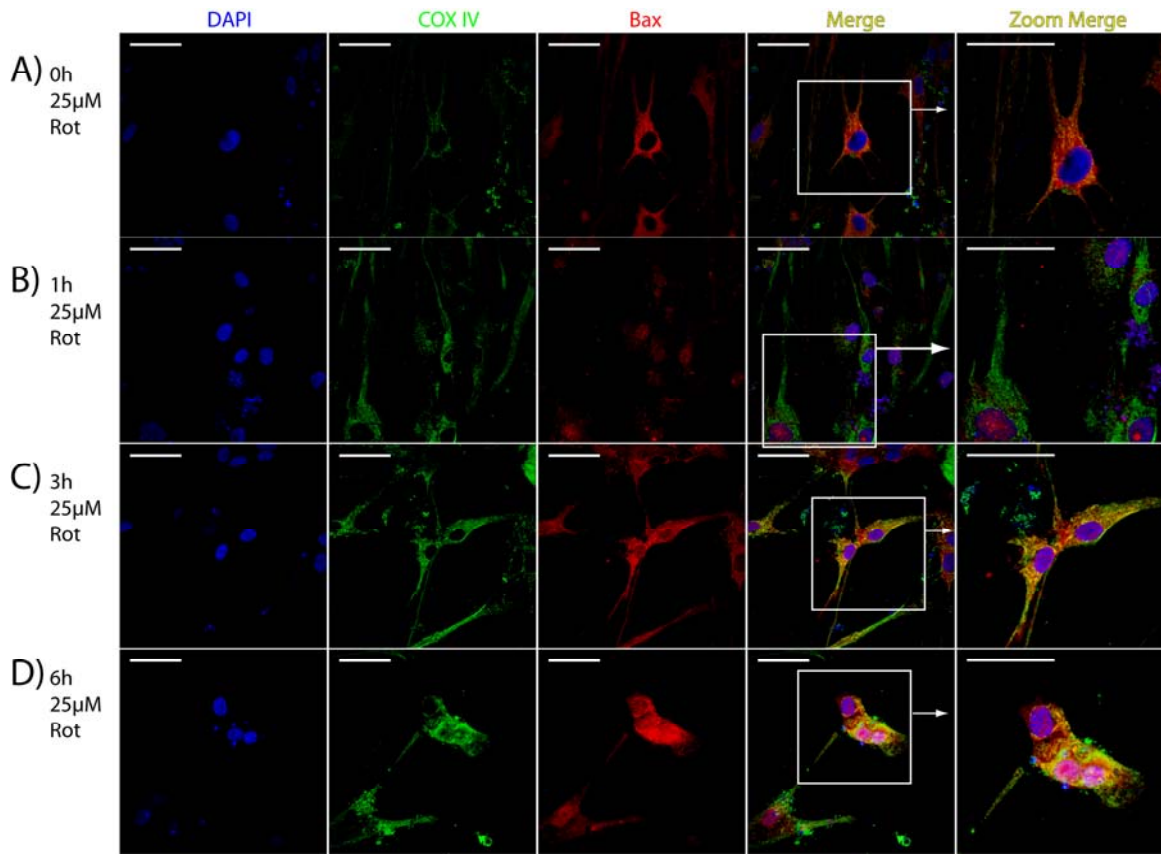


Figure 20. 25μM rotenone treatment shifts Bax to nuclei at 1h and to mitochondria at 6h insult.

A) Primary neurons at 0h 25μM rotenone insult have little to no nuclear Bax fluorescence and no mitochondrial Bax localization. Representative 60X confocal florescent micrograph of a region of interest (ROI) within primary neuronal cultures. B) Primary neurons at 1h 25μM rotenone insult have increased nuclear Bax fluorescence and no mitochondrial Bax localization. Representative 60X confocal florescent micrograph of a region of interest (ROI) within primary neuronal cultures. C) Primary neurons at 3h 25μM rotenone insult have increased nuclear Bax fluorescence and little mitochondrial Bax localization. Representative 60X confocal florescent micrograph of a region of interest (ROI) within primary neuronal cultures. D) Primary neurons at 6h 25μM rotenone insult have increased nuclear Bax fluorescence and increased mitochondrial Bax localization. Representative 60X confocal florescent micrograph of a region of interest (ROI) within primary neuronal cultures. Scale bars = 20μm.

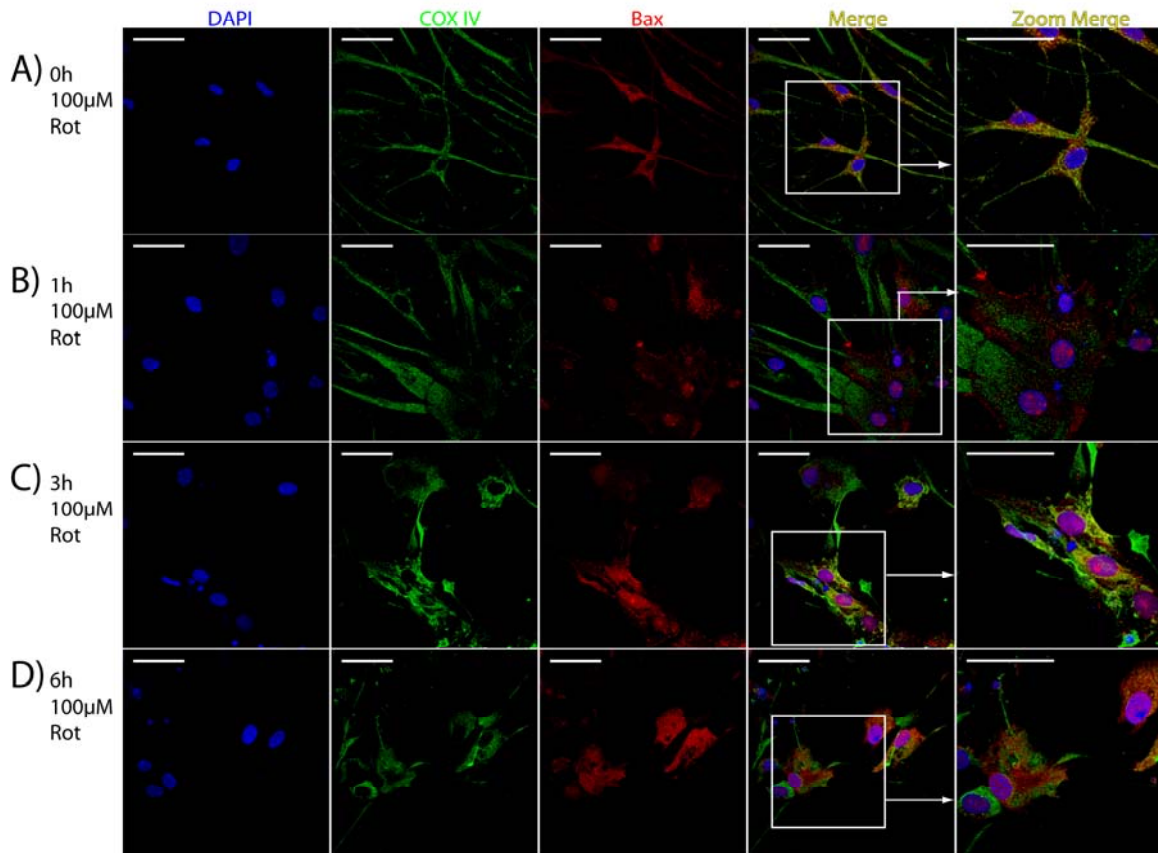


Figure 21. 100 μ M rotenone treatment shifts Bax to nuclei at 1h.

A) Primary neurons at 0h 100 μ M rotenone insult have little to no nuclear Bax fluorescence and no mitochondrial Bax localization. Representative 60X confocal fluorescent micrograph of a region of interest (ROI) within primary neuronal cultures. B) Primary neurons at 1h 100 μ M rotenone insult have increased nuclear Bax fluorescence and no mitochondrial Bax localization. Representative 60X confocal fluorescent micrograph of a region of interest (ROI) within primary neuronal cultures. C) Primary neurons at 3h 100 μ M rotenone insult have increased nuclear Bax fluorescence and no mitochondrial Bax localization. Representative 60X confocal fluorescent micrograph of a region of interest (ROI) within primary neuronal cultures. D) Primary neurons at 6h 100 μ M rotenone insult have increased nuclear Bax fluorescence and no mitochondrial Bax localization. Representative 60X confocal fluorescent micrograph of a region of interest (ROI) within primary neuronal cultures. Scale bars = 20 μ m.

neonatal HI (Gill et al., unpublished observations). Furthermore, we observed no mitochondrial Bax localization after 6h 100 μ M rotenone (Fig. 21A-D).

100 μ M rotenone insult shifts Bax to nuclei at 1h and to ER at 6h.

Recent reports have used high doses of rotenone to induce necrotic or necrotic-like cell death, although its exact mechanism of action has not been defined (Bal-Price and Brown, 2000; Casarejos et al., 2006; Leist et al., 1999). We have recently observed increased oxidative stress increases Bax-mediated activation of ER cell death signaling cascades in an *in vivo* rat model of neonatal HI (Gill et al., unpublished observations). Therefore, we wanted to ascertain whether the increased oxidative stress of 100 μ M rotenone insult would increase ER Bax localization. Using high magnification confocal microscopy, we observed increases of Bax in ER as assessed by colocalization of Bax with the ER marker, protein disulfide isomerase (PDI), at 6h after 100 μ M rotenone insult when compared to 0h control cultures (Fig. 22D). As with 25 μ M rotenone insult, we, also, observed a dramatic increase in nuclear Bax after 1h 100 μ M rotenone insult when compared to 0h control cultures (Fig. 22B). Furthermore, we observed no ER Bax localization after 6h 25 μ M rotenone (Fig. 23A-D).

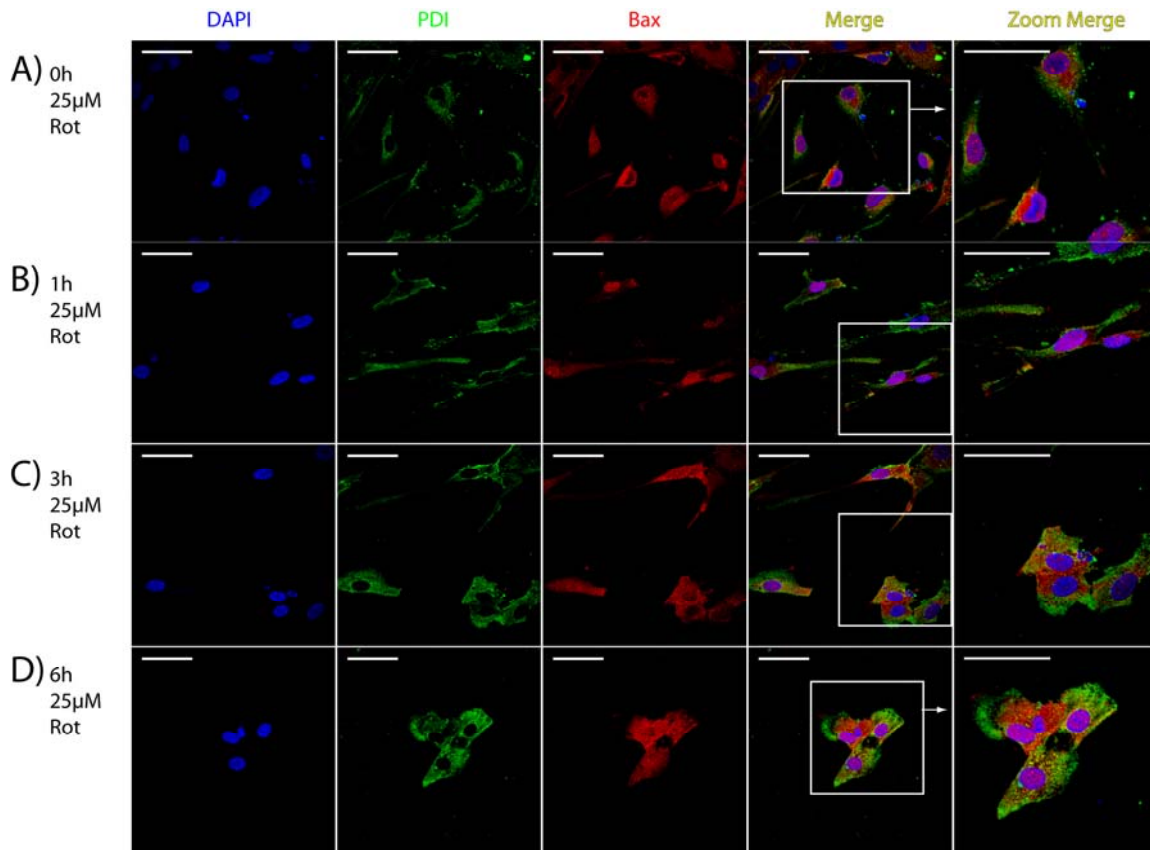


Figure 22. 25μM rotenone treatment shifts Bax to nuclei at 1h.

A) Primary neurons at 0h 25μM rotenone insult have little to no nuclear Bax fluorescence and no ER Bax localization. Representative 60X confocal florescent micrograph of a region of interest (ROI) within primary neuronal cultures. B) Primary neurons at 1h 25μM rotenone insult have increased nuclear Bax fluorescence and no ER Bax localization. Representative 60X confocal florescent micrograph of a region of interest (ROI) within primary neuronal cultures. C) Primary neurons at 3h 25μM rotenone insult have increased nuclear Bax fluorescence and little ER Bax localization. Representative 60X confocal florescent micrograph of a region of interest (ROI) within primary neuronal cultures. D) Primary neurons at 6h 25μM rotenone insult have increased nuclear Bax fluorescence and little ER Bax localization. Representative 60X confocal florescent micrograph of a region of interest (ROI) within primary neuronal cultures. Scale bars = 20μm.

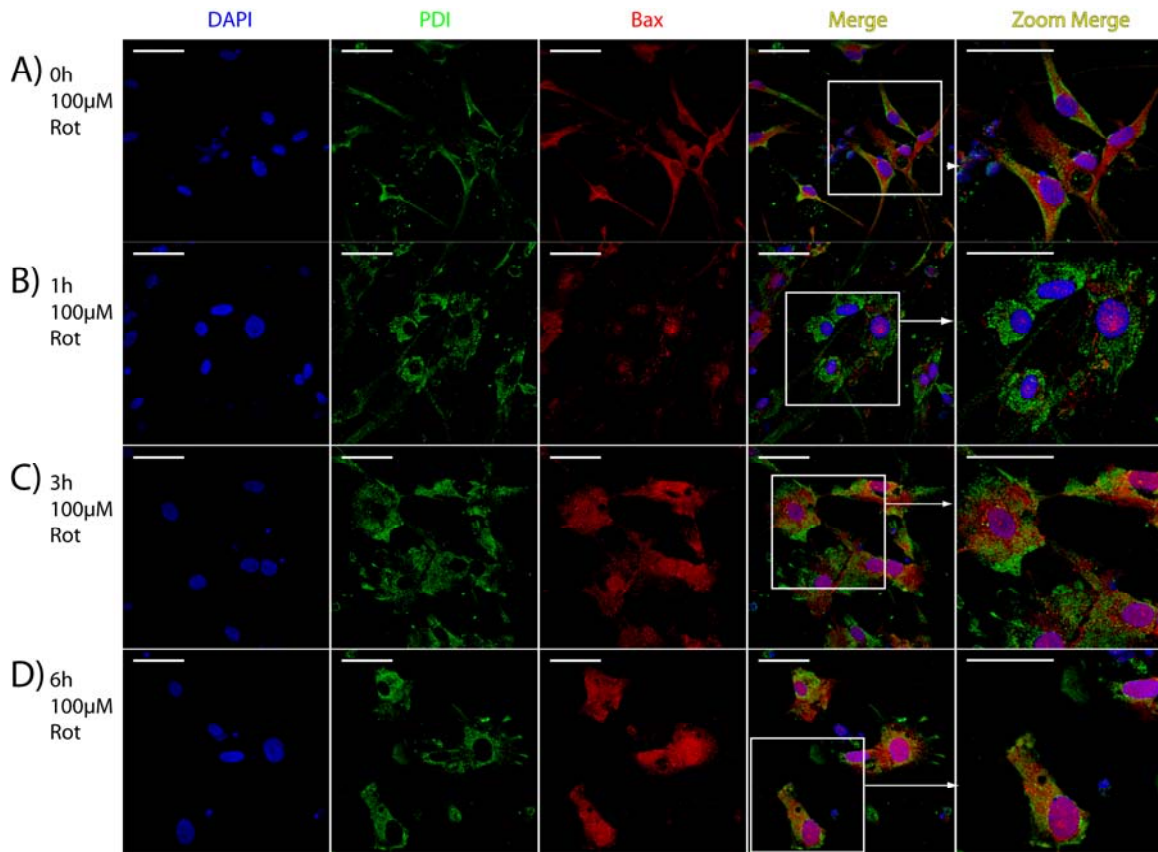


Figure 23. 100μM rotenone treatment shifts Bax to nuclei at 1h and to ER at 6h.

A) Primary neurons at 0h 100μM rotenone insult have little to no nuclear Bax fluorescence and no ER Bax localization. Representative 60X confocal florescent micrograph of a region of interest (ROI) within primary neuronal cultures. B) Primary neurons at 1h 100μM rotenone insult have increased nuclear Bax fluorescence and no ER Bax localization. Representative 60X confocal florescent micrograph of a region of interest (ROI) within primary neuronal cultures. C) Primary neurons at 3h 100μM rotenone insult have increased nuclear Bax fluorescence and little ER Bax localization. Representative 60X confocal florescent micrograph of a region of interest (ROI) within primary neuronal cultures. D) Primary neurons at 6h 100μM rotenone insult have increased nuclear Bax fluorescence and increased ER Bax localization. Representative 60X confocal florescent micrograph of a region of interest (ROI) within primary neuronal cultures. Scale bars = 20μm.

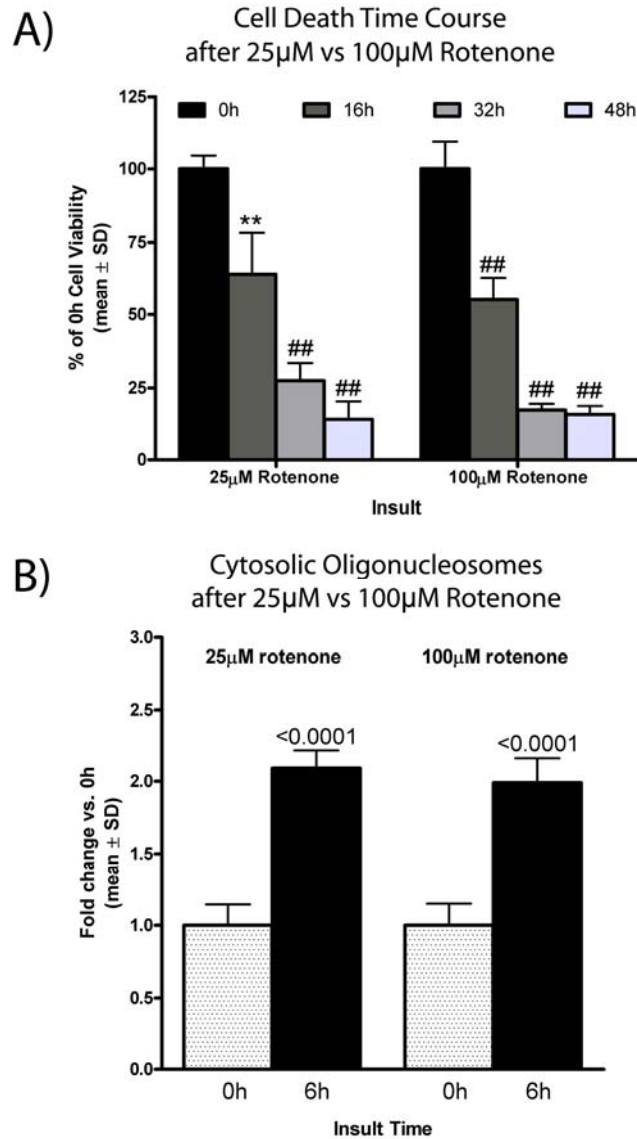


Figure 24. Supplementary data

A) 25 μ M and 100 μ M rotenone insults produce similar time courses for cell death. LDH cytotoxicity data gathered at various time points of 25 μ M and 100 μ M rotenone insults. Data are represented as % cell viability of 0h control cultures \pm S.D. B) 25 μ M and 100 μ M rotenone insults produce similar cytosolic oligonucleosome levels. Cell death ELISA data gathered at 6h of 25 μ M and 100 μ M rotenone insults. Data are represented as fold change of 0h control cultures \pm S.D. p-values above columns denote significance relative to 0h control cultures. ** denotes $p < 0.01$, ## denotes $p < 0.001$ when compared to 0h control cultures.

25μM rotenone insult increases nuclear Bax at 1h insult and mitochondrial Bax at 6h insult.

In order to quantitate the extent of nuclear and mitochondrial Bax localization after 25μM rotenone insult, we conducted blind cell counts of randomly selected confocal images from our 25μM rotenone-treated cultures at 1h (Fig. 26A, B) and 6h (Fig. 27A, B) insult. We found an increase in the number of cells expressing Bax colocalized with the nuclear stain, DAPI, at 1h ($87.5 \pm 13\%$; $p < 0.001$) (Fig. 26D) insult in 25μM rotenone-treated primary neuronal cultures than in 0h control-treated cultures. In addition, there were significantly more cells labeled with colocalized Bax and COXIV at 6h ($40.0 \pm 8.7\%$; $p < 0.01$) (Fig. 27D) insult in 25μM rotenone-treated primary neuronal cultures than in 0h control-treated cultures. These findings concurred with our high magnification immunocytochemical data.

100μM rotenone insult increases nuclear Bax at 1h insult and ER Bax at 6h insult.

In order to quantitate the extent of nuclear and ER Bax localization after 100μM rotenone insult, we conducted blind cell counts of randomly selected confocal images from our 100μM rotenone-treated cultures at 1h (Fig. 28A, B) and 6h (Fig. 29A, B) insult. We found an increase in the number of cells expressing Bax colocalized with the nuclear stain, DAPI, at 1h ($88.6 \pm 14\%$; $p < 0.001$) (Fig. 28D) insult in 100μM rotenone-treated primary neuronal cultures

than in 0h control-treated cultures. In addition, there were significantly more cells labeled with colocalized Bax and PDI at 6h ($19.7 \pm 2.6\%$; $p < 0.01$) (Fig. 29D) insult in 100 μ M rotenone-treated primary neuronal cultures than in 0h control-treated cultures. These findings concurred with our high magnification immunocytochemical data.

25 μ M rotenone insult increases caspase-mediated cleavage of the cytoskeletal protein α -fodrin.

In vivo and *in vitro* studies of activation of mitochondrial-mediated cell death as apoptotic and mediated by mitochondrial Bax localization (Putcha et al., 1999; Tsuruta et al., 2004). If 25 μ M rotenone insult produces apoptotic cell death, we hypothesized that Bax-mediated cell death pathways should be involved.

In order to measure the contributions of both apoptosis and necrosis to the 25 μ M and 100 μ M rotenone-induced cell death, we measured the cleavage of the cytosolic cytoskeletal protein, α -fodrin, which has been widely reported to yield protease-specific cleavage fragments: a 150kD fragment resulting from cumulative ER calpain- and caspase-mediated cleavage (contributing to both apoptosis and necrosis), a 145kD fragment resulting from ER calpain-mediated cleavage alone (contributing to necrosis) and a 120kD fragment resulting from cytosolic caspase-mediated cleavage (contributing to apoptosis alone (Blomgren et al., 2001; Cryns et al., 1996; Vanags et al., 1996)]. Our preliminary data

demonstrates 25 μ M rotenone insult increases the caspase- / calpain-cleaved 150kD α -fodrin fragment levels, as well as the caspase-cleaved 120kD α -fodrin fragment levels, when compared to 0h control cultures (Fig. 30A-C). This result confirms 25 μ M rotenone insult produces an apoptotic cell death.

100 μ M rotenone insult increases calpain-mediated cleavage of the cytoskeletal protein α -fodrin.

Early *in vitro* studies of activation of ER-mediated cell death described the cell death phenotype as necrotic-like (Kalai et al., 2003; Yoneda et al., 2001). If 100 μ M rotenone insult produces a necrotic-like cell death, we hypothesized that ER-mediated cell death pathways should be involved.

Our preliminary data demonstrates 100 μ M rotenone insult increases the caspase- / calpain-cleaved 150kD α -fodrin fragment levels, as well as the calpain-cleaved 145kD α -fodrin fragment levels, when compared to 0h control cultures and 25 μ M rotenone insult cultures (Fig. 30A, B, D) Surprisingly, 100 μ M rotenone insult, also, increases the caspase-cleaved 120kD α -fodrin fragment to that of 25 μ M rotenone-treated cultures when compared to 0h control cultures, suggesting an apoptotic-like component to 100 μ M rotenone-induced cell death (Fig. 30A, C). To confirm this result, we measured cytosolic oligonucleosomes, a marker of apoptotic cell death, and in concordance with the fodrin data, we observed that 25 μ M and 100 μ M rotenone insults increased cytosolic oligonucleosome levels to similar values (for 25 μ M rotenone, 2.09 ± 0.12 ;

$p < 0.0001$ / for 100 μ M rotenone, 1.99 ± 0.17 ; $p < 0.0001$) (Fig. 24B) at 6h insult when compared to 0h control cultures. These results suggest that 100 μ M rotenone insult produces an apoptotic / necrotic cell death as opposed to a true necrotic cell death.

Discussion

Oxidative stress, energy depletion and cell death phenotype

Numerous reports have linked increased oxidative stress and energy depletion with increased probability of necrosis (Almeida and Bolanos, 2001; Cole and Perez-Polo, 2004; Mehta et al., 2007). Until recently, this was the extent of the published research, because necrosis has been classically defined as a passive event (Edinger and Thompson, 2004). Recent reports have begun to focus on a programmed necrotic cell death, which possesses many of the phenotypic markers of passive necrosis, but involves the activation and coordination of intracellular signaling cascades (Ditsworth et al., 2007). Several models have been proposed to study programmed necrosis, but the majority have involved DNA-damage inducing agents (Moubarak et al., 2007), while few involve the combined components of oxidative stress and energy depletion.

In this report, we have developed a reliable *in vitro* primary cortical neuron model, which uses different doses of the mitochondrial complex I inhibitor, rotenone (thereby allow selective increasing or decreasing oxidative stress and energy depletion), to initiate both apoptosis and necrosis. We found that despite

possessing similar cell death time courses, 25 μ M rotenone insult produces an apoptotic-like, while 100 μ M rotenone insult produces a necrotic-like cell death phenotype (Fig. 19). The benefit of this neuronal culture system lies in the uniformity of cell death time course, thereby increasing the ease involved in investigating apoptotic cell death.

25 μ M rotenone insult induces mitochondrial Bax localization to activate the intrinsic mitochondrial cell death pathway.

Classically, the Bcl-2 family has been described as regulators of the intrinsic mitochondrial cell death pathway (Linseman et al., 2004; Precht et al., 2005). A recent shift in Bcl-2 family research proposes a disinhibition hierarchical model of regulation (Kim et al., 2006a). This hierarchical model suggests an interaction between anti-apoptotic and BH3-only proteins, which serve as activators of Bax and Bak (Kim et al., 2006a), as opposed to a direct interaction between multi-domain pro- and anti-apoptotic Bcl-2 family members. The consequences of this type of regulation remain under investigation, but one could speculate that this model allows for increased capability and dynamics in cell death signal processing by the Bcl-2 family of proteins. Despite this model debate, Bax translocation to the mitochondria and subsequent release of cytochrome c release into the cytosol remains a canon in cell death literature (Cho et al., 2006; Hu et al., 2003; Precht et al., 2005).

Our observation that application of an apoptotic stimulus (25 μ M rotenone) increased mitochondrial Bax localization (Fig. 20, 27), which increased caspase 3 cleavage, increased cytosolic oligonucleosomes and caspase-mediated cleavage of α -fodrin supports this model (Fig. 19A, 24B, 30C, respectively). Therefore, the apoptotic stimulus (25 μ M rotenone) used in our model follows previous findings regarding Bax-mediated activation of mitochondrial apoptotic signaling, thus validating our model of apoptosis.

100 μ M rotenone insult induces ER Bax localization to activate ER cell death signaling.

Recently, Edinger et al. (2004) have suggested that, in addition to passive necrosis, there exists programmed necrosis, possessing passive necrotic phenotypic features, which could play a developmental role as an alternative to apoptotic programmed cell death (Edinger and Thompson, 2004; Golstein and Kroemer, 2007; Proskuryakov et al., 2003). Furthermore, recent studies suggest programmed necrosis involves ER Ca²⁺-activated calpain activation, as well as mitochondrial AIF extrusion, itself an outcome of calpain-mediated cleavage (Moubarak et al., 2007; Polster et al., 2005; Sanges et al., 2006; Sanges and Marigo, 2006). Regarding Bax, Scorrano et al. (2003) have shown ER targeting of Bax increases cell death, which could not be inhibited by apoptotic antagonists, via manipulation of ER Ca²⁺ levels (Oakes et al., 2005; Oakes et al., 2003; Scorrano et al., 2003). Based on these findings, we hypothesized that Bax

ER localization would promote activation of ER, specifically calpain-mediated, cell signaling cascades.

We found application of 100 μ M rotenone, a necrotic-like stimulus (Fig. 19), increased ER Bax localization (Fig. 22, 29), which increased calpain-mediated cleavage of α -fodrin (Fig. 30D). These data support previous research, which has linked ER cell death signaling and necrotic-like cell death (Hu et al., 2005a), as well as, those reports, which have linked ER and Bax (Chae et al., 2004; Nutt et al., 2002b; Scorrano et al., 2003; Zong et al., 2003). However, this report is the first to link all three findings together in an *in vitro* trauma model.

25 μ M and 100 μ M rotenone insult induces nuclear Bax localization.

Cancer literature has reported nuclear Bax localization (Godlewski et al., 2001; Mandal et al., 1998; Nishita et al., 1998; Salah-eldin et al., 2000) and suggests a role for Bax in p53 nuclear activity (Raffo et al., 2000). Recently *in vivo*, we have demonstrated that hypoxia-ischemia insult induces early intra- and peri-nuclear Bax localization, which correlates with Ser15 phosphorylation-mediated activation of p53 (Gill et al., unpublished observations). While, determination of the *in vivo* function of nuclear Bax is currently underway, we sought to ascertain whether 25 μ M and / or 100 μ M rotenone insult increased nuclear Bax.

Surprisingly, we observed both rotenone treatments induced early nuclear Bax localization agreeing with our *in vivo* observations and previous cancer

research. Based on our *in vivo* findings, Bax was peri- and intra-nuclear in its localization after 25 μ M and 100 μ M rotenone insults. To our knowledge, this is the first *in vitro* primary neuronal culture trauma model to show nuclear Bax localization after insult. For purposes of investigating p53 activation, attempts to prepare a nuclear fraction in these rotenone models were made, but were unsuccessful as nuclear protein yield from this neuronal plating density was too low for western blot analysis. Thus, together with our *in vivo* data, we hypothesize that the nuclear localization of Bax, early after trauma, is a common mechanism across multiple CNS trauma models.

Conclusion

Using P5 primary cortical neurons and rotenone, we used a high (100 μ M) and a low (25 μ M) rotenone dose, as respective necrotic-like and apoptotic stimuli, we observed both treatments induced early nuclear Bax localization. In addition, we found that the apoptotic stimulus increased mitochondrial Bax localization and caspase-mediated cleavage of α -fodrin, while the necrotic-like stimulus increased ER Bax localization and calpain-mediated cleavage of α -fodrin. This report is the first to link ER Bax, ER cell death signaling and necrotic-like cell death. We conclude that apoptotic and necrotic-like stimuli promote differential Bax localization and subsequent differential activation of cognate cell death signaling cascades to induce expression of their characteristic phenotypic cell morphologies. Furthermore, we hypothesize the nuclear localization of Bax

early after trauma to be a common mechanism across multiple CNS trauma models.

CHAPTER IV

Effects of FK506 and 100% O₂ therapy on Bax-mediated activation of cell death signaling cascades and resulting cell death phenotype

Our previous research has shown *in vivo* neonatal HI and *in vitro* 25μM and 100μM rotenone insults can promote early shifts in Bax localization to the nucleus followed by later shifts of Bax to the mitochondria and ER. Our *in vitro* data suggests that the nature of the insult can dictate Bax localization, with necrotic-like stimuli promoting ER Bax localization and apoptotic stimuli promoting mitochondrial Bax localization, and subsequently the cell death phenotype through activation of respective organelle cell death signaling cascades. However, evidence presented thus far has been correlative.

Using the clinically approved immunosuppressant, FK506, which has been demonstrated to possess neuroprotective properties, and 100% O₂ hyperoxia therapy, used in treatment of children suspected to have suffered a hypoxic-ischemic insult, we provide novel mechanistic evidence supporting the coordinating role of Bax in the activation of cognate organelle cell death signaling cascades and, through selective activation of organelle cell death cascades, can shift the cell death phenotype after trauma. Using FK506, we demonstrate an inhibition of rotenone-induced Bax localization to the nucleus, mitochondria and ER. Furthermore, this localization inhibition decreases rotenone-mediated activation of cognate organelle cell death signaling, and inhibits rotenone-

mediated cell death, suggesting that a common mechanism is involved in promoting Bax localization to organelles after trauma. Using 100% O₂, we surprisingly demonstrate that 100% O₂ increases HI-induced tissue trauma. Furthermore, this increased damage is not apoptotic, but rather necrotic-like and inflammatory, through selective Bax-mediated upregulation of ER cell death signaling cascades. This result confirms our *in vitro* data, linking Bax-mediated activation of ER cell death signaling and necrotic-like cell death.

Introduction

Our previous research has shown *in vivo* neonatal HI and *in vitro* 25μM and 100μM rotenone insults can promote early shifts in Bax localization to the nucleus followed by later shifts of Bax to the mitochondria and ER. Our *in vitro* data suggests that the nature of the insult can dictate Bax localization, with necrotic-like stimuli promoting ER Bax localization and apoptotic stimuli promoting mitochondrial Bax localization, and subsequently the cell death phenotype through activation of respective organelle cell death signaling cascades. These data support previous research, which has linked activation of intrinsic mitochondria cell death signaling apoptotic cell death (Ferrer et al., 2003; Wei et al., 2001) and ER cell death signaling with necrotic-like cell death (Fujita et al., 2002; Hu et al., 2005a; Nakagawa et al., 2000; Yoneda et al., 2001). In spite of these ongoing investigations, evidence for Bax-mediated coordination of the activation of cell death signaling cascades, including its canonical

mitochondrial site of action, and the effects this coordination has on cell death phenotype is noticeably absent in literature.

Recent cancer cell biology studies have shown chemotherapeutics to promote Bax localization to other organelles in addition to mitochondria, such as the nucleus and ER (Gajkowska et al., 2004; Godlewski et al., 2001; Salah-eldin et al., 2000), where Bax promotes cell death via manipulation of Ca^{2+} homeostasis (Nutt et al., 2002a; Nutt et al., 2002b; Oakes et al., 2005; Oakes et al., 2003). In addition, cancer literature has reported nuclear Bax localization (Godlewski et al., 2001; Mandal et al., 1998; Nishita et al., 1998; Salah-eldin et al., 2000) and suggest a role for Bax in p53 nuclear activity (Raffo et al., 2000). In addition, Bax overexpression in SY5Y cells localizes full-length Bax to both the nuclear envelope and the inside of the nucleus, with N-terminal Bax cleavage locking it in the nucleus (Karlsson et al., 2007). Furthermore, porcine models of global fetal hypoxia suggest nuclear envelope-associated Bax regulates nuclear Ca^{2+} (Ashraf et al., 2001), hinting at Bax regulation of Ca^{2+} homeostasis in all organelles in response to oxidative stress. Yet despite these findings, there is a noticeable dearth in literature, which suggest a coordinating role for Bax after trauma in the activation of multiple cell death signaling cascades.

Recently, focus in cell death literature has shifted from the study of individual cell death signaling cascade to the holistic approach of studying the cross-talk / interplay between the signaling cascades. Reports have linked nuclear and mitochondrial cell signaling: AIF nuclear translocation (Hong et al.,

2004), caspase 3-mediated cleavage of PARP-1 (Martin et al., 2005) and Puma and p53-mediated Bax mitochondrial translocation (Chipuk et al., 2004; Chipuk et al., 2003; Zhao et al., 2005). In addition, reports have associated ER and nuclear cell death cascades: calpain-mediated PARP-1 cleavage (Moubarak et al., 2007), p53-mediated activation of ER scotin (Bourdon et al., 2002) and p73 α -mediated activation of scotin and ER stress (Ramadan et al., 2005; Terrinoni et al., 2004). Furthermore, reports have connected ER and mitochondrial cell death signaling: calpain-mediated AIF cleavage and activation (Polster et al., 2005), IRE1-mediated JNK activation to trigger intrinsic mitochondrial cell death (Lee et al., 2007; Yoneda et al., 2001) and Bax and Bak localization to the ER to promote release of ER Ca²⁺ (Nutt et al., 2002a; Oakes et al., 2003; Scorrano et al., 2003). Despite this recent focus, few studies exist, which actually link a phenotypic or functional outcome to this crosstalk.

In this report, we provide novel mechanistic *in vitro* and *in vivo* evidence for Bax coordination of multiple cognate organelle cell death signaling cascades. Using a different dose rotenone insult model in primary cortical neurons, we found 1h pretreatment with immunosuppressive and neuroprotective FK506 inhibited high and low dose rotenone-mediated Bax relocalization and cell death signaling, *in toto*. Using 100% O₂ as an intervention in the *in vivo* Rice-Vannucci neonatal HI model, we show 100% O₂ increases T2-weighted MRI lesion volumes, via increased inflammatory and necrotic signaling, with no amelioration of cortical apoptotic signaling when compared to HI alone. Furthermore, 100%

O₂ increased ER calpain activation and increased ER Bax protein levels, suggesting that 100% O₂ increases HI-induced Bax-mediated activation of ER cell death signaling to increase inflammation and injury by increasing necrotic-like cell death. Taken together, these findings are the first to show Bax-mediated coordination of multi-organelle cell death signaling and demonstrate a link between ER Bax, ER cell death signaling and necrotic-like cell death, all of which can be inhibited via FK506. This report is the first to provide evidence for a FK506-inhibited common trauma-induced Bax activation step.

Materials and Methods

Materials. All chemicals were purchased from Sigma-Aldrich (Saint Louis, MO). N, N-bisacrylamide was purchased from Bio-rad Laboratories (Hercules, CA). Surgical instruments were purchased from Roboz Surgical Instrument Company (Gaithersburg, MD) and 5-0 P3 surgical silk was purchased from Ethicon (Somerville, NJ).

Animal Care for in vitro primary neuronal cultures. E15 pregnant Wistar rat dams (Charles Rivers Laboratories, Wilmington, MA) were housed upon arrival in 12h light-dark cycle with access to food and water *ad libitum*. The day of birth was designated P0. On P5, the day of primary neuron isolation, pups were removed from the dam and kept housed on an electrical warming pad surgery.

Animal Care for in vivo HI. E15 pregnant Wistar rat dams (Charles Rivers Laboratories, Wilmington, MA) were housed upon arrival in 12h light-dark cycle with access to food and water *ad libitum*. The day of birth was designated P0. On P1, litters were culled to ten pups. On P7, the day of HI insult, all pups were removed from the dam, sexed, weighed and randomly assigned to HI-injured groups of variable survival duration or sham groups of variable survival duration. In lieu of using the contralateral hemisphere as the control group, sham groups were utilized because the model of hypoxia-ischemia insult described below produced injury to both the contralateral and ipsilateral cortices, as measured by increased cytosolic cleaved caspase 3 expression and increased cytosolic oligonucleosome formation at 3h post hypoxia-ischemia (Figure 9A-C). For survival time course analyses at multiple time points after HI insult, multiple dams were ordered and housed as described above, except that on P1 after culling to ten pups, the pups were mixed among the dams to minimize potential, confounding litter effects among the multiple groups.

Isolation and culture maintenance of P5 primary cortical neurons. Isolation of primary cortical neurons was carried out following Brewer et al. (1997) with modifications in the isolation method. Prior to extraction of brain tissue, papain (40U / mL) was partially activated by incubation at 37°C for 30min in Hibernate A medium (BrainBits, Carbondale, IL) containing 2% **B**-27, 1% penicillin-streptomycin-neomycin (PSN), 50g / mL **g**entamycin and 0.5mM **L**-glutamine (HA-BPGL) (Invitrogen, Carlsbad, CA). After activation, the papain

solution was filtered (0.22 μ m) and pre-sterilized DnaseI (20U / mL) was added. The enzyme solution was stored at 4°C until use, but no longer than 1.5h.

On P5, Wistar rat pups were deeply anesthetized in an isoflurane-filled gas chamber and then decapitated. Quickly, meninges were removed and cortices from the anterior tuber cinereum to anterior of the occipital cortex (encompassing the parietal cortex) were placed in a glass Petri dish in a laminar flow hood (from here sterile technique should be strictly adhered). Cortices were chopped in 1-2mm blocks and then placed in HA-BPGL medium (2 mL / 2 cortices). Then, minced cortices were enzymatically dissociated in an orbitally, rotating (170rpm) incubator for 30 min at 30°C in the previously made papain / DNaseI solution.

After enzymatic dissociation, the enzyme solution was aspirated and the tissue was incubated for 5min in warmed (30°C) HA-BPGL (4mL). Next, the cortices were triturated 10X and allowed to sediment for 2min. After the tissue has settled, the supernatant was removed and carefully layered Nycoprep 1.077A / HA-BPGL step gradient (1ml each of 22.1%, 29.4%, 36.3% and 51.4% Nycoprep 1.077A) (Accurate Chemical, Westbury, NY). This trituration process was repeated twice more. The layered, cell containing supernatant was centrifuged at 800g for 15min at room temperature, which separates neurons, astrocytes, oligodendroglia and microglia based on cell density. The neuron containing fraction was removed and resuspended in 6mL warmed, HA-BPGL to dilute the Nycoprep 1.077A. Again, the neuron containing solution was

centrifuged at 200g for 1min at room temperature. The neuron-containing pellet was resuspended in Neurobasal-A medium (Invitrogen, Carlsbad, CA) containing the same proportions of BPGL (NA-BPGL) + 5ng / mL basic fibroblast growth factor (bFGF). Neurons were plated at 3.2×10^4 neurons / cm² on poly-D-lysine / β -laminin coated tissue culture plates and incubated for 1.5h at 37°C in 5% CO₂. After incubation, the medium was exchanged for fresh FGF-containing NA-BPGL to remove non-attached cells and cultured at 37°C in 5% CO₂. Day of isolation was deemed 0 days *in vitro* (0DIV).

On 3DIV, fresh media was applied to the neuronal cultures. On 4DIV, 3 μ M cytosine arabinofuranoside (AraC) was added for 48h to kill contaminating proliferating glial cells. On 7DIV, AraC-containing medium was removed and fresh media was applied to culture. Observed at 8DIV, this isolation and culture maintenance protocol yielded a very low glial-contaminating culture (~8-10% GFAP+ cells on 8DIV) (Fig. 18A-C).

Rotenone and FK506 experimental protocols. All primary neuronal culture experiments were carried out at 8DIV. Rotenone and FK506 were made into stock solutions with DMSO and stored at room temperature and -20°C, respectively. Control medium used for 6 and 16h incubations contained 0.66% DMSO, as that was the maximal concentration of DMSO added in any combination of FK506 and rotenone. Neuronal cultures were washed once with experimental medium and were incubated for various times, with either 25 μ M (apoptotic stimulus) or 100 μ M (necrotic-like) rotenone. Unless specified, control

0h cultures were washed once with experimental medium and, then, immediately processed. Pre-treatment with FK506, consisted of incubating cultures for 1h in different FK506 concentrations, and, then, the FK506-containing medium was aspirated and the cultures were washed once in experimental medium \pm the same concentration of FK506 and then incubated for various times in experimental medium \pm the same concentration of FK506. Pretreated 0h (0h+) control cultures were pre-treated for 1h, washed once with experimental medium and then processed. For experiments involving, confocal microscopy or western blot analyses, we used an n=3 (or 4 for FK506 experiments). For ELISA experiments, we used an n=4 run in triplicate wells.

Surgical protocols (Hypoxia-ischemia and hypoxia-ischemia insult plus hyperoxia therapy). Hypoxia-ischemia (HI) insult involving a unilateral, permanent ligation of the common carotid was performed as described elsewhere (Hu et al., 2005b; Vannucci et al., 1988) with minor modifications. Briefly, anesthesia was induced in P7 rat pups by 7-minute incubation in 5% isoflurane, balanced with blood-gas grade 100% O₂, in a 37°C E-Z anesthesia chamber (Euthanex Corp., Palmer, PA) with maintenance of anesthesia at 2.0% isoflurane. As prolonged neuroprotective effects have been observed with isoflurane incubations of greater than 1h (Loepke et al., 2006), care was taken to ensure that no pup was anesthetized for longer than 0.75h. After a mid-neckline incision, the left common carotid was isolated and ischemia was induced by electrocauterization at two points, one rostral and one caudal, along the isolated

artery using a ball-end cauterizer. Double electrocauterization cut the left common carotid in the majority of surgeries (>95%). In those cases in which the blood vessel did not sever, the artery was cut between the two cauterization points using micro-spring scissors to prevent reperfusion across cauterization points. Furthermore, care was taken not to damage the vagal nerve which runs parallel and dorsal (underneath) the common carotid artery. After cauterization, the mid-neckline incision was sutured with 5-0 P3 surgical silk and the pup was returned to a normoxic (20.8% O₂) 37°C chamber until the effects of the anesthesia dissipated (5-10 min). Sham pups were anesthetized, given the mid-neckline incision and, then, sutured. Isolation of the left common carotid was not performed on sham pups as isolation of the artery can produce minor (<1-2s) ischemia-reperfusion events (unreported observational finding). The total time for performing ischemia surgery on a litter of pups was approximately 1h. After the last pup recovered from anesthesia, the pups were returned to the dam for a 2.5h recovery period to prevent any potential isoflurane-mediated respiratory complications during the hypoxia component of the HI injury.

After the 2.5h recovery period, all pups were removed from the dam and placed either in a normoxic 37°C chamber (sham) or hypoxic (8.0% O₂ balanced with blood-gas grade nitrogen) 37°C chamber for 1.5h. A small pet intensive care unit (ICU) (Harvard Apparatus, Boston, MA) was used for the hypoxia chamber as its larger volume promoted greater inertia of oxygen levels and its heated internal water bath reduced temperature variations commonly observed

with small chambers wrapped in heated water pads (unreported observational finding). After the 1.5h period, designated 0h survival, pups were returned to the dam until their randomly assigned survival time point. Cortices were collected from sham (0h) and HI-injured pups at 0.5, 1, 2, 3, 6, 12, 24, 48 and 72h survival times after HI (n=3 / time point).

For hypoxia-ischemia insult plus hyperoxia therapy (HHI), HI insult was performed as described above except that immediately after the 1.5h hypoxic period, the groups receiving hyperoxia therapy were incubated in 100% blood-gas grade O₂ for 2h, while the sham pups and HI-alone pups remained in a normoxic 37°C chamber. After the 2h period, all pups were returned to the dam until their randomly assigned survival time point. The end of the hypoxic component remained the designated 0h survival point. Cortices were collected from sham (3h) (n=3), HI-injured (3h) (n=3) and HI-injured + hyperoxia therapy pups (3h) (n=4).

Cytosolic fractionation of P5 primary cortical neurons. At the designated rotenone insult duration, neurons were washed once with ice cold PBS. Then, primary neurons were suspended in ice-cold fractionation buffer (FB) (in mM: 10 HEPES, 0.5 EGTA, 2 EDTA, 10 DTT, 250 sucrose) containing 1 Roche Complete Protease Inhibitor Tablet (Roche Applied Sciences, Indianapolis, IN) and 100µl Phosphatase Inhibitor Cocktail II (Sigma-Aldrich, Saint Louis) per every 10mL of FB, and were scraped from wells using a plastic policeman into a 1.5mL centrifuge tube. Cells and protein extracts were kept on ice or in a 4°C

cold room throughout the duration of the fractionation. Neurons were lysed via three 5s pulses at 15W using the KONTES micro ultrasonic cell disruptor (KONTES, Vineland, NJ). Cells were placed in ice after each 5s pulse to prevent overheating of the sample. After cell disruption, homogenates were incubated on ice for 10min. Then, homogenates were centrifuged for 30min at 14000rpm to pellet any nuclei, mitochondria or unbroken cells. The supernatant (cytosolic fraction) was removed and stored in aliquots at -80°C until further analysis.

Subcellular Fractionation of P7 Wistar rat pup cortices. At the designated survival time point after HI or HHI, pups were deeply anesthetized in an isoflurane-filled gas chamber and then decapitated. Whole brains were removed and both contralateral and ipsilateral cortices, from the anterior tuber cinereum to anterior of the occipital cortex (encompassing the parietal cortex), were isolated and flash frozen in liquid nitrogen. Cortical tissue was stored at -80°C until processed. All of the following fractionation steps were carried in ice or a 4°C cold room.

Each isolated cortex was suspended in ice-cold fractionation buffer (FB) (in mM: 10 HEPES, 0.5 EGTA, 2 EDTA, 10 DTT, 250 sucrose) containing 1 Roche Complete Protease Inhibitor Tablet (Roche Applied Sciences, Indianapolis, IN) and 100µl Phosphatase Inhibitor Cocktail II (Sigma-Aldrich, Saint Louis) per every 10mL of FB. Cortices were disrupted by 30 strokes in a tight-fitting dounce homogenizer (Wheaton Science, Millville, NJ). Homogenates were centrifuged for 20min at 1000g to pellet nuclei and unbroken cells. To aid

in the enrichment of the fractionation procedure, we employed a 50-80 supernatant removal process. Briefly, 50% of the supernatant was removed to a new chilled tube [labeled supernatant 1 (S1)] and FB roughly equivalent to half of the supernatant volume taken off was added to the pellet. The nuclear pellet was resuspended, and, again, the homogenate was centrifuged for 20min at 1000g to repellet nuclei and any remaining unbroken cells. Now 80% of the supernatant was removed and placed in the S1 tube. The remaining supernatant was discarded and the nuclear pellet was resuspended in pellet buffer (PB) (in mM: 20 HEPES, 400 NaCl, 1 EDTA, 1 EGTA, 1 DTT, 1 PMSF) containing 1 Roche Complete Protease Inhibitor Tablet and 100µl Phosphatase Inhibitor Cocktail II per every 10mL of PB. The suspended nuclear pellet was shaken at 1400rpm on an orbital shaker for 30min and then centrifuged at 14000rpm for 10 min. To minimize repetitive freeze-thaw cycles, the supernatant (nuclear fraction) was stored in aliquots at -80°C until further analysis.

While processing the nuclear fraction, the supernatant in the S1 tube was centrifuged at 3300g for 10min to pellet any remaining nuclei and unbroken cells. The supernatant was removed to a new chilled tube (M) and the pellet was discarded. The supernatant in the M tube was centrifuged at 10000g for 20min to pellet heavy and light mitochondria. As with the original 1000g step, which used the 50-80 supernatant removal steps, 50% of the supernatant was removed to a new chilled tube (S2), the pellet was resuspended and centrifuged again at 10000g for 20min. 80% of the supernatant was removed to the S2 tube and the

remaining supernatant was discarded. The mitochondrial pellet was resuspended in PB and then was briefly pulse-sonicated (30kHz, <2s). After sonication, the sonicated resuspension (mitochondrial fraction) was stored in aliquots at -80°C until further analysis.

While processing the mitochondrial fraction, the supernatant in the S2 tube was centrifuged at 15000g for 10min to pellet any remaining light mitochondria. The supernatant was then removed to a new chilled tube (E) and the pellet was discarded. The supernatant in the E tube was centrifuged at 100000g for 1h to pellet rough and smooth endoplasmic reticulum (ER). The supernatant (cytosolic fraction) was removed and stored in aliquots at -80°C until further analysis. The ER pellet was resuspended in PB and, then, was briefly pulse-sonicated (30kHz, <2s). After sonication, the sonicated resuspension (ER fraction) was stored in aliquots at -80°C until further analysis. Using Lamin-B₁, IκB-α, cytochrome c oxidase IV (COXIV) and protein disulfide isomerase (PDI) as respective nuclear, cytosolic, mitochondrial and ER markers, we observed that this subcellular fractionation protocol yielded highly enriched nuclear, cytosolic, mitochondrial and ER fractions (Figure 2A).

Western Blot Analysis. Protein concentration of subcellular fractions was determined via the bicinchoninic acid (BCA) assay (Pierce, Rockford, IL). 50μg of protein were separated via electrophoresis on a 10% or 12% SDS-polyacrylamide gel, depending upon the main protein of interest for analysis. Protein was transferred overnight at 4°C in transfer buffer [in mM: 25 Tris base,

192 glycine, 10% (v/v) methanol] to a PDVF membrane (Millipore, Billerica, MA). Protein-containing PDVF membranes were blocked for 1h at room temperature in blocking buffer (BB) [4% bovine serum albumin (BSA), 0.2% Tween-20 in Tris-buffered saline (TBS, pH 7.4)]. Following blocking, membranes were washed 2X in wash buffer (WB) [0.2% Tween-20 in Tris-buffered saline (TBS, pH 7.4)]. Next, membranes were incubated overnight (or 1h at room temperature) with primary antibody diluted in primary antibody buffer (PAB) [1% bovine serum albumin (BSA), 0.2% Tween-20 in Tris-buffered saline (TBS, pH 7.4)]. The following primary antibodies [with their dilution used] were examined: mouse anti-Bax (6A7 clone) [1:1000], rabbit anti-IL-1 β [1:500], mouse anti-poly-ADP-ribose polymerase 1 (PARP-1) (clone C-2-10) [1:500], mouse anti-Lamin B₁ [1:1000] (Invitrogen, Carlsbad, CA), rabbit anti-I κ B- α [1:1000] (Santa Cruz Biotechnology, Santa Cruz, CA), mouse anti-COXIV [1:4000] (Abcam, Cambridge, MA), rabbit anti-high mobility group protein 1 (HMG1/HMGB1) [1:1000], rabbit anti-caspase 12 (C-terminus) [1:1000] (Millipore, Billerica, MA), mouse anti-PDI [1:1000] (Assay Designs, Inc., Ann Arbor, MI), mouse anti-alpha fodrin [1:1000] (BIOMOL International, LP, Plymouth Meeting, PA), rabbit anti-phospho-p53 (Ser15) [1:1000], rabbit anti-cleaved caspase 3 [1:1000], rabbit anti-apoptosis inducing factor (AIF) [1:500] (Cell Signaling Technologies, Inc., Danvers, MA) and mouse anti- β -actin [1:50000] (Sigma-Aldrich, Saint Louis, MO). After incubation with the primary antibody, membranes were washed 6X 10min in WB. Following these washes, the membranes were incubated 1h at room temperature with the

appropriate secondary antibody diluted in secondary antibody buffer (SAB) [0.5% bovine serum albumin (BSA), 0.2% Tween-20 in Tris-buffered saline (TBS, pH 7.4)]. The following secondary antibodies were employed: goat anti-mouse-POD, rat adsorbed, and goat anti-rabbit F(ab')₂-POD, human and mouse adsorbed (Southern Biotech, Birmingham, AL). All secondary antibodies were diluted 1:3000, except for mouse anti- β -actin for which the secondary antibody was diluted 1:15000. Following incubation with the secondary antibody, membranes were washed 6X 10min in WB and, then, developed using the enhanced chemiluminescence (ECL) system (GE Healthcare, Piscataway, NJ). Films were scanned and densitometric analyses were performed using AlphaEase software (Alpha Innotech, San Leandro, CA). Samples were normalized first to β -actin values and then represented as fold values relative to sham.

Lactate Dehydrogenase (LDH) release cytotoxicity assay. The release of intracellular LDH can be used as a measure of cell death for insult paradigms >12-24h and can be used as a marker of necrosis-induced plasma membrane rupture for insult paradigms <10-12h. The release of intracellular LDH was detected using the Cytotoxicity Detection Kit® (Roche Applied Sciences, Indianapolis, IN), by following the manufacturer's protocol. All steps were carried out at room temperature. Briefly, 100 μ L of LDH-containing medium from control, different dose rotenone-treated, FK506-treated and FK506-pretreated, and different dose rotenone-treated primary neuronal cultures were transferred in triplicate to a 96-

well microplate. Then, the samples were incubated in 100µL of the supplied reaction buffer, containing diaphorase / NAD⁺ / iodotetrazolium chloride, from 20min to 1hr on a rotary shaker (250rpm). During this incubation, multiple readings at 405nm were recorded using a Dynex MRX™ microplate reader (Dynex Technologies, Chantilly, VA). High controls (HC) consisted of medium from control cells lysed with 2% Triton X-100 for 10min at 37°C. Low controls (LC) were medium without incubation with cells. Absorbance values (Abs.) at 490nm (630 nm reference) were represented as % of control cell viability ± S.D., determined via the following equation:

$$\% \text{ cell viability} = 100 - [(Abs - LC) / (HC - LC)] * 100$$

ELISA detection of cytosolic oligonucleosome formation. As a measure of apoptotic cell death, the presence of cytosolic oligonucleosomes (DNA+histone complexes resulting from cleavage at the interlinker regions between histones on DNA) was detected using the Cell Death Detection ELISA® (Roche Applied Sciences, Indianapolis, IN), by following the manufacturer's protocol. All steps were carried out at room temperature. Briefly, a 96-well microplate was coated for 1.5h with a mouse monoclonal antibody, diluted in supplied coating buffer (clone H11-4 to the histones H2A, H2B, H3 and H4). The plate was then incubated in the supplied incubation buffer for 0.5h. 50µg of cytosolic protein from each sample loaded in triplicate wells was diluted in incubation buffer. The cytosolic samples were incubated for 1.5h. After incubation, the microplate was washed 3X with supplied wash buffer and then incubated for 1.5h in a peroxidase

conjugated antibody to DNA, diluted in incubation buffer. The microplate, again, was washed 3X in wash buffer and then incubated for 5 min to 1h in 2,2-azino-bis(3-ethylbenzthiazoline-6-sulphonic acid) (ABTS) substrate solution on a rotary shaker (250rpm). During this incubation, multiple readings at 405nm were recorded using a Dynex MRX™ microplate reader (Dynex Technologies, Chantilly, VA). Absorbance values at 405nm were represented as fold change relative to sham absorbance values at 405nm.

Cell preparation for immunofluorescent staining. Rotenone treatment duration was selected based on the time point at which biochemical markers demonstrated a difference between the apoptotic and necrotic-like stimuli (Fig. 2A, B). At these time points, neurons, plated on Assistent glass cover slips (No. 1.5 thickness) (Harvard Apparatus, Holliston, MA), were washed once with ice cold PBS and, then, fixed with 4% paraformaldehyde / 10% sucrose PBS for 15min at room temperature. Fixed cells were washed 3X 5mins in 1XPBS, subsequently post-fixed with ice cold methanol for 5min at -20°C, and then allowed to air dry at room temperature for 30min.

After air drying, neurons were washed 3X for 5min in immunocytochemistry wash buffer (IWB) (1X PBS, 0.45µm filter-sterilized, pH 7.4). Then, neurons were blocked for 1h with IWB+ 5%(v/v) normal goat serum (NGS)+ 0.3% Triton X-100. After removal of the blocking solution, neurons were incubated overnight in a humidified chamber with the primary antibodies diluted in IWB+ 1%(v/v) normal goat serum (NGS) + 0.3% Triton X-100. The following

primary antibodies [with their dilutions used] were examined: rabbit anti-Bax (N-terminus) [1:200] (Millipore, Billerica, MA), mouse anti-PDI [1:100] (Assay Designs, Inc., Ann Arbor, MI) and mouse anti-ATP synthase β [1:100] (Abcam, Cambridge, MA). Following overnight incubation, neurons were washed 3X for 5min in IWB. Then, neurons were incubated for 1h with appropriate fluorescent secondary antibodies diluted in IWB. The following secondary antibodies [and their dilutions] were employed: AlexaFluor 568 goat anti-rabbit [1:1000] and AlexaFluor 488 goat anti-mouse [1:1000] (Invitrogen, Carlsbad, CA). Again, neurons were washed 3X for 5min in high salt IWB (IWB + 4.676g NaCl / 200mL of IWB). Following these wash steps, Vectashield mounting medium containing DAPI (Vector Labs, Burlingame, CA) was applied to the neurons and were placed on top of glass slides and sealed with clear nail polish. Fluorescent stained slides were stored in the dark at -20°C until viewing. Sets of slides to be used for comparison studies using the same primary antibodies were performed on the same day to eliminate inter-experimental variance.

Confocal microscopy. Fluorescent stained slides were viewed using the Biorad Radiance 2100 laser scanning system (Carl Zeiss, Thornwood, NY) fitted onto a Nikon Eclipse E800 microscope (Nikon, Melville, NY). Images were collected using LaserSharp 2000 software (Carl Zeiss, Thornwood, NY). Fluorescence was detected using the following laser and emission filter sets: for cyan fluorophores, a 405nm laser with an HQ442/45 emission filter, for green fluorophores, a 488nm laser with an HQ515/30 emission filter, and for red

fluorophores, a 568nm laser with an E600LP emission filter. Two dichroic mirrors were placed along the optical path to prevent fluorescence bleed-through- a 500DCLPXR mirror for the cyan and green fluorophores and a 560DCLPXR for the green and red fluorophores. A third 100% deflection mirror was used when imaging the cyan fluorophore.

Control neurons were used to set the baseline parameters for laser intensity, gain and offset for slides stained with the same primary antibodies. Using the SETCOL lookup table (LUT), the three parameters were chosen which maximized the width of the gray scale with few red (high intensity) pixels and few green (low intensity) pixels. Optimal pinhole size was computer generated for each laser at each objective. For the Fluor 40X oil (NA 1.3), the pinhole settings were as follows: for 405nm, 0.9mm, for 488nm, 1.1mm and for 568, 1.3mm. For the Plan Apo 60X oil (NA 1.4), the pinhole settings were as follows: for 405nm, 1.3mm, for 488nm, 1.5mm and for 568nm, 1.8mm. After the parameters had been selected, the settings were maintained for all images taken involving the same primary antibodies and the entire image set was collected on the same day.

Images were scanned using the sequential scan setting for the three lasers, set at a scan rate of 50 lines per second (lps), and using a Kalman averaging (N=6) to minimize background signal. A 60X oil PlanAPO objective (NA 1.4) was used to acquire images for analyzing the presence of Bax colocalization with particular subcellular organelles, a 20X Plan APO (NA 0.75)

for characterizing cell types after primary isolation and a Fluor 40X oil objective (NA 1.3) was used to acquire images for the blind counting of the cells within regions of interests (ROIs) which exhibited Bax colocalization with a particular subcellular organelle. Sets of 40X confocal images for each primary antibody combination were counted by the same blind reviewers to minimize reviewer-to-reviewer variability. Prior to analysis, collected images were deconvolved using a 2D iterative deconvolution plug-in based on the DAMAS algorithm (Brooks and Humphreys, 2004; Dougherty, 2005) for NIH ImageJ shareware (<http://rsb.info.nih.gov/ij/>). *Magnetic Resonance Imaging*. T2-weighted magnetic resonance images (MRI) were acquired with a Bruker 7 Tesla MRI scanner using a quadrature surface coil. For MRI scans, P7 and P8 Wistar rat pups, anesthetized with 2.5% isoflurane, were placed on a custom built Plexiglas bed. Respiratory rate, EKG, oxygen saturation and body temperature were continuously monitored during the MRI scans and a feedback-controlled warm air heating system maintained body temperature at $37.0 \pm 0.1^{\circ}\text{C}$. T2-MRI data were acquired as dual echo fast spin echo (FSE) images using the following imaging parameters: TR (repetition time) = 5s, TE (echo time) = 10.096ms, acquisition matrix = 256 pixels x 256 pixels, field of view = 35mm (resulting spatial resolution = 0.1367mm x 0.1367 mm) and slice thickness = 0.5mm. Each brain scan consisted of 25-30 contiguous slice locations with each resulting slice image equaling the average of 4 images at that location. Total scan time for each brain was 16min.

Lesion volume analysis of T2-MRI scans were analyzed using the MeasureStack plug-in for NIH ImageJ shareware (<http://rsb.info.nih.gov/ij/>). Briefly, cortices of MRI brain scans were blocked around the parietal cortex from just posterior to the hippocampal formation until just anterior to the caudal occipital cortex. ROIs, at each slice, were placed around lesions within the cortex and, then, the lesion volumes for each blocked cortical region were calculated. MRI lesion volume rendering was performed using the 360° 3D Stack Macro plug-in for NIH ImageJ shareware (<http://rsb.info.nih.gov/ij/>).

Statistical Analysis. Statistical analyses were performed using GraphPad Prism 5 software (GraphPad Software, San Diego, CA). For analyses involving two groups, a student's t-test was performed and a p-value less than 0.05 was considered significant. If variances for the two groups were deemed significantly different, a Welch correction was added to the student's t-test. For analyses involving two or more groups, a one-way analysis of variance (ANOVA) was performed with a Tukey-Kramer post-hoc test to compare groups. A p-value of less than 0.05 was deemed significant. A chi-squared test, including calculation of relative risk, was performed for MRI lesion volume analyses.

Results

FK506 reduces both 25 μ M and 100 μ M rotenone-induced cell death

Reports have shown FK506, an immunophilin used in chemotherapeutic treatment regimens as an immunosuppressant, possesses neuroprotective

properties mediated primarily by its inhibition of protein phosphatase 2B (PP2B, or calcineurin) and, in part, due to an unknown cytoprotective mechanism (Almeida et al., 2004; Manakova et al., 2005; Pardo et al., 2006; Shou et al., 2004). In addition, FK506 treatment has been shown to reduce mitochondria Bax translocation and apoptotic cell death induced by 3-nitropropionic acid (Almeida et al., 2004). Therefore, we sought to ascertain the neuroprotective effects of FK506 on different dose rotenone models of apoptotic and necrotic-like cell death.

We found 16h (the empirically determined insult time producing 50% cell death treatment in both treatments) with FK506 had no effect on cell viability when compared to control cells exposed to the same concentration of DMSO used to solubilize FK506 (Fig. 25A). In addition for both 25 μ M and 100 μ M, we found a 1h pretreatment and maintained treatment with FK506 throughout insult dose-dependently increased cell viability [for 25 μ M rotenone: 0.1 μ M FK506, ($106 \pm 5.6\%$; $p < 0.001$), 1 μ M FK506, ($103 \pm 13\%$; $p < 0.001$), 10 μ M FK506, ($99.1 \pm 11\%$; $p < 0.001$), / for 100 μ M rotenone: 0.01 μ M FK506, ($89.9 \pm 4.4\%$; $p < 0.001$), 0.1 μ M FK506, ($90.3 \pm 7.5\%$; $p < 0.001$), 1 μ M FK506, ($93.3 \pm 6.8\%$; $p < 0.001$), 10 μ M FK506, ($97.6 \pm 1.2\%$; $p < 0.001$)], with 1 μ M FK506 yielding greatest neuroprotection, when compared to 16h insult alone (Fig. 25B-C).

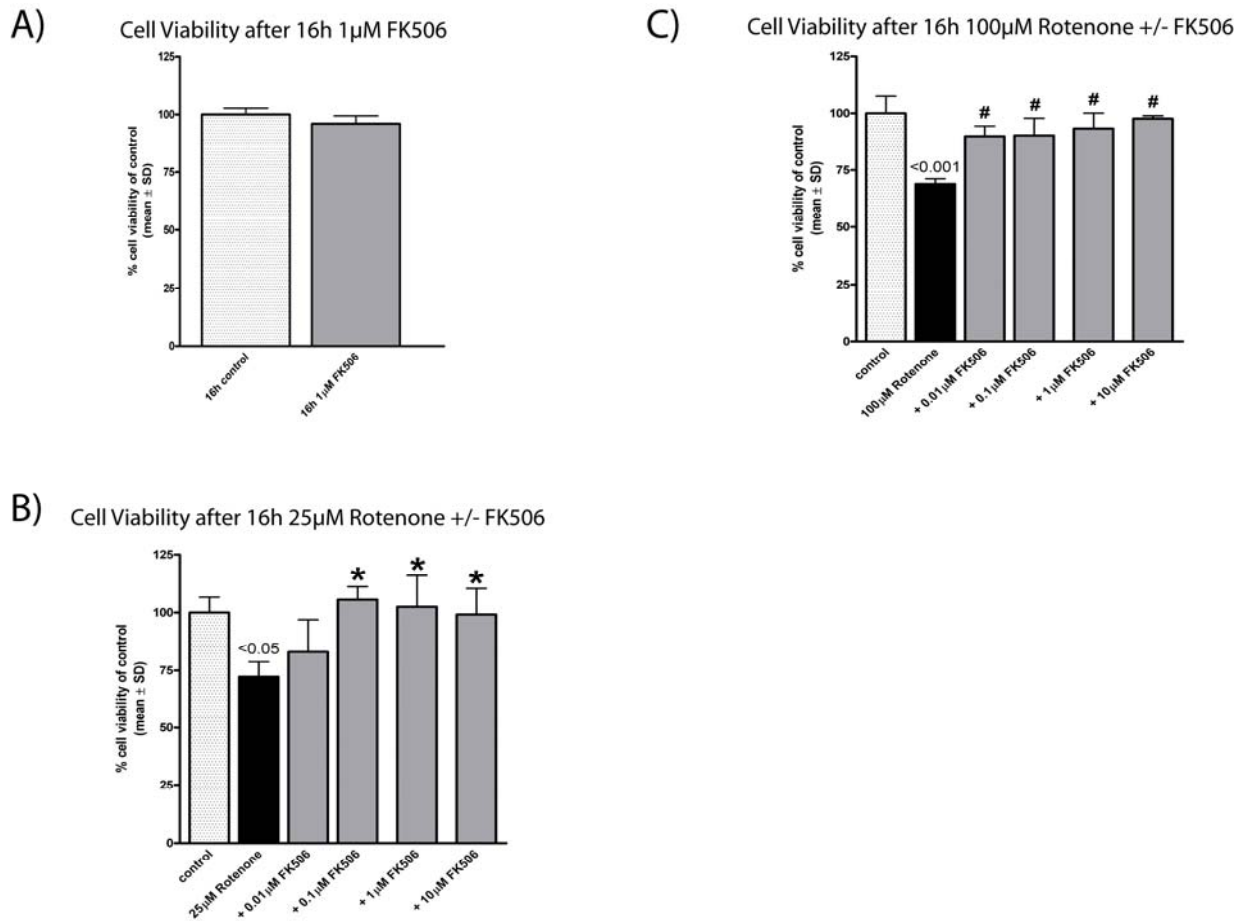


Figure 25. FK506 reduces both 25μM and 100μM rotenone-induced cell death.

A) 1μM FK506 has no effect on cell viability. LDH cytotoxicity data gathered at 16h of 25μM and 100μM rotenone insults. Data are represented as % cell viability of 0h control cultures ± S.D. B) FK506 pretreatment dose-dependently decreases 25μM rotenone-induced cell death at 16h (0.1μM FK506, (106 ± 5.6%; p<0.001), 1μM FK506, (103 ± 13%; p<0.001), 10μM FK506, (99.1 ± 11%; p<0.001). LDH cytotoxicity data gathered at 16h of 25μM insults ± FK506. Data are represented as % cell viability of 0h control cultures ± S.D. C) FK506 pretreatment dose-dependently decreases 100μM rotenone-induced cell death at 16h (0.01μM FK506, (89.9 ± 4.4%; p<0.001), 0.1μM FK506, (90.3 ± 7.5%; p<0.001), 1μM FK506, (93.3 ± 6.8%; p<0.001), 10μM FK506, (97.6 ± 1.2%; p<0.001). LDH cytotoxicity data gathered at 16h of 100μM insults ± FK506. Data are represented as % cell viability of 0h control cultures ± S.D. p-values above columns denote significance relative to 0h control cultures.

FK506-pretreatment reduces 25μM rotenone-induced increases in nuclear Bax at 1h insult and mitochondrial Bax at 6h insult.

Because FK506 has been shown to prevent mitochondrial Bax localization in other *in vitro* trauma models, we hypothesized that the observed FK506-mediated decreases in cell death from 25μM rotenone insult (Fig. 25B) resulted from inhibition of 25μM rotenone-induced mitochondrial Bax localization. In accordance, we observed 1h pretreatment and maintained treatment with 1μM FK506 throughout insult of primary neuronal cultures reduced mitochondrial Bax levels when compared to FK506-untreated cultures after 6h 25μM rotenone insult ($16.9 \pm 10\%$; $p < 0.05$) (Fig. 27C, D). Surprisingly, FK506 treatment also reduced nuclear Bax levels after 1h 25μM rotenone insult to 0h control values ($13.0 \pm 18\%$; $p < 0.001$) (Fig. 26D), and maintained this decreased nuclear Bax even at 6h 25μM rotenone insult ($32.5 \pm 10\%$; $p < 0.001$) (Fig. 26C, D). These results suggest a common FK506-mediated inhibitory mechanism for preventing localization of Bax to the mitochondria and nucleus after 25μM rotenone insult.

FK506-pretreatment reduces 100μM rotenone-induced increases in nuclear Bax at 1h insult and ER Bax at 6h insult.

Because we observed FK506 to prevent nuclear and mitochondrial Bax localization in our apoptotic rotenone model, we hypothesized that the observed FK506-mediated decreases in cell death from 100μM rotenone insult (Fig. 25C) resulted from inhibition of 100μM rotenone-induced ER Bax localization. In

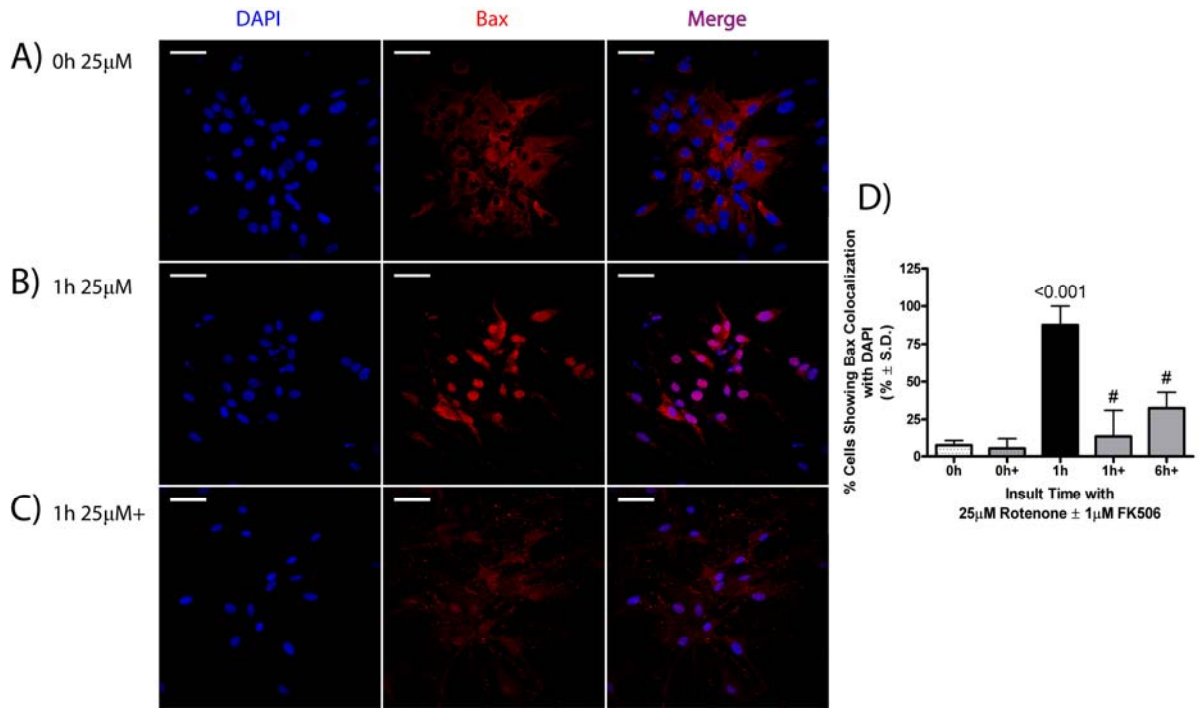


Figure 26. FK506-pretreatment reduces 25μM rotenone-induced increases in nuclear Bax at 1h insult.

A) Primary neurons at 0h 25μM rotenone insult have little to no nuclear Bax fluorescence. Representative 40X confocal fluorescent micrograph of a region of interest (ROI) within primary neuronal cultures. B) Primary neurons at 1h 25μM rotenone insult have increased nuclear Bax fluorescence. Representative 40X confocal fluorescent micrograph of a region of interest (ROI) within primary neuronal cultures. C) FK506-treated primary neurons at 1h 25μM rotenone insult have little nuclear Bax fluorescence. Representative 40X confocal fluorescent micrograph of a region of interest (ROI) within primary neuronal cultures. D) Blinded cell counts of representative ROIs from 0h control, 1h 25μM rotenone insult and FK506-treated at 1h 25μM rotenone insult. Values represent percentage of cells demonstrating colocalization of Bax with the nuclear marker, DAPI. Data are presented as mean percentage of cells expressing colocalization ± S.D. p-values above columns denote significance relative to 0h control cultures. # denotes p<0.001 when compared to 1h 25μM rotenone insult. Scale bars = 50μm.

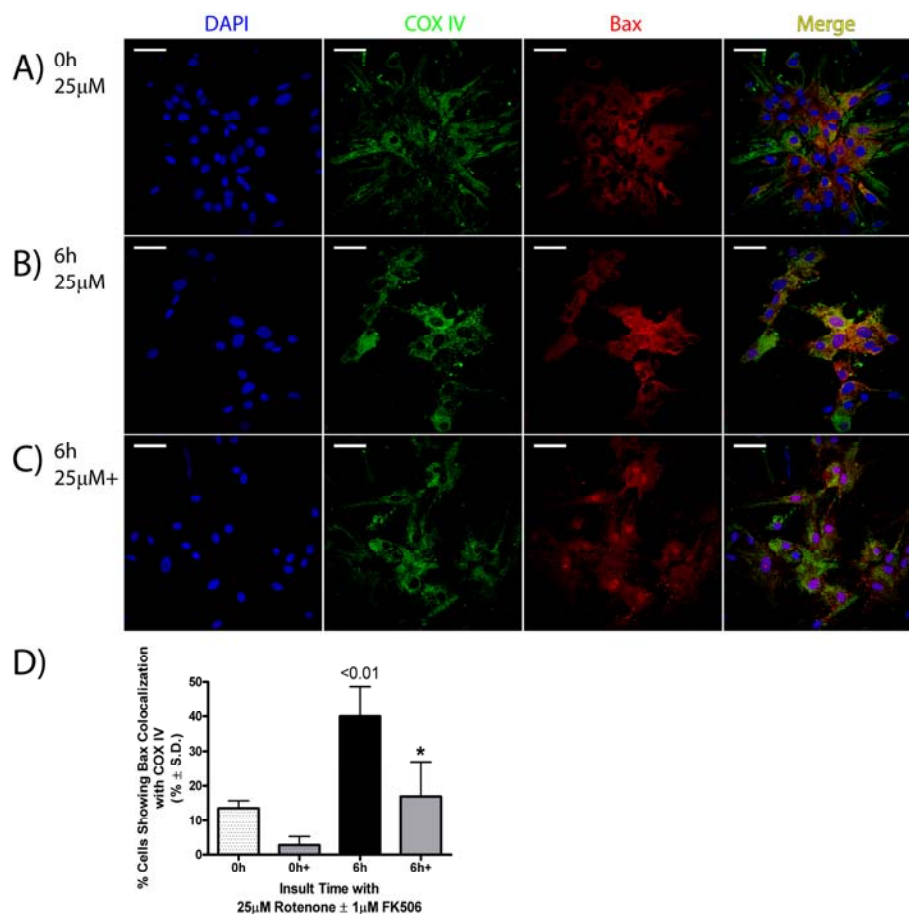


Figure 27. FK506-pretreatment reduces 25μM rotenone-induced increase in mitochondrial Bax at 6h insult.

A) Primary neurons at 0h 25μM rotenone insult have little to no mitochondrial Bax localization. Representative 40X confocal florescent micrograph of a region of interest (ROI) within primary neuronal cultures. B) Primary neurons at 6h 25μM rotenone insult have increased mitochondrial Bax colocalization. Representative 40X confocal florescent micrograph of a region of interest (ROI) within primary neuronal cultures. C) FK506-treated primary neurons at 6h 25μM rotenone insult have little mitochondrial Bax colocalization. Representative 40X confocal florescent micrograph of a region of interest (ROI) within primary neuronal cultures. D) Blinded cell counts of representative ROIs from 0h control, 6h 25μM rotenone insult and FK506-treated at 6h 25μM rotenone insult. Values represent percentage of cells demonstrating colocalization of Bax with the mitochondrial marker, COX IV. Data are presented as mean percentage of cells expressing colocalization ± S.D. p-values above columns denote significance relative to 0h control cultures. * denotes $p < 0.05$ when compared to 6h 25μM rotenone insult. Scale bars = 50μm.

agreement, we observed 1h pretreatment and maintained treatment with 1 μ M FK506 throughout insult of primary neuronal cultures reduced mitochondrial Bax levels to 0h control values when compared to FK506-untreated cultures after 6h 100 μ M rotenone insult ($4.06 \pm 3.5\%$; $p < 0.05$) (Fig. 29C, D). In agreement with our 25 μ M observation, FK506 treatment also reduced nuclear Bax levels after 1h 100 μ M rotenone insult to 0h control values ($9.40 \pm 4.5\%$; $p < 0.001$) (Fig. 28D), and maintained this decreased nuclear Bax even at 6h 100 μ M rotenone insult ($17.3 \pm 9.6\%$; $p < 0.001$) (Fig. 28C, D). Taken together with the 25 μ M rotenone insult findings, these results suggest a common FK506-mediated inhibitory mechanism for preventing localization of Bax to the mitochondria, ER and nucleus after 25 μ M and 100 μ M rotenone insults.

FK506-pretreatment reduces 25 μ M rotenone-mediated increases in caspase-mediated cleavage of the cytoskeletal protein α -fodrin.

In vivo and *in vitro* studies have illustrated activation of mitochondrial-mediated cell death to be apoptotic and mediated by mitochondrial Bax localization (Goping et al., 1998; Koubi et al., 2005). If 25 μ M rotenone insult produces apoptotic cell death, we hypothesized that Bax-mediated cell death pathways should be involved.

If Bax coordinates the activation of mitochondrial cell death signaling (i.e. caspase 3 activation), then, FK506 treatment, which we have shown to decrease

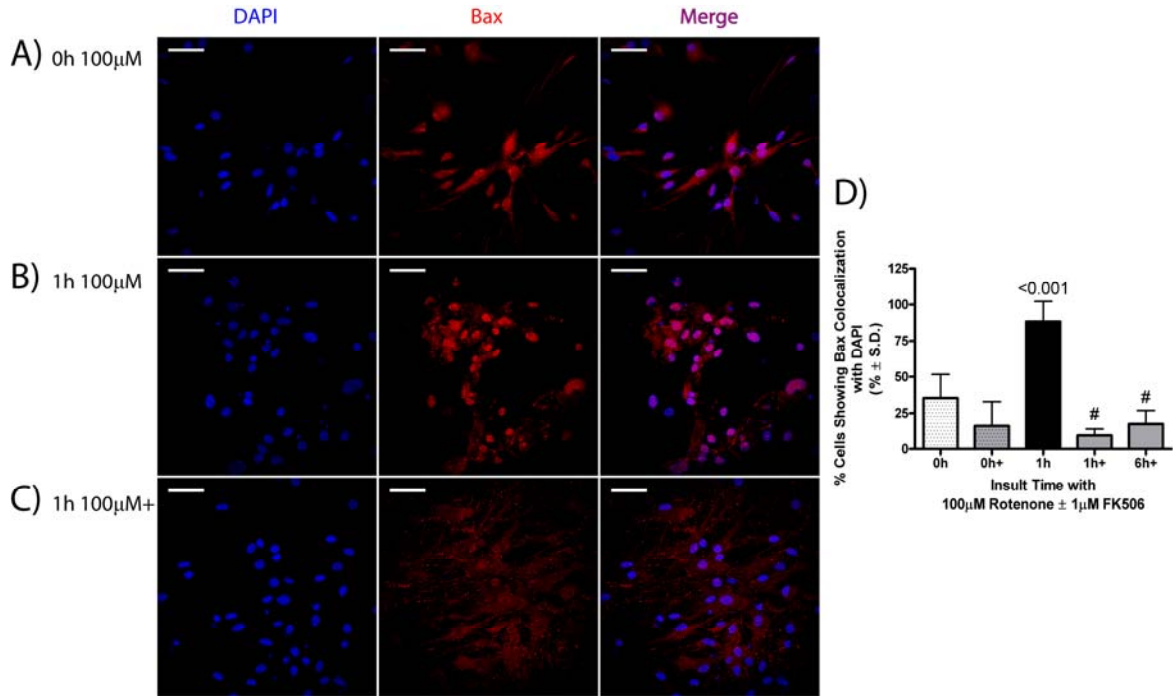


Figure 28. FK506-pretreatment reduces 100μM rotenone-induced increases in nuclear Bax at 1h insult.

A) Primary neurons at 0h 100μM rotenone insult have little to no nuclear Bax fluorescence. Representative 40X confocal florescent micrograph of a region of interest (ROI) within primary neuronal cultures. B) Primary neurons at 1h 100μM rotenone insult have increased nuclear Bax fluorescence. Representative 40X confocal florescent micrograph of a region of interest (ROI) within primary neuronal cultures. C) FK506-treated primary neurons at 1h 100μM rotenone insult have little nuclear Bax fluorescence. Representative 40X confocal florescent micrograph of a region of interest (ROI) within primary neuronal cultures. D) Blinded cell counts of representative ROIs from 0h control, 1h 100μM rotenone insult and FK506-treated at 1h 100μM rotenone insult. Values represent percentage of cells demonstrating colocalization of Bax with the nuclear marker, DAPI. Data are presented as mean percentage of cells expressing colocalization ± S.D. p-values above columns denote significance relative to 0h control cultures. # denotes p<0.001 when compared to 1h 25μM rotenone insult. Scale bars = 50μm.

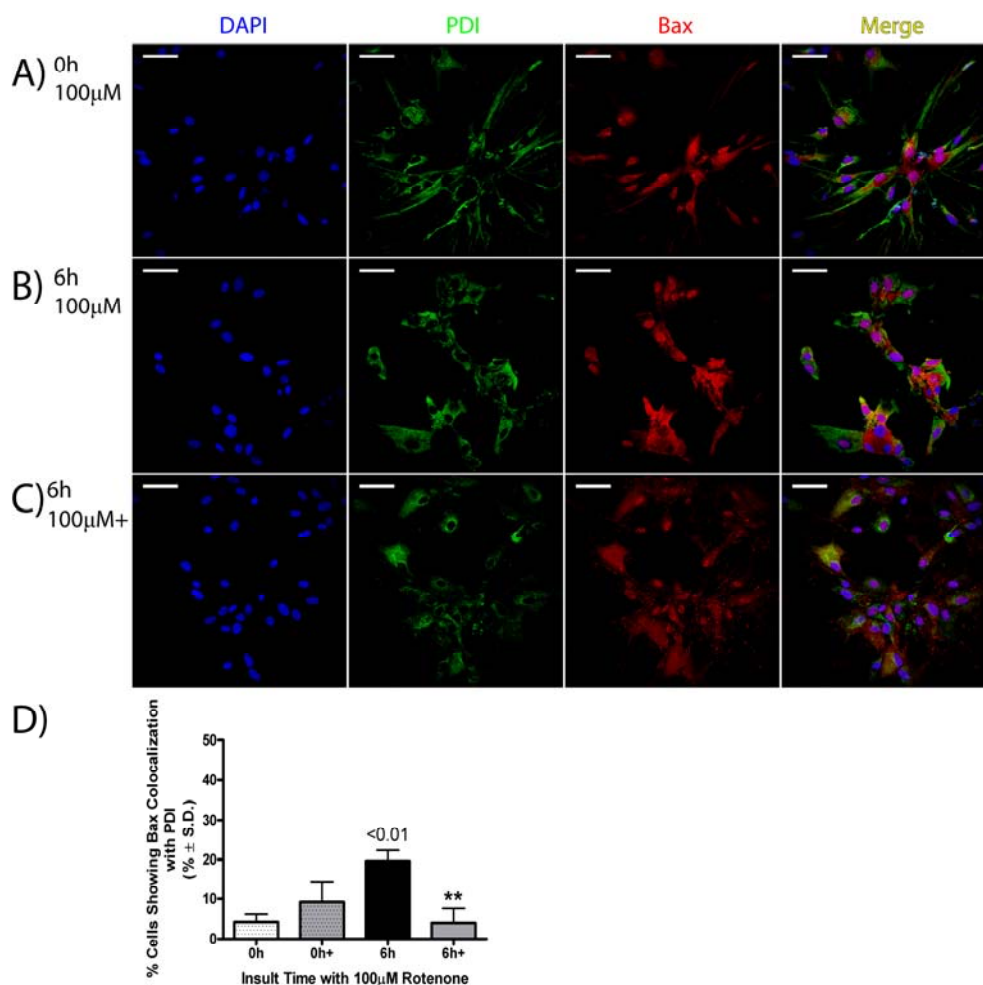


Figure 29. FK506-pretreatment reduces 100μM rotenone-induced increase in ER Bax at 6h insult.

A) Primary neurons at 0h 100μM rotenone insult have little to no ER Bax localization. Representative 40X confocal florescent micrograph of a region of interest (ROI) within primary neuronal cultures. B) Primary neurons at 6h 100μM rotenone insult have increased ER Bax colocalization. Representative 40X confocal florescent micrograph of a region of interest (ROI) within primary neuronal cultures. C) FK506-treated primary neurons at 6h 100μM rotenone insult have little ER Bax colocalization. Representative 40X confocal florescent micrograph of a region of interest (ROI) within primary neuronal cultures. D) Blinded cell counts of representative ROIs from 0h control, 6h 100μM rotenone insult and FK506-treated at 6h 100μM rotenone insult. Values represent percentage of cells demonstrating colocalization of Bax with the ER marker, PDI. Data are presented as mean percentage of cells expressing colocalization ± S.D. p-values above columns denote significance relative to 0h control cultures. ** denotes p<0.01 when compared to 6h 100μM rotenone insult. Scale bars = 50μm.

mitochondrial Bax localization, should, also, decrease calpain activity. In agreement, our preliminary data illustrates FK506 treatment decreased 25 μ M rotenone-induced increases in the 150kD and 120kD α -fodrin fragment levels to near 0h control culture values (Fig. 30A-C). This result substantiates our hypothesis that Bax coordinates the activation of mitochondrial cell death signaling to induce apoptotic cell death.

FK506-pretreatment reduces 100 μ M rotenone-mediated increases in calpain-mediated cleavage of the cytoskeletal protein α -fodrin.

Early *in vitro* studies of activation of ER-mediated cell death described the cell death phenotype as necrotic-like (Kalai et al., 2003; Yoneda et al., 2001). If 100 μ M rotenone insult produces a necrotic-like cell death, we hypothesized that ER-mediated cell death pathways should be involved.

If Bax coordinates the activation of ER cell death signaling (i.e. calpain activation), then, FK506 treatment, which we have shown to decrease ER Bax localization, should, also, decrease calpain activity. In agreement, our preliminary data illustrates FK506 treatment decreased 100 μ M rotenone-induced increases in the 150kD and 145kD α -fodrin fragment levels to near 0h control culture values (Fig. 30A, B, D). This result substantiates our hypothesis that Bax coordinates the activation of ER cell death signaling to induce necrotic-like cell death. In addition, FK506 treatment, also, decreased 100 μ M rotenone-induced increases in the 120kD α -fodrin fragment levels to 0h control culture values (Fig.

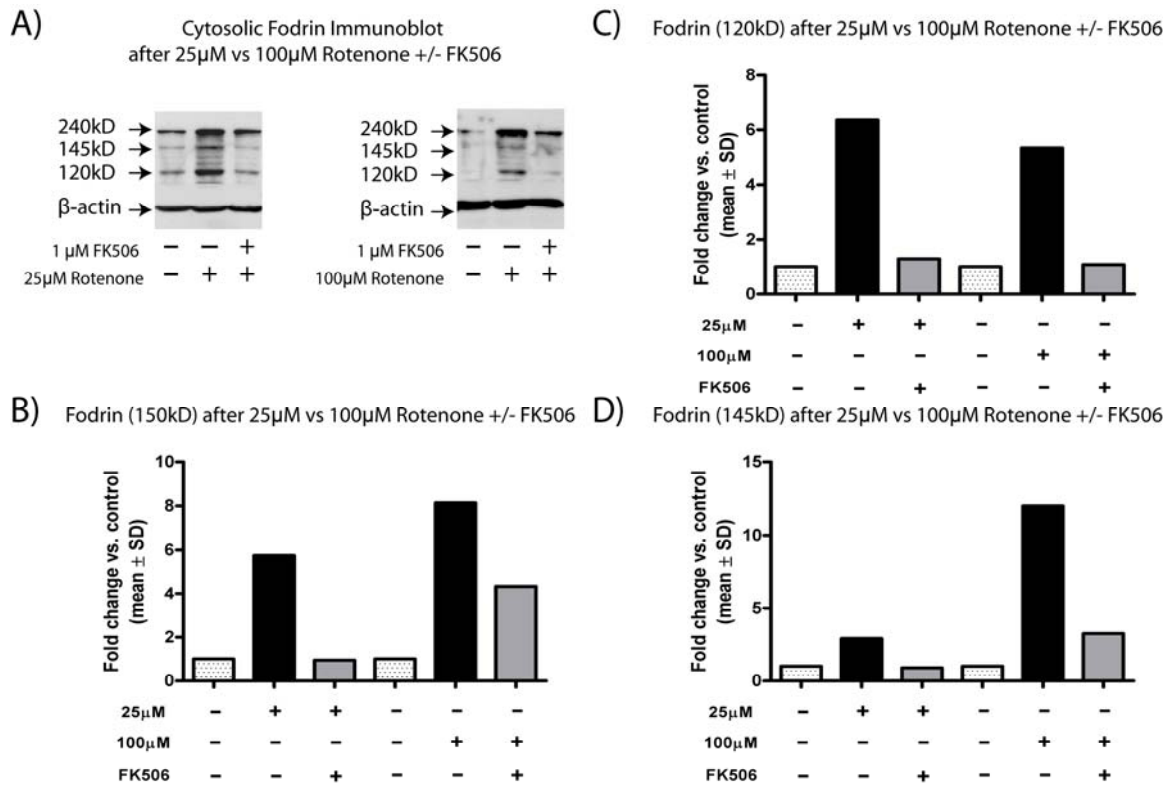


Figure 30. FK506 treatment inhibits 100 μ M rotenone-induced increases in calpain- and caspase-mediated cleavage of α -fodrin, and inhibits 25 μ M rotenone-induced increases in caspase-mediated cleavage of α -fodrin. (Preliminary data)

A) Representative western blots for cleaved α -fodrin at 0h control, 6h insult and FK506-treated 6h insult for both 25 μ M and 100 μ M rotenone. Below, Representative western blots for β -actin. B) FK506 treatment decreases 25 μ M and 100 μ M rotenone-mediated generation of the 150kD α -fodrin fragment. Densitometric values for the 150kD α -fodrin fragment. Densitometric data were normalized to β -actin and are represented as fold change of sham. C) FK506 treatment decreases 25 μ M and 100 μ M rotenone-mediated generation of the caspase-cleaved 120kD α -fodrin fragment. Densitometric values for the 120kD α -fodrin fragment. Densitometric data were normalized to β -actin and are represented as fold change of sham. D) FK506 treatment decreases 100 μ M rotenone-mediated generation of the calpain-cleaved 145kD α -fodrin fragment. Densitometric values for the 145kD α -fodrin fragment. Densitometric data were normalized to β -actin and are represented as fold change of sham.

30C), supporting the coordinating role for Bax in multiple organelle subcellular cell death signaling cascades.

At 24h post HI, hyperoxia therapy Increases HI-induced lesion volume size

The standard clinical treatment for preterm or term newborns suspected of experiencing a hypoxic-ischemic insult is treatment by placement in a warm incubator supplemented with 100% O₂ until they have “pinked up” (pulse oxymetry saturations of 92-96% in term infants and 88-92% in preterm infants). Variable FiO₂ levels are permitted during resuscitation, but if the infant’s condition does not improve after 90 seconds, then a FiO₂ of 1 (100% O₂) is recommended, as it effectively increases the infant’s APGAR (Activity, Pulse, Grimace, Appearance, Respiration) score (Bissinger and Ohning, 2006; de Menezes and Shaw, 2006; Raju, 2006c).

In order to assess the benefit of hyperoxia therapy on HI-injured cortices, we modeled the clinical scenario of hyperoxia therapy by adding to the Rice-Vannucci model of neonatal HI a 2h exposure to 100% O₂. Immediately after the hypoxia component, we saturated the 37°C hypoxia chamber with 100% O₂ until the chamber oxymeter read 100% (<2 minutes) and, then, incubated the HI-injured pups for 2h in the hyperoxic chamber (see Materials and Methods). We hypothesized that 2h 100% hyperoxia therapy would decrease the HI-induced cortical lesion volume in 24h post HI-injured pups as measured by T2-weighted magnetic resonance imaging (T2-MRI). As expected, 24h post-HI cortices

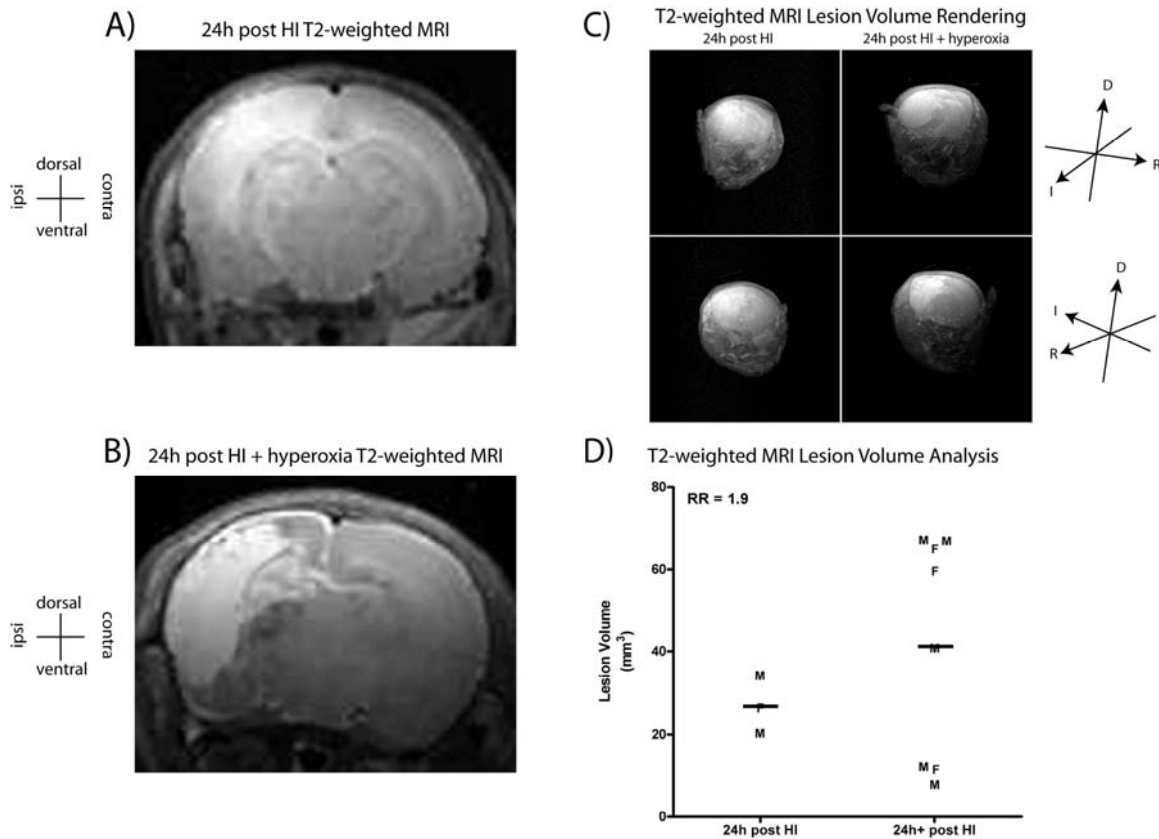


Figure 31. At 24h post HI, hyperoxia therapy increases HI-induced lesion volume size.

A) HI increases injury lesion volume within the ipsilateral cortices of 24h post HI-injured animals. Representative T2-weighted magnetic resonance image (T2-MRI) of a HI-injured rat pup brain at 24h post HI. B) Hyperoxia therapy increases lesion volume within the ipsilateral cortices of 24h post HI-injured animals when compared to untreated 24h post HI-injured animals. Representative T2-MRI of a HI-injured + 2h 100% hyperoxia-treated rat pup brain at 24h post HI. C) Hyperoxia therapy does not change the HI-induce injury localization, but rather enhances the degree of the injury. 3D lesion volume rendering comparing hyperoxia-treated and untreated HI-injured rat pup brains at 24h post HI. XYZ coordinate graphs are included for orientation purposes. D = dorsal, I = ipsilateral and R = rostral. 3D renderings were blocked around the parietal cortex, eliminating brain regions anterior to the hippocampal formation. D) Hyperoxia therapy increases lesion volume within the ipsilateral cortices of 24h post HI-injured animals when compared to untreated 24h post HI-injured animals [24h post HI: $27.00 \pm 7.0 \text{ mm}^3$ vs. 24h post HI + hyperoxia: $41.55 \pm 27.0 \text{ mm}^3$, relative risk = 1.875]. Quantification of lesion volume size from T2-MRIs of HI-injured and HI + hyperoxia rat pup brains. Data are represented as a fold change of sham \pm S.D.

showed dramatic injury in the ipsilateral parietal cortex (Fig. 31A). However, hyperoxia therapy did not decrease but rather increased ipsilateral T2-MRI cortical lesion volume at 24h post HI when compared to 24 post HI-injured cortices with no hyperoxia exposure ($41.6 \pm 27 \text{ mm}^3$; relative risk = 1.9) (Fig. 31B, D).

Hyperoxia therapy does not decrease apoptotic cell death signaling, but does increase inflammatory signaling after HI

In order to characterize the exacerbating effects of hyperoxia on HI-mediated cell death, we selected the 3h post HI time point because it is at this time after HI that there was significant activation of apoptotic cell death cascades (Fig. 11). First, we hypothesized that hyperoxia therapy increased ipsilateral cortical lesion volume via increasing apoptosis relative to HI alone-treatment. To test this hypothesis, we measured the levels of cytosolic caspase 3 cleavage and cytosolic oligonucleosome levels. Interestingly, at 3h post HI, hyperoxia (3hHHI) did not increase either cytosolic cleaved caspase 3 or cytosolic oligonucleosome levels in hyperoxia-treated, ipsilateral cortices when compared to ipsilateral cortices from HI-injured pups with no hyperoxia treatment (3hHI) at 3h post-HI, although in both groups HI did significantly increase cytosolic cleaved caspase 3 [(3hHI, 3.13 ± 1.4 ; $p < 0.05$) (3hHHI, 2.90 ± 0.54 ; $p < 0.05$)] and cytosolic oligonucleosome levels [(3hHI, 1.85 ± 0.49 ; $p < 0.05$) (3hHHI, 1.76 ± 0.30 ; $p < 0.05$)] relative to sham-treated cortices (Fig. 32A, B)]. As another marker for

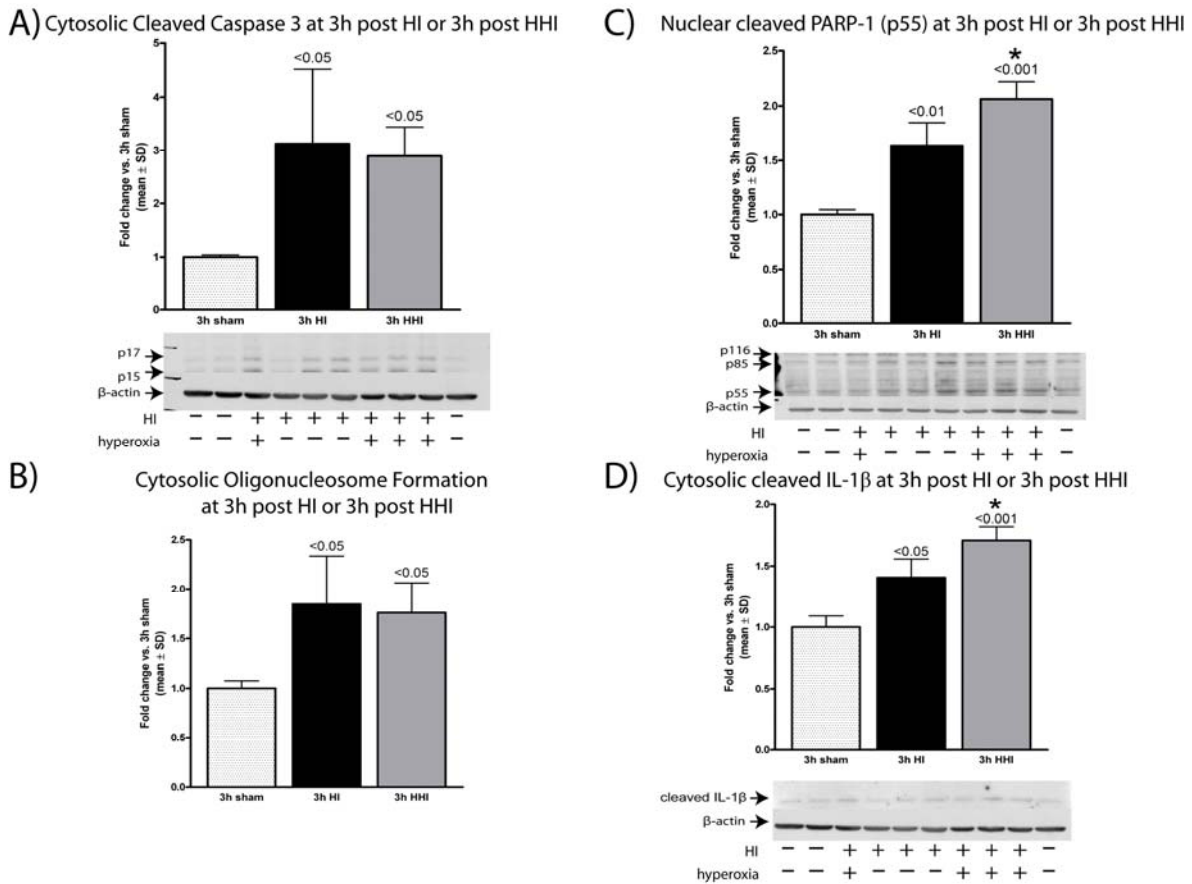


Figure 32. Hyperoxia therapy does not decrease apoptotic cell death signaling, but does increase inflammatory signaling.

A) Hyperoxia therapy has no effect on cytosolic cleaved caspase 3 levels within the ipsilateral cortices of 3h post HI-injured animals when compared to untreated 3h post HI-injured animals [3hHI; 3.126 ± 1.39 ($p<0.05$), 3hHHI; 2.897 ± 0.54 ($p<0.05$) vs. sham (1.000 ± 0.04)]. Densitometric values for cytosolic cleaved caspase 3 (p17 + p15) levels in 3h sham, 3h post HI-injured and 3h post HI-injured + hyperoxia cortices. Below, representative Western blot for cytosolic cleaved caspase 3 and β -actin levels at 3h post HI. B) Hyperoxia therapy has no effect on cytosolic oligonucleosome levels within the ipsilateral cortices of 3h post HI-injured animals when compared to untreated 3h post HI-injured animals [3hHI; 1.848 ± 0.49 ($p<0.05$), 3hHHI; 1.761 ± 0.30 ($p<0.05$) vs. sham (1.000 ± 0.08)]. Cytosolic oligonucleosomes levels in 3h sham, 3h post HI-injured, and 3h post HI-injured + hyperoxia cortices. Data are represented as fold change of sham \pm S.D. C) Hyperoxia therapy increases nuclear 55kD cleaved PARP-1 levels within the ipsilateral cortices of 3h post HI-injured animals when compared to untreated 3h post HI-injured animals [3hHI; 1.636 ± 0.21 ($p<0.01$), 3hHHI; 2.063 ± 0.16 ($p<0.001$) vs. sham (1.000 ± 0.05); $p<0.05$, 3hHI vs. 3hHHI]. Densitometric values for nuclear 55kD cleaved PARP-1 levels in 3h sham, 3h post HI-injured and 3h post HI-injured + hyperoxia

cortices. Below, representative Western blot for nuclear cleaved PARP-1 and β -actin levels at 3h post HI. D) Hyperoxia therapy increases cytosolic cleaved interleukin 1-beta (IL-1 β) levels within the ipsilateral cortices of 3h post HI-injured animals when compared to untreated 3h post HI-injured animals [3hHI; 1.405 ± 0.15 ($p < 0.05$), 3hHHI; 1.711 ± 0.11 ($p < 0.001$) vs. sham (1.000 ± 0.09): $p < 0.05$, 3hHI vs. 3hHHI]. Densitometric values for cytosolic cleaved IL-1 β levels in 3h sham, 3h post HI-injured and 3h post HI-injured + hyperoxia cortices. Below, representative Western blot for cytosolic cleaved IL-1 β and β -actin levels at 3h post HI. Densitometric data were normalized to β -actin and are represented as fold change of sham \pm S.D. Numerical value above column bars denotes p-value when compared to sham. *; $p < 0.05$ when compared to HI alone.

apoptotic signaling, we measured the nuclear levels of the cleaved 85kD poly-ADP ribose polymerase 1 (PARP-1) fragment. Again, hyperoxia did not significantly increase nuclear 85kD PARP-1 levels in the hyperoxia-treated, ipsilateral cortices when compared to ipsilateral cortices from HI-injured pups with no hyperoxia treatment at 3h after HI, although both groups also had increased levels of 85kD PARP-1 fragments [(3hHI, 2.74 ± 0.20 ; $p < 0.001$) (3hHHI, 3.27 ± 0.31 ; $p < 0.001$)] (Fig. 35C).

Since the hyperoxia treatment had no effect on apoptosis, we hypothesized that the hyperoxia-induced increases in lesion volume observed by MRI could be due to increased necrosis in the hyperoxia-treated, HI-injured ipsilateral cortex relative to HI-injured cortices with no hyperoxia treatment. To test this hypothesis, we asked if the nuclear levels of cleaved 55kD PARP-1 fragment would increase and the levels of high mobility group box 1 (HMGB1) protein would decrease, both changes widely used as cellular markers for necrosis, after hyperoxia treatment of HI.

Hyperoxia treatment of HI increased nuclear 55kD PARP-1 levels significantly ($p < 0.05$) in ipsilateral cortices compared to ipsilateral cortices from HI-injured pups with no hyperoxia treatment at 3h, and both groups had increased nuclear 55kD PARP-1 levels relative to the sham-treated pups [(3hHI, 1.64 ± 0.21 ; $p < 0.01$) (3hHHI, 2.06 ± 0.16 ; $p < 0.001$)] (Fig.32C). Furthermore at 3h post HI, there was significantly decreased ($p < 0.05$) nuclear HMGB1 levels in the hyperoxia-treated, ipsilateral cortices compared to ipsilateral cortices from HI-injured pups with no hyperoxia treatment (Fig. 35A). This hyperoxia-induced increase in necrosis should result in increased inflammatory signaling. We measured cytosolic cleaved interleukin 1-beta (IL-1 β), a known marker of cellular inflammation, to determine if the hyperoxia treatment of HI was stimulating inflammation. Hyperoxia treatment of HI resulted in increased ($p < 0.05$) ipsilateral cortical cleaved IL-1 β levels at the 3h post HI time point compared to pups exposed to HI without hyperoxia treatment and both groups also had higher levels of cleaved IL-1 β levels compared to the sham-treated pups [(3hHI, 1.41 ± 0.15 ; $p < 0.05$) (3hHHI, 1.71 ± 0.11 ; $p < 0.001$)] (Fig. 32D). Thus, hyperoxia-increased lesion volumes in the HI-injured cortices also stimulated inflammation.

Hyperoxia therapy increases calpain-mediated but not caspase-mediated cleavage of cytosolic α -fodrin

Early *in vitro* studies of activation of ER-mediated cell death described the cell death phenotype as necrotic-like (Kalai et al., 2003; Yoneda et al., 2001). If

hyperoxia-treatment increases HI-induced ipsilateral cortical lesion volume through increased inflammation, we hypothesized that ER-mediated cell death pathways could be involved.

In order to measure the contributions of both apoptosis and necrosis to the hyperoxia-mediated increases in lesion size volume, we measured the cleavage of the cytosolic cytoskeletal protein, α -fodrin, which has been widely reported to yield protease-specific cleavage fragments: a 150kD fragment resulting from cumulative ER calpain and cytosolic caspase 3-mediated cleavage (contributing to both apoptosis and necrosis), a 145kD fragment resulting from ER calpain-mediated cleavage alone (contributing to necrosis) and a 120kD fragment resulting from cytosolic caspase 3-mediated cleavage (contributing to apoptosis alone (Blomgren et al., 2001; Cryns et al., 1996; Vanags et al., 1996)). The hyperoxia treatment increased cytosolic cleaved 150kD ($p < 0.05$) and 145kD ($p < 0.05$) α -fodrin levels but had no effect on cytosolic cleaved 120kD α -fodrin ipsilateral cortical levels compared to the non-hyperoxia treated cortices at 3h post-HI and both the hyperoxia-treated and non-treated HI groups had increased levels of 150kD [(3hHI, 1.60 ± 0.13 ; $p < 0.05$) (3hHHI, 2.18 ± 0.32 ; $p < 0.01$)], 145kD [(3hHI, 1.77 ± 0.15 ; $p < 0.05$) (3hHHI, 2.46 ± 0.33 ; $p < 0.001$)] and 120kD [(3hHI, 1.78 ± 0.16 ; $p < 0.01$) (3hHHI, 1.59 ± 0.19 ; $p < 0.05$)] compared to sham-treated pups (Fig. 33A-D). Thus, hyperoxia increased activation of ER calpain-mediated cell death relative to mitochondria-mediated cell death, indicative of increased cell death with necrotic characteristics.

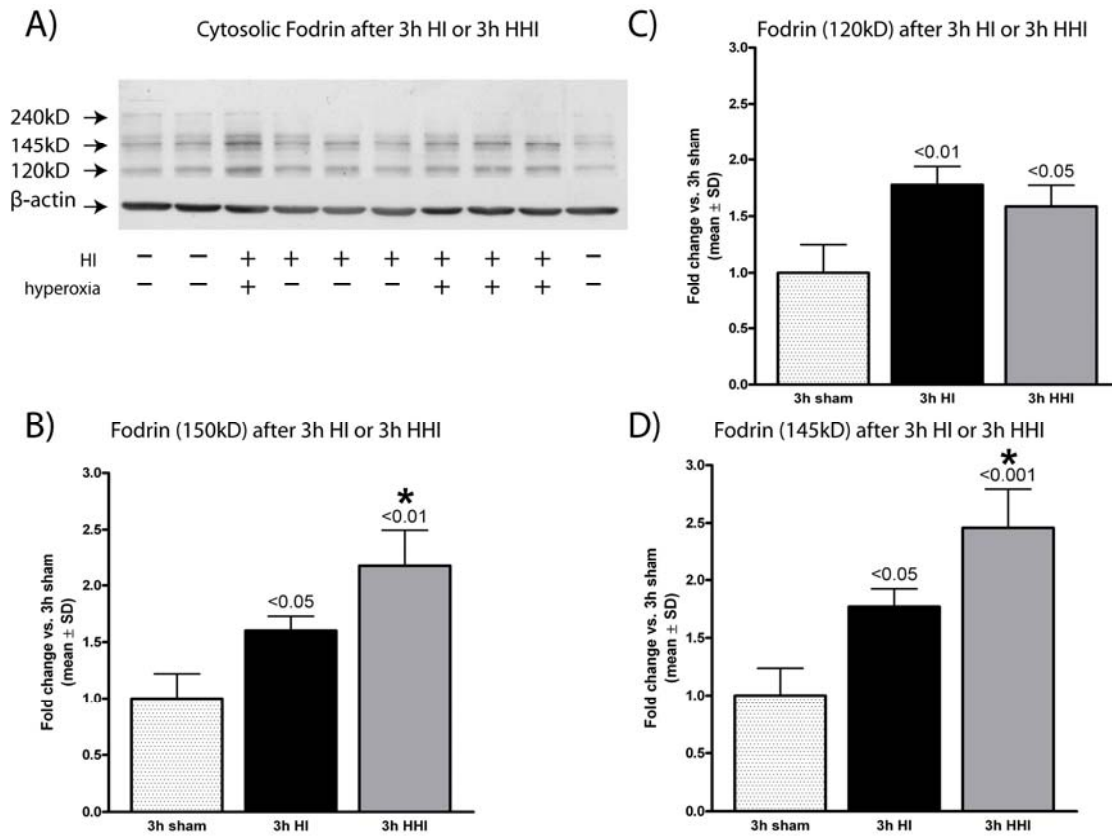


Figure 33. Hyperoxia therapy increases calpain-mediated but has no effect on caspase-mediated cleavage of cytosolic α -fodrin.

A) Western blot of cytosolic cleaved α -fodrin levels in 3h sham, 3h post HI-injured, and 3h post HI-injured + hyperoxia cortices. β -actin was used as a loading control. B) Hyperoxia therapy increases cytosolic 150kD cleaved α -fodrin levels within the ipsilateral cortices of 3h post HI-injured animals when compared to untreated 3h post HI-injured animals [3hHI; 1.602 ± 0.13 ($p<0.05$), 3hHHI; 2.175 ± 0.32 ($p<0.01$) vs. sham (1.000 ± 0.22): $p<0.05$, 3hHI vs. 3hHHI]. Densitometric values for the cytosolic 150kD cleaved α -fodrin fragment levels in 3h sham, 3h post HI-injured and 3h post HI-injured + hyperoxia cortices. C) Hyperoxia therapy has no effect on cytosolic 120kD cleaved α -fodrin levels within the ipsilateral cortices of 3h post HI-injured animals when compared to untreated 3h post HI-injured animals [3hHI; 1.776 ± 0.16 ($p<0.01$), 3hHHI; 1.586 ± 0.19 ($p<0.05$) vs. sham (1.000 ± 0.22)]. Densitometric values for the cytosolic 120kD cleaved α -fodrin fragment levels in 3h sham, 3h post HI-injured and 3h post HI-injured + hyperoxia cortices. D) Hyperoxia therapy increases cytosolic 145kD cleaved α -fodrin levels within the ipsilateral cortices of 3h post HI-injured animals when compared to untreated 3h post HI-injured animals [3hHI; 1.771 ± 0.15 ($p<0.05$), 3hHHI; 2.459 ± 0.33

($p < 0.001$) vs. sham (1.000 ± 0.24); $p < 0.05$, 3hHI vs. 3hHHI]. Densitometric values for the cytosolic 145kD cleaved α -fodrin fragment levels in 3h sham, 3h post HI-injured and 3h post HI-injured + hyperoxia cortices. Densitometric data were normalized to β -actin and are represented as fold change of sham \pm S.D. Numerical value above column bars denotes p-value when compared to sham. *; $p < 0.05$ when compared to HI alone.

Hyperoxia therapy increases ER Bax levels but not nuclear and mitochondrial

Bax levels

ER Bax is known to promote a greater release of Ca^{2+} and activation of ER calpain-mediated cell death (Nutt et al., 2002b; Oakes et al., 2005; Oakes et al., 2003; Scorrano et al., 2003; Zong et al., 2003). Thus, since hyperoxia therapy selectively increased calpain-mediated cleavage but not caspase 3-mediated cleavage, we hypothesized that, if hyperoxia therapy increased ER-mediated cell death, then, there should be a selective increase in ER Bax levels but not mitochondrial Bax levels in the hyperoxia-treated ipsilateral cortices of HI-injured pups compared to their HI alone-treated cohorts.

When we measured Bax levels in each subcellular fraction, hyperoxia treatment of HI did not significantly increase mitochondrial or nuclear Bax levels but did significantly increase ($p < 0.05$) ER Bax levels when compared to HI exposure alone, although both hyperoxia-treated and untreated pups exposed to HI showed higher Bax levels in mitochondria [(3hHI, 1.50 ± 0.063 ; $p < 0.05$) (3hHHI, 1.64 ± 0.16 ; $p < 0.05$)], nuclei [(3hHI, 1.55 ± 0.27 ; $p < 0.05$) (3hHHI, 1.73 ± 0.25 ; $p < 0.05$)] and ER [(3hHI, 1.87 ± 0.17 ; $p < 0.05$) (3hHHI, 2.77 ± 0.21 ; $p < 0.001$)] compared to the sham-treated pups (Fig. 34B-D). Thus, hyperoxia therapy increases HI-induced cortical lesion volume through increased Bax-

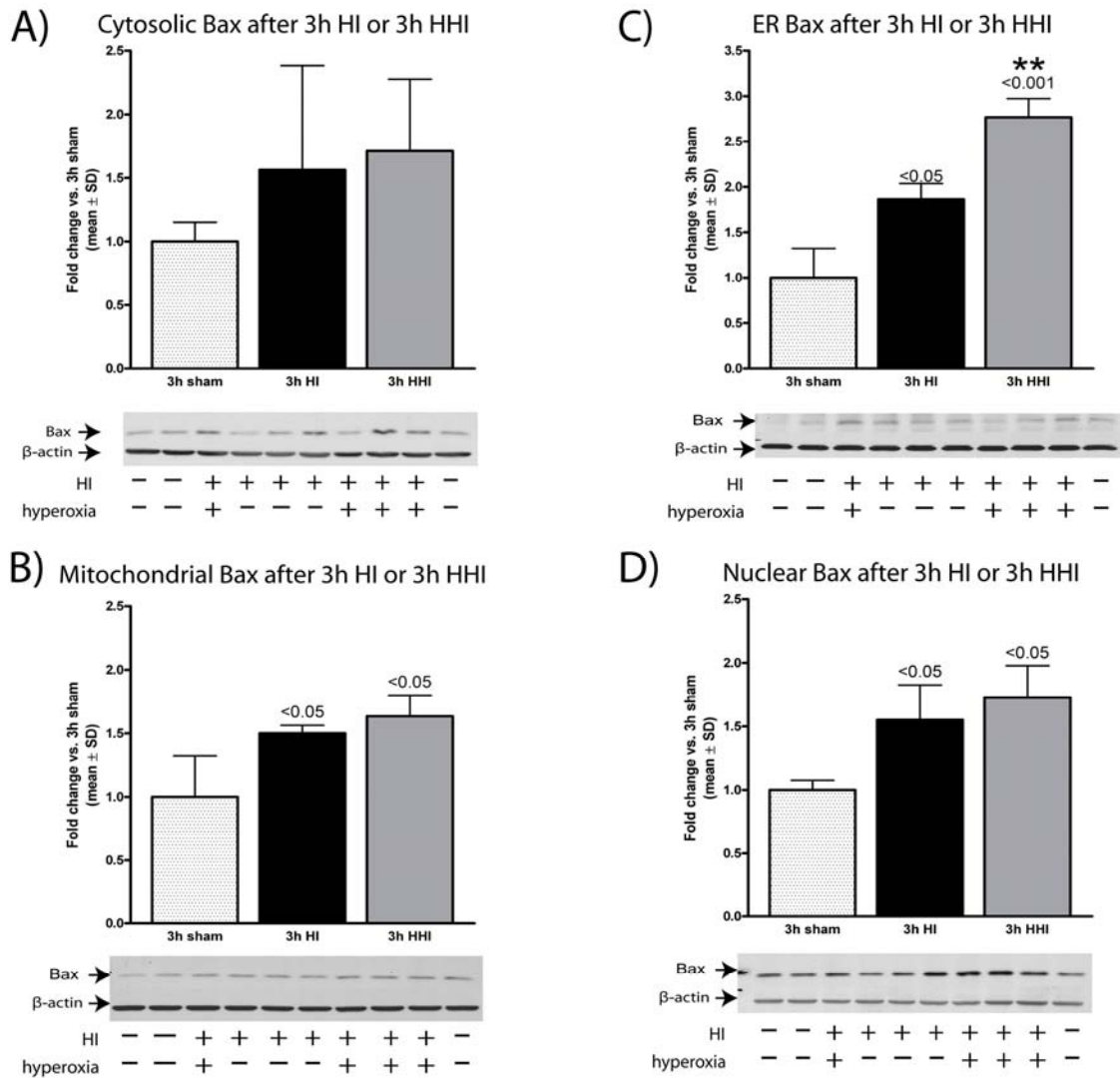


Figure 34. Hyperoxia therapy increases ER but has no effect on nuclear and mitochondrial Bax levels.

A) Hyperoxia therapy has no effect on cytosolic Bax levels within the ipsilateral cortices of 3h post HI-injured animals when compared to untreated 3h post HI-injured animals [3hHI; 1.563 ± 0.82 , 3hHHI; 1.713 ± 0.56 and sham (1.000 ± 0.15)]. Densitometric values for cytosolic Bax levels in 3h sham, 3h post HI-injured, and 3h post HI-injured + hyperoxia cortices. Below, representative Western blot for cytosolic Bax and β -actin levels at 3h post HI. B) Hyperoxia therapy has no effect on mitochondrial Bax levels within the ipsilateral cortices of 3h post HI-injured animals when compared to untreated 3h post HI-injured animals [3hHI; 1.500 ± 0.06 ($p < 0.05$), 3hHHI; 1.635 ± 0.16 ($p < 0.05$) vs. sham (1.000 ± 0.32)]. Densitometric values for mitochondrial Bax levels in 3h sham, 3h post HI-injured, and 3h post HI-injured + hyperoxia cortices. Below, representative

Western blot for nuclear Bax and β -actin levels at 3h post HI. C) Hyperoxia therapy increases ER Bax levels within the ipsilateral cortices of 3h post HI-injured animals when compared to untreated 3h post HI-injured animals [3hHI; 1.865 ± 0.17 ($p < 0.05$), 3hHHI; 2.767 ± 0.21 ($p < 0.001$) vs. sham (1.000 ± 0.32): $p < 0.05$, 3hHI vs. 3hHHI]. Densitometric values for ER Bax levels 3h sham, 3h post HI-injured, and 3h post HI-injured + hyperoxia cortices. Below, representative Western blot for ER Bax and β -actin levels at 3h post HI. D) Hyperoxia therapy has no effect on nuclear Bax levels within the ipsilateral cortices of 3h post HI-injured animals when compared to untreated 3h post HI-injured animals [3hHI; 1.551 ± 0.27 ($p < 0.05$), 3hHHI; 1.726 ± 0.25 ($p < 0.05$) vs. sham (1.000 ± 0.08)]. Densitometric values for nuclear Bax levels in 3h sham, 3h post HI-injured, and 3h post HI-injured + hyperoxia cortices. Below, representative Western blot for nuclear Bax and β -actin levels at 3h post HI. Densitometric data were normalized to β -actin and are represented as fold change of sham \pm S.D. Numerical value above column bars denotes p-value when compared to sham. **: $p < 0.01$ when compared to HI alone.

mediated activation of ER calpain-mediated cell death, which also increases inflammation and cell death with necrotic features.

Discussion

Inhibitory effects of FK506 on rotenone-induced Bax localization and activation of cognate cell death signaling cascades

Reports have shown FK506, an immunophilin used in chemotherapeutic treatment regimens as an immunosuppressant, possesses neuroprotective properties mediated primarily by its inhibition of protein phosphatase 2B (PP2B, or calcineurin) and, in part, due to an unknown cytoprotective mechanism (Almeida et al., 2004; Manakova et al., 2005; Pardo et al., 2006; Shou et al., 2004). In addition, FK506 treatment has been shown to reduce mitochondrial Bax translocation and apoptotic cell death induced by 3-nitropropionic acid

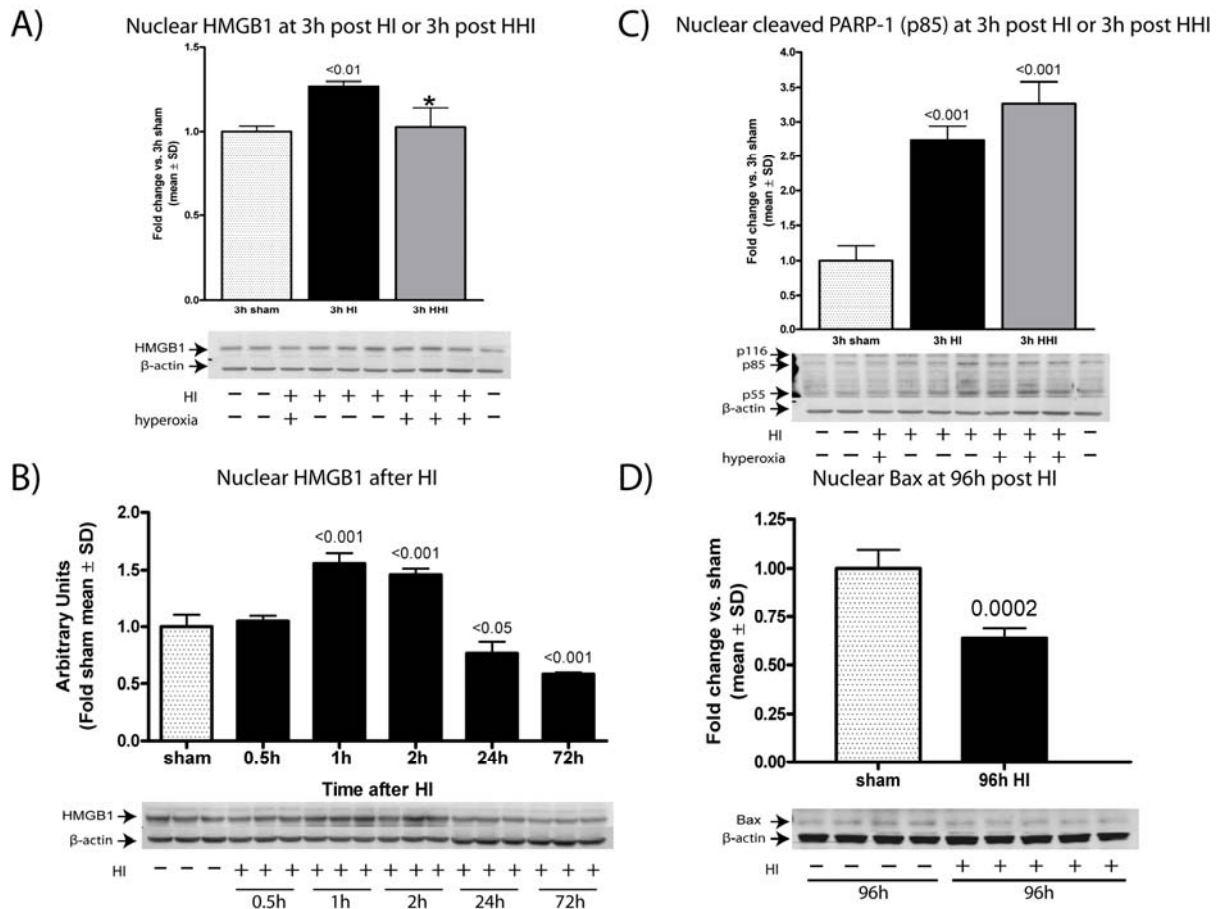


Figure 35. Supplementary data II

A) Hyperoxia therapy decreases nuclear high mobility group box protein 1 (HMGB1) levels within the ipsilateral cortices of 3h post HI-injured animals when compared to untreated 3h post HI-injured animals [3hHI; 1.268 ± 0.03 ($p < 0.01$), 3hHHI; 1.028 ± 0.11 (ns) vs. sham (1.000 ± 0.03): $p < 0.05$, 3hHI vs. 3hHHI]. Densitometric values for nuclear HMGB-1 levels in 3h sham, 3h post HI-injured and 3h post HI-injured + hyperoxia cortices. Below, representative Western blot for nuclear HMGB1 and β -actin levels at 3h post HI. B) HI initially increases nuclear HMGB1 levels in the ipsilateral cortex of 1 and 2h post HI-injured animals [1.559 ± 0.09 ($p < 0.001$) and 1.461 ± 0.05 ($p < 0.001$), respectively, vs. sham (1.000 ± 0.10)] but, then, decreases nuclear HMGB1 levels in the ipsilateral cortex of 24 and 72h post HI-injured animals [0.7651 ± 0.103 ($p < 0.05$) and 0.5819 ± 0.015 ($p < 0.001$), respectively]. Densitometric values for nuclear Bax levels in sham and HI-injured cortices at various survival times post HI. Below, representative Western blot for nuclear HMGB1 and β -actin levels at various survival time points after HI. C) Hyperoxia therapy has no effect on nuclear 85kD cleaved PARP-1 levels within the ipsilateral cortices of 3h post HI-injured animals when compared to untreated 3h post HI-injured animals [3hHI; 2.735 ± 0.20 ($p < 0.001$), 3hHHI; 3.265 ± 0.31 ($p < 0.001$) vs.

sham (1.000 ± 0.22)). Densitometric values for nuclear 85kD cleaved PARP-1 levels in 3h sham, 3h post HI-injured and 3h post HI-injured + hyperoxia cortices. Below, representative Western blot for nuclear cleaved PARP-1 and β -actin levels at 3h post HI. D) HI decreases nuclear Bax levels in the ipsilateral cortex of 96h post HI-injured animals [0.6385 ± 0.051 ($p=0.0002$) vs. sham (1.000 ± 0.10)]. Below, representative Western blot for nuclear Bax and β -actin levels at 96h post HI. Densitometric data were normalized to β -actin and are represented as fold change of sham \pm S.D. Numerical value above column bars denotes p-value when compared to sham. *; $p<0.05$ when compared to HI alone.

(Almeida et al., 2004). Furthermore, in vitro research using cancer cell lines and cerebellar granule cells have demonstrated differential phosphorylation of Bax dictates its activation (Ashraf et al., 2001; Gardai et al., 2004; Linseman et al., 2004), with Ser184 phosphorylation sequestering Bax in the cytosol and Ser163 and Thr167 promoting its activation and mitochondrial localization (Ashraf et al., 2001; Gardai et al., 2004; Linseman et al., 2004). These reports suggest the phosphorylation state of Bax plays a major role its conformation change and activation.

Interestingly, we observed pretreatment and maintained treatment through insult with FK506 dose-dependently inhibited 25 μ M and 100 μ M rotenone-induced cell death (Fig. 25). In addition, we found that FK506 treatment inhibited 25 μ M and 100 μ M rotenone-induced nuclear, mitochondria and ER localization (Fig. 26, 27, 28, 29). Furthermore, our preliminary data demonstrates FK506 treatment, also, inhibited caspase- and calpain-mediated cleavage of α -fodrin (Fig. 30). Taken as a whole, the data presented in the paper provide mechanistic evidence of an FK506-inhibited activation step in Bax localization after rotenone-induced trauma. In addition, inhibition of Bax localization and activation of

cognate cell death signaling cascades inhibits rotenone-induced cell death, thus providing the first evidence for a coordinating role for Bax in activation of multiple cell death signaling cascades to dictate cell death phenotype.

Hyperoxia treatment increases HI-induced lesion volume via ER stimulation of necrosis and inflammation

Mitochondria-mediated apoptosis has been well-characterized to involve Bcl-2 family-regulated signaling pathways (Dejean et al., 2005; Ferrer et al., 2003; Koubi et al., 2005; Putcha et al., 1999; Wei et al., 2001), while necrosis has been classically defined as a passive event (Cole and Perez-Polo, 2004; Yuan et al., 2003). Recently, Edinger et al. (2004) have suggested that, in addition to passive necrosis, there exists programmed necrosis, possessing passive necrotic phenotypic features, which could play a developmental role as an alternative to apoptotic programmed cell death (Edinger and Thompson, 2004; Golstein and Kroemer, 2007; Proskuryakov et al., 2003). Like apoptosis, there exist markers of programmed necrosis, such as nuclear release of HMGB1 (Ditsworth et al., 2007; Jiang and Pisetsky, 2007; Scaffidi et al., 2002) and differential cleavage of PARP-1 (Ditsworth et al., 2007; Gobeil et al., 2001), and recent studies suggest programmed necrosis involves ER Ca^{2+} -activated calpain activation, as well as mitochondrial AIF extrusion, itself an outcome of calpain-mediated cleavage (Moubarak et al., 2007; Polster et al., 2005; Sanges et al., 2006; Sanges and Marigo, 2006). Furthermore, chronic treatment of animals

undergoing CNS trauma with anti-apoptotic agents has been shown not to inhibit cell death, but rather in a regulated manner, shift the cell death phenotype to necrotic phenotype with increased inflammation (Cittelly et al., 2007; Gobeil et al., 2001; Rabuffetti et al., 2000).

In order to model the clinical setting, we modified the Rice-Vannucci model with a 2h isobaric 100% O₂ intervention after the hypoxia exposure to determine if 100% O₂ decreased HI-induced cortical lesion volumes by decreasing Bax-mediated activation of nuclear-, mitochondrial- and/or ER-mediated cell death cascades. Surprisingly, the 100% O₂ treatment increased the HI-induced cortical lesion volume, as well as, increased, by almost two-fold, the likelihood of incurring a more severe lesion (Fig. 31). Furthermore, we observed no increase in cortical apoptosis, but rather an increase in necrotic cell death signaling and inflammation (Fig. 32). In agreement with no increase in HI-induced apoptosis, we observed no increase in mitochondrial Bax levels with 100% O₂. Instead, 100% O₂ augmented HI-induced increases in ER Bax levels concurrent with increased calpain activity (Fig. 33, 34), suggesting 100% O₂ therapy increases HI-induced Bax-mediated activation of ER cell death signaling to increase inflammation and injury by increasing necrotic-like cell death (Fig. 36). We recently have demonstrated long-term reduced locomotor recovery in a rodent model of spinal cord injury due to early increased inflammation (Cittelly et al., 2007). Furthermore, recent reports have linked neonatal infection to multiple CNS disorders, ranging from schizophrenia to autism (Babulas et al., 2006;

Bager et al., 2004; Fatemi et al., 2005). This report and these recent findings support the concept that early cell death signaling produces injury with detrimental outcomes persisting long after cell death and inflammatory cascades have subsided.

Conclusion

In this report, we provide novel mechanistic *in vitro* and *in vivo* evidence for Bax coordination of multiple cognate organelle cell death signaling cascades. Using a different dose rotenone insult model in primary cortical neurons, we found 1h pretreatment with immunosuppressive and neuroprotective FK506 inhibited high and low dose rotenone-mediated Bax relocalization and cell death signaling, *in toto*. Using 100% O₂ as an intervention in the *in vivo* Rice-Vannucci neonatal HI model, we show 100% O₂ increases T2-weighted MRI lesion volumes, via increased inflammatory and necrotic signaling, with no amelioration of cortical apoptotic signaling when compared to HI alone. Furthermore, 100% O₂ increased ER calpain activation and increased ER Bax protein levels, suggesting that 100% O₂ increases HI-induced Bax-mediated activation of ER cell death signaling to increase inflammation and injury by increasing necrotic-like cell death. Taken together, these findings are the first to show Bax-mediated coordination of multi-organelle cell death signaling and demonstrate a link between ER Bax, ER cell death signaling and necrotic-like cell death, all of which

can be inhibited via FK506. This report is the first to provide evidence for a FK506-inhibited common trauma-induced Bax activation step.

CHAPTER V

Conclusions and Future Directions

In conclusion, we report here for the first time *in vivo*, a distinct subcellular time course for Bax in the HI-injured cortex, with Bax localizing first to the nucleus as early as 30 minutes after HI, then to mitochondria and, finally, to the ER. Furthermore, we report that Bax localization to these organelles coordinates with activation of each organelle's cognate cell death cascade, suggesting a new role for Bax, thus providing the first evidence in support of the proposed role for Bax in coordinating the cell death signaling at multiple subcellular organelles.

Using P5 primary cortical neurons, we used a high (100 μ M) and a low (25 μ M) rotenone dose, as respective necrotic-like and apoptotic stimuli, we observed both treatments induced early nuclear Bax localization. In addition, we found that the apoptotic stimulus increased mitochondrial Bax localization and caspase-mediated cleavage of α -fodrin, while the necrotic-like stimulus increased ER Bax localization and calpain-mediated cleavage of α -fodrin. This report is the first to link ER Bax, ER cell death signaling and necrotic-like cell death. We conclude that apoptotic and necrotic-like stimuli promote differential Bax localization and subsequent differential activation of cognate cell death signaling cascades to induce expression of their characteristic phenotypic cell morphologies (Fig. 36A-C). Furthermore, we hypothesize the nuclear localization

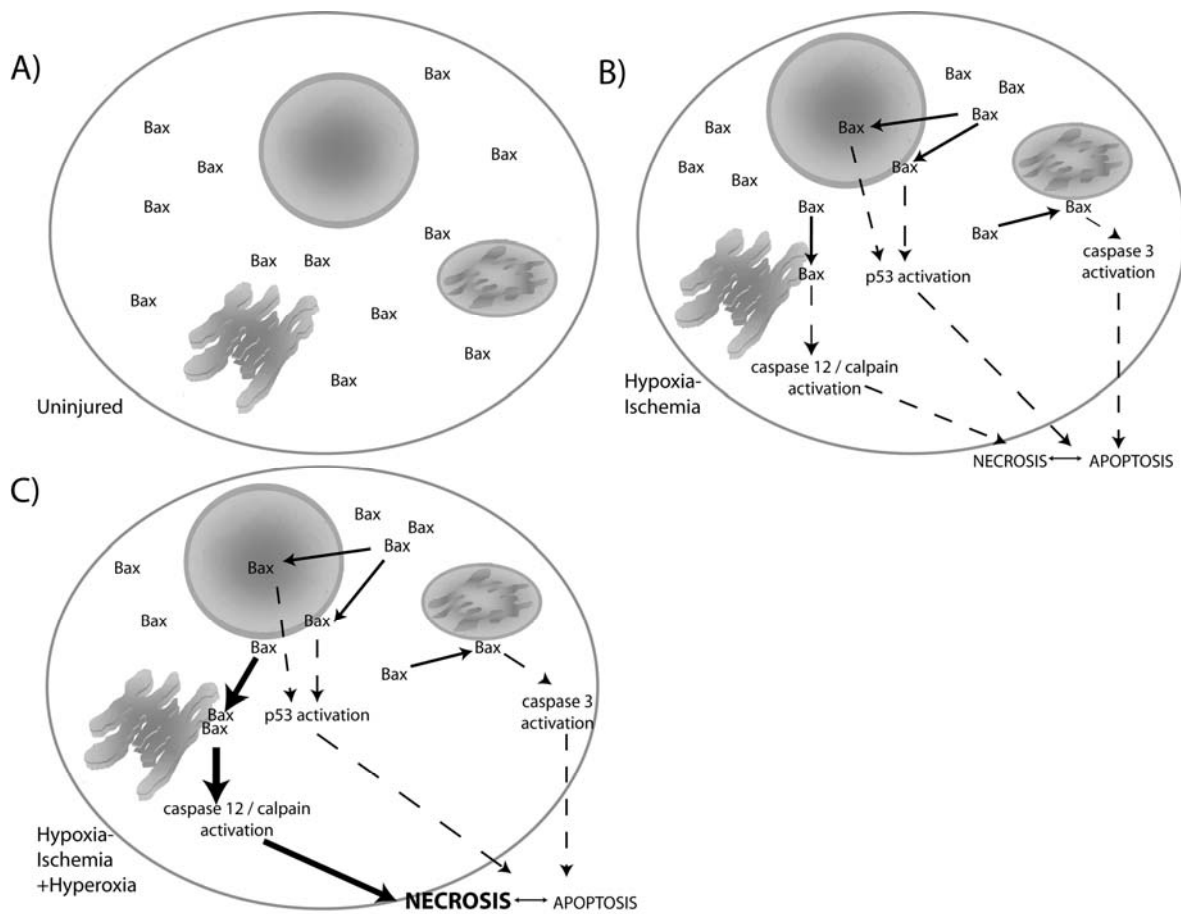


Figure 36. Schematic representations for Bax localization in sham, HI-injured and 100% O₂-treated HI-injured cortices.

A) Schematic illustrating the cytosolic localization of Bax within cells of the uninjured cortex, with little Bax association with the nucleus, mitochondria or ER. B) After hypoxic ischemic insult, Bax shifts to the nucleus, mitochondria and ER to activate each organelle's cognate cell death signaling cascade. We hypothesize that the tissue's integration of the differential activation of these organelle cell death cascades determines the cell death phenotype after HI insult, with increased mitochondria cell death signaling promoting increased apoptotic-like cell death and increased ER cell death signaling promoting increased necrotic-like cell death. C) 100% O₂ therapy increases HI-injured cortical lesion volume via selectively increasing Bax-mediated activation of ER cell death signaling resulting in increased necrosis and inflammation. This finding supports our hypothesis that selective activation of ER cell death signaling vs. mitochondrial cell death signaling will increase the necrotic phenotype resulting from HI insult and underscores the importance for the re-investigation of 100% O₂ as a clinical therapeutic in neonatal HI.

of Bax early after trauma to be a common mechanism across multiple CNS trauma models.

Finally in this report, we provide novel mechanistic *in vitro* and *in vivo* evidence for Bax coordination of multiple cognate organelle cell death signaling cascades. Using a different dose rotenone insult model in primary cortical neurons, we found 1h pretreatment with immunosuppressive and neuroprotective FK506 inhibited high and low dose rotenone-mediated Bax relocalization and cell death signaling, *in toto*. Using 100% O₂ as an intervention in the *in vivo* Rice-Vannucci neonatal HI model, we show 100% O₂ increases T2-weighted MRI lesion volumes, via increased inflammatory and necrotic signaling, with no amelioration of cortical apoptotic signaling when compared to HI alone. Furthermore, 100% O₂ increased ER calpain activation and increased ER Bax protein levels, suggesting that 100% O₂ increases HI-induced Bax-mediated activation of ER cell death signaling to increase inflammation and injury by increasing necrotic-like cell death. Taken together, these findings are the first to show Bax-mediated coordination of multi-organelle cell death signaling and demonstrate a link between ER Bax, ER cell death signaling and necrotic-like cell death, all of which can be inhibited via FK506. Lastly, this report is the first to provide evidence for a FK506-inhibited common trauma-induced Bax activation step.

Based on these findings, investigations into cell death signaling need to consider a more holistic approach and not focus on solely one specific

site of action. Recent reports and the data presented here are changing the long-time standing view of two types of cell death- apoptosis and necrosis. In actuality, there exists a spectrum of cell death phenotype, each dictated by the integration by the cell of external and internal cell death signals. The consequences of these different cell deaths is manifested in the CNS's response to trauma, which can affect not only the short-term functioning, but also the long term functioning even into adulthood. Furthermore, these data stress the tremendous impact immediate cell death signaling events have on the long term progression of the neurological disorder. This speaks to the importance of combinatorial therapeutic treatment of acute trauma, with specific treatments designed to inhibit not cell death as a whole but inhibit cell death, which can exacerbate injury predominantly through unchecked augmentation of Inflammation, at several points in the trauma's destructive progression.

Based on these findings, continued investigation into the coordinating role of Bax in the activation of multiple cognate cell death signaling cascades is warranted. In particular, the ER role for Bax, because of its necrotic / inflammatory consequences, and the nuclear role for Bax, as it seems to be a generalized mechanism to trauma in the CNS, demand further research, not only into their pathway, but also in the inhibition of these pathways as possible therapeutics for early death signals in disease progression. Furthermore, re-investigation of the clinical use of 100% O₂ as a therapy for HIE is required based on these findings, especially because the incidence of low birth weight

infants (the population of neonates who are at greatest risk for suffering HIE and PVH-IVH) is increasing. Perhaps an O₂ dosing paradigm is in order as the benefits of oxygen are readily apparent in terms of heart and lung function. Lastly, further investigation of the neuroprotective effects of FK506 are in order, especially in regards to the observed inhibitory step in Bax activation that FK506 can inhibit. Perhaps, through these investigations a more efficient neuroprotective compound can be developed, which can selectively target Bax away from necrotic-like cell death signaling and towards apoptotic death signaling, as a means to minimize an inevitable trauma do to acute injury.

REFERENCES

- Aggarwal S, Gollapudi S, Gupta S (1999) Increased TNF- α -induced apoptosis in lymphocytes from aged humans: changes in TNF- α receptor expression and activation of caspases. *J Immunol* 162:2154-2161.
- Akhtar RS, Geng Y, Klocke BJ, Latham CB, Villunger A, Michalak EM, Strasser A, Carroll SL, Roth KA (2006) BH3-only proapoptotic Bcl-2 family members Noxa and Puma mediate neural precursor cell death. *J Neurosci* 26:7257-7264.
- Almeida A, Bolanos JP (2001) A transient inhibition of mitochondrial ATP synthesis by nitric oxide synthase activation triggered apoptosis in primary cortical neurons. *J Neurochem* 77:676-690.
- Almeida S, Domingues A, Rodrigues L, Oliveira CR, Rego AC (2004) FK506 prevents mitochondrial-dependent apoptotic cell death induced by 3-nitropropionic acid in rat primary cortical cultures. *Neurobiol Dis* 17:435-444.
- Annibale D (2006) Periventricular Hemorrhage-Intraventricular Hemorrhage. Date Retrieved: 07/07. <http://www.emedicine.com/ped/topic2595.htm>
- Appella E, Anderson CW (2001) Post-translational modifications and activation of p53 by genotoxic stresses. *Eur J Biochem* 268:2764-2772.
- Ashraf QM, Zanelli SA, Mishra OP, Ivoria-Papadopoulos M (2001) Phosphorylation of Bcl-2 and Bax proteins during hypoxia in newborn piglets. *Neurochem Res* 26:1-9.
- Ashwal S, Tone B, Tian HR, Chong S, Obenaus A (2007) Comparison of two neonatal ischemic injury models using magnetic resonance imaging. *Pediatr Res* 61:9-14.
- Babulas V, Factor-Litvak P, Goetz R, Schaefer CA, Brown AS (2006) Prenatal exposure to maternal genital and reproductive infections and adult schizophrenia. *Am J Psychiatry* 163:927-929.
- Back SA, Craig A, Kayton RJ, Luo NL, Meshul CK, Allcock N, Fern R (2007a) Hypoxia-ischemia preferentially triggers glutamate depletion from oligodendroglia and axons in perinatal cerebral white matter. *J Cereb Blood Flow Metab* 27:334-347.
- Back SA, Han BH, Luo NL, Chricton CA, Xanthoudakis S, Tam J, Arvin KL, Holtzman DM (2002) Selective vulnerability of late oligodendrocyte progenitors to hypoxia-ischemia. *J Neurosci* 22:455-463.

Back SA, Riddle A, McClure MM (2007b) Maturation-dependent vulnerability of perinatal white matter in premature birth. *Stroke* 38:724-730.

Bager P, Nielsen NM, Bihrmann K, Frisch M, Hjalgrim H, Wohlfart J, Koch-Henriksen N, Melbye M, Westergaard T (2004) Childhood infections and risk of multiple sclerosis. *Brain* 127:2491-2497.

Bal-Price A, Brown GC (2000) Nitric-oxide-induced necrosis and apoptosis in PC12 cells mediated by mitochondria. *J Neurochem* 75:1455-1464.

Basso E, Fante L, Fowlkes J, Petronilli V, Forte MA, Bernardi P (2005) Properties of the permeability transition pore in mitochondria devoid of Cyclophilin D. *J Biol Chem* 280:18558-18561.

Bell CW, Jiang W, Reich CF, III, Pisetsky DS (2006) The extracellular release of HMGB1 during apoptotic cell death. *Am J Physiol Cell Physiol* 291:C1318-C1325.

Bender LM, Morgan MJ, Thomas LR, Liu ZG, Thorburn A (2005) The adaptor protein TRADD activates distinct mechanisms of apoptosis from the nucleus and the cytoplasm. *Cell Death Differ* 12:473-481.

Bhat RV, DiRocco R, Marcy VR, Flood DG, Zhu Y, Dobrzanski P, Siman R, Scott R, Contreras PC, Miller M (1996) Increased expression of IL-1 β converting enzyme in hippocampus after ischemia: selective localization in microglia. *J Neurosci* 16:4146-4154.

Bissinger RL, Ohning BL (2006) Neonatal Resuscitation. Date Retrieved: 07/07. <http://www.emedicine.com/ped/topic2598.htm>.

Blomgren K, Zhu C, Wang X, Karlsson JO, Leverin AL, Bahr BA, Mallard C, Hagberg H (2001) Synergistic activation of caspase-3 by m-calpain after neonatal hypoxia-ischemia: a mechanism of "pathological apoptosis"? *J Biol Chem* 276:10191-10198.

Boehning D, Patterson RL, Sedaghat L, Glebova NO, Kurosaki T, Snyder SH (2003) Cytochrome c binds to inositol (1,4,5) trisphosphate receptors, amplifying calcium-dependent apoptosis. *Nat Cell Biol* 5:1051-1061.

Bourdon JC, Renzing J, Robertson PL, Fernandes KN, Lane DP (2002) Scotin, a novel p53-inducible proapoptotic protein located in the ER and the nuclear membrane. *J Cell Biol* 158:235-246.

Bredesen DE, Rao RV, Mehlen P (2006) Cell death in the nervous system. *Nature* 443:796-802.

Brooks TF, Humphreys WM (2004) A Deconvolution Approach for the Mapping of Acoustic Sources (DAMAS) Determined from Phased Microphone Arrays. American Institute of Aeronautics and Astronautics. Date Retrieved: 07/07. <http://hdl.handle.net/2002/15629>

Camins A, Verdaguer E, Folch J, Pallas M (2006) Involvement of calpain activation in neurodegenerative processes. *CNS Drug Rev* 12:135-148.

Cao G, Pei W, Ge H, Liang Q, Luo Y, Sharp FR, Lu A, Ran R, Graham SH, Chen J (2002) In Vivo Delivery of a Bcl-xL Fusion Protein Containing the TAT Protein Transduction Domain Protects against Ischemic Brain Injury and Neuronal Apoptosis. *J Neurosci* 22:5423-5431.

Casarejos MJ, Menendez J, Solano RM, Rodriguez-Navarro JA, Garcia de YJ, Mena MA (2006) Susceptibility to rotenone is increased in neurons from parkin null mice and is reduced by minocycline. *J Neurochem* 97:934-946.

Chae HJ, Kim HR, Xu C, Bailly-Maitre B, Krajewska M, Krajewski S, Banares S, Cui J, Digicaylioglu M, Ke N, Kitada S, Monosov E, Thomas M, Kress CL, Babendure JR, Tsien RY, Lipton SA, Reed JC (2004) BI-1 regulates an apoptosis pathway linked to endoplasmic reticulum stress. *Mol Cell* 15:355-366.

Cheung EC, Melanson-Drapeau L, Cregan SP, Vanderluit JL, Ferguson KL, McIntosh WC, Park DS, Bennett SA, Slack RS (2005) Apoptosis-inducing factor is a key factor in neuronal cell death propagated by BAX-dependent and BAX-independent mechanisms. *J Neurosci* 25:1324-1334.

Chinopoulos C, Zam-Vizi V (2006) Calcium, mitochondria and oxidative stress in neuronal pathology. Novel aspects of an enduring theme. *FEBS J* 273:433-450.

Chipuk JE, Bouchier-Hayes L, Kuwana T, Newmeyer DD, Green DR (2005) PUMA couples the nuclear and cytoplasmic proapoptotic function of p53. *Science* 309:1732-1735.

Chipuk JE, Kuwana T, Bouchier-Hayes L, Droin NM, Newmeyer DD, Schuler M, Green DR (2004) Direct activation of Bax by p53 mediates mitochondrial membrane permeabilization and apoptosis. *Science* 303:1010-1014.

Chipuk JE, Maurer U, Green DR, Schuler M (2003) Pharmacologic activation of p53 elicits Bax-dependent apoptosis in the absence of transcription. *Cancer Cell* 4:371-381.

Cho HJ, Kim JK, Kim KD, Yoon HK, Cho MY, Park YP, Jeon JH, Lee ES, Byun SS, Lim HM, Song EY, Lim JS, Yoon DY, Lee HG, Choe YK (2006) Upregulation of Bcl-2 is associated with cisplatin-resistance via inhibition of Bax translocation in human bladder cancer cells. *Cancer Lett* 237:56-66.

Chu D, Qiu J, Grafe M, Fabian R, Kent TA, Rassin D, Nesic O, Werrbach-Perez K, Perez-Polo R (2002) Delayed cell death signaling in traumatized central nervous system: hypoxia. *Neurochem Res* 27:97-106.

Cittelly DM, Nesic-Taylor O, Perez-Polo JR (2007) Phosphorylation of Bcl-x(L) after spinal cord injury. *J Neurosci Res* 85:1894-1911.

Colbourne F, Sutherland GR, Auer RN (1999) Electron microscopic evidence against apoptosis as the mechanism of neuronal death in global ischemia. *J Neurosci* 19:4200-4210.

Cole K, Perez-Polo JR (2004) Neuronal trauma model: in search of Thanatos. *Int J Dev Neurosci* 22:485-496.

Cryns VL, Bergeron L, Zhu H, Li H, Yuan J (1996) Specific cleavage of alpha-fodrin during Fas- and tumor necrosis factor-induced apoptosis is mediated by an interleukin-1beta-converting enzyme/Ced-3 protease distinct from the poly(ADP-ribose) polymerase protease. *J Biol Chem* 271:31277-31282.

Culmsee C, Mattson MP (2005) p53 in neuronal apoptosis. *Biochem Biophys Res Commun* 331:761-777.

Culmsee C, Zhu C, Landshamer S, Becattini B, Wagner E, Pellecchia M, Blomgren K, Plesnila N (2005) Apoptosis-inducing factor triggered by poly(ADP-ribose) polymerase and Bid mediates neuronal cell death after oxygen-glucose deprivation and focal cerebral ischemia. *J Neurosci* 25:10262-10272.

D'Alessio M, De NM, Coppola S, Gualandi G, Pugliese L, Cerella C, Cristofanon S, Civitareale P, Ciriolo MR, Bergamaschi A, Magrini A, Ghibelli L (2005) Oxidative Bax dimerization promotes its translocation to mitochondria independently of apoptosis. *FASEB J* 19:1504-1506.

D'Amours D, Sallmann FR, Dixit VM, Poirier GG (2001) Gain-of-function of poly(ADP-ribose) polymerase-1 upon cleavage by apoptotic proteases: implications for apoptosis. *J Cell Sci* 114:3771-3778.

de Menezes MS, Shaw DW (2006) Hypoxic-Ischemic Brain Injury in the Newborn. Date Retrieved: 07/07. <http://www.emedicine.com/neuro/topic696.htm>.

DeGracia DJ, Montie HL (2004) Cerebral ischemia and the unfolded protein response. *J Neurochem* 91:1-8.

Degterev A, Huang Z, Boyce M, Li Y, Jagtap P, Mizushima N, Cuny GD, Mitchison TJ, Moskowitz MA, Yuan J (2005) Chemical inhibitor of nonapoptotic cell death with therapeutic potential for ischemic brain injury. *Nat Chem Biol* 1:112-119.

Dejean LM, Martinez-Caballero S, Guo L, Hughes C, Teijido O, Ducret T, Ichas F, Korsmeyer SJ, Antonsson B, Jonas EA, Kinnally KW (2005) Oligomeric Bax is a component of the putative cytochrome c release channel MAC, mitochondrial apoptosis-induced channel. *Mol Biol Cell* 16:2424-2432.

Derugin N, Ferriero DM, Vexler ZS (1998) Neonatal reversible focal cerebral ischemia: a new model. *Neurosci Res* 32:349-353.

Ditsworth D, Zong WX, Thompson CB (2007) Activation of poly(ADP)-ribose polymerase (PARP-1) induces release of the pro-inflammatory mediator HMGB1 from the nucleus. *J Biol Chem* 282:17845-17854.

Dougherty RP (2005) Extensions of DAMAS and Benefits and Limitations of Deconvolution in Beamforming. *American Institute of Aeronautics and Astronautics* 2005-2961.

Edinger AL, Thompson CB (2004) Death by design: apoptosis, necrosis and autophagy. *Curr Opin Cell Biol* 16:663-669.

Fatemi SH, Pearce DA, Brooks AI, Sidwell RW (2005) Prenatal viral infection in mouse causes differential expression of genes in brains of mouse progeny: a potential animal model for schizophrenia and autism. *Synapse* 57:91-99.

Ferrer I, Friguls B, Dalfo E, Justicia C, Planas AM (2003) Caspase-dependent and caspase-independent signalling of apoptosis in the penumbra following middle cerebral artery occlusion in the adult rat. *Neuropathol Appl Neurobiol* 29:472-481.

Ferrer I, Planas AM (2003) Signaling of cell death and cell survival following focal cerebral ischemia: life and death struggle in the penumbra. *J Neuropathol Exp Neurol* 62:329-339.

Festjens N, Vanden BT, Vandenabeele P (2006) Necrosis, a well-orchestrated form of cell demise: signalling cascades, important mediators and concomitant immune response. *Biochim Biophys Acta* 1757:1371-1387.

Fiskum G, Starkov A, Polster BM, Chinopoulos C (2003) Mitochondrial mechanisms of neural cell death and neuroprotective interventions in Parkinson's disease. *Ann N Y Acad Sci* 991:111-119.

Formigli L, Papucci L, Tani A, Schiavone N, Tempestini A, Orlandini GE, Capaccioli S, Orlandini SZ (2000) Aponecrosis: morphological and biochemical exploration of a syncretic process of cell death sharing apoptosis and necrosis. *J Cell Physiol* 182:41-49.

Formigli L, Zecchi OS, Capaccioli S, Poupon MF, Bani D (2002) Energy-dependent types of cell death in MCF-7 breast cancer cell tumors implanted into nude mice. *Cells Tissues Organs* 170:99-110.

Fujita E, Kouroku Y, Jimbo A, Isoai A, Maruyama K, Momoi T (2002) Caspase-12 processing and fragment translocation into nuclei of tunicamycin-treated cells. *Cell Death Differ* 9:1108-1114.

Gajkowska B, Wojewodzka U, Gajda J (2004) Translocation of Bax and Bid to mitochondria, endoplasmic reticulum and nuclear envelope: possible control points in apoptosis. *J Mol Histol* 35:11-19.

Gardai SJ, Hildeman DA, Frankel SK, Whitlock BB, Frasch SC, Borregaard N, Marrack P, Bratton DL, Henson PM (2004) Phosphorylation of Bax Ser184 by Akt regulates its activity and apoptosis in neutrophils. *J Biol Chem* 279:21085-21095.

Gobeil S, Boucher CC, Nadeau D, Poirier GG (2001) Characterization of the necrotic cleavage of poly(ADP-ribose) polymerase (PARP-1): implication of lysosomal proteases. *Cell Death Differ* 8:588-594.

Godlewski MM, Motyl MA, Gajkowska B, Wareski P, Koronkiewicz M, Motyl T (2001) Subcellular redistribution of BAX during apoptosis induced by anticancer drugs. *Anticancer Drugs* 12:607-617.

Golstein P, Kroemer G (2007) Cell death by necrosis: towards a molecular definition. *Trends Biochem Sci* 32:37-43.

Goping IS, Gross A, Lavoie JN, Nguyen M, Jemmerson R, Roth K, Korsmeyer SJ, Shore GC (1998) Regulated targeting of BAX to mitochondria. *J Cell Biol* 143:207-215.

Goto S, Xue R, Sugo N, Sawada M, Blizzard KK, Poitras MF, Johns DC, Dawson TM, Dawson VL, Crain BJ, Traystman RJ, Mori S, Hurn PD (2002) Poly(ADP-ribose) polymerase impairs early and long-term experimental stroke recovery. *Stroke* 33:1101-1106.

Gould TW, Buss RR, Vinsant S, Prevette D, Sun W, Knudson CM, Milligan CE, Oppenheim RW (2006) Complete dissociation of motor neuron death from motor dysfunction by Bax deletion in a mouse model of ALS. *J Neurosci* 26:8774-8786.

Ha HC, Hester LD, Snyder SH (2002) Poly(ADP-ribose) polymerase-1 dependence of stress-induced transcription factors and associated gene expression in glia. *Proc Natl Acad Sci U S A* 99:3270-3275.

Hailer NP, Vogt C, Korf HW, Dehghani F (2005) Interleukin-1 β exacerbates and interleukin-1 receptor antagonist attenuates neuronal injury and microglial activation after excitotoxic damage in organotypic hippocampal slice cultures. *Eur J Neurosci* 21:2347-2360.

Hartley A, Stone JM, Heron C, Cooper JM, Schapira AH (1994) Complex I inhibitors induce dose-dependent apoptosis in PC12 cells: relevance to Parkinson's disease. *J Neurochem* 63:1987-1990.

Hegde R, Srinivasula SM, Zhang Z, Wassell R, Mukattash R, Cilenti L, DuBois G, Lazebnik Y, Zervos AS, Fernandes-Alnemri T, Alnemri ES (2002) Identification of Omi/HtrA2 as a mitochondrial apoptotic serine protease that disrupts inhibitor of apoptosis protein-caspase interaction. *J Biol Chem* 277:432-438.

Hetz C, Bernasconi P, Fisher J, Lee AH, Bassik MC, Antonsson B, Brandt GS, Iwakoshi NN, Schinzel A, Glimcher LH, Korsmeyer SJ (2006) Proapoptotic BAX and BAK modulate the unfolded protein response by a direct interaction with IRE1 α . *Science* 312:572-576.

Hillion JA, Takahashi K, Maric D, Ruetzler C, Barker JL, Hallenbeck JM (2005) Development of an ischemic tolerance model in a PC12 cell line. *J Cereb Blood Flow Metab* 25:154-162.

Hong SJ, Dawson TM, Dawson VL (2004) Nuclear and mitochondrial conversations in cell death: PARP-1 and AIF signaling. *Trends Pharmacol Sci* 25:259-264.

Hu Q, Chang J, Tao L, Yan G, Xie M, Wang Z (2005a) Endoplasmic reticulum mediated necrosis-like apoptosis of HeLa cells induced by Ca²⁺ oscillation. *J Biochem Mol Biol* 38:709-716.

Hu X, Han W, Li L (2007) Targeting the Weak Point of Cancer by Induction of Necroptosis. *Autophagy* 3.

Hu X, Nesic-Taylor O, Qiu J, Rea HC, Fabian R, Rassin DK, Perez-Polo JR (2005b) Activation of nuclear factor-kappaB signaling pathway by interleukin-1 after hypoxia/ischemia in neonatal rat hippocampus and cortex. *J Neurochem* 93:26-37.

Hu X, Qiu J, Grafe MR, Rea HC, Rassin DK, Perez-Polo JR (2003) Bcl-2 family members make different contributions to cell death in hypoxia and/or hyperoxia in rat cerebral cortex. *Int J Dev Neurosci* 21:371-377.

Hu X, Rea HC, Wiktorowicz JE, Perez-Polo JR (2006) Proteomic analysis of hypoxia/ischemia-induced alteration of cortical development and dopamine neurotransmission in neonatal rat. *J Proteome Res* 5:2396-2404.

Ikeda T, Mishima K, Aoo N, Harada K, Liu AX, Egashira N, Iwasaki K, Fujiwara M, Ikenoue T (2006) Rehabilitative training tasks improve spatial learning impairment in the water maze following hypoxic-ischemic insult in neonatal rats. *Pediatr Res* 59:61-65.

Jackson GR (1991) Effects of NGF on hydrogen peroxide toxicity in PC12 rat pheochromocytoma. (Doctoral Dissertation, University of Texas-Medical Branch, 1991).

Jackson GR, Morgan BC, Werrbach-Perez K, Perez-Polo JR (1991) Antioxidant effect of retinoic acid on PC12 rat pheochromocytoma. *Int J Dev Neurosci* 9:161-170.

Jakob U, Muse W, Eser M, Bardwell JC (1999) Chaperone activity with a redox switch. *Cell* 96:341-352.

Jatana M, Singh I, Singh AK, Jenkins D (2006) Combination of systemic hypothermia and N-acetylcysteine attenuates hypoxic-ischemic brain injury in neonatal rats. *Pediatr Res* 59:684-689.

Jessenberger V, Jentsch S (2002) Deadly encounter: ubiquitin meets apoptosis. *Nat Rev Mol Cell Biol* 3:112-121.

Jiang W, Pisetsky DS (2007) Mechanisms of Disease: the role of high-mobility group protein 1 in the pathogenesis of inflammatory arthritis. *Nat Clin Pract Rheumatol* 3:52-58.

Kalai M, Lamkanfi M, Denecker G, Boogmans M, Lippens S, Meeus A, Declercq W, Vandenabeele P (2003) Regulation of the expression and processing of caspase-12. *J Cell Biol* 162:457-467.

Kaneko M, Nomura Y (2003) ER signaling in unfolded protein response. *Life Sci* 74:199-205.

Karbowski M, Norris KL, Cleland MM, Jeong SY, Youle RJ (2006) Role of Bax and Bak in mitochondrial morphogenesis. *Nature* 443:658-662.

Karlsson J, Pietras A, Beckman S, Pettersson HM, Larsson C, Pahlman S (2007) Arsenic trioxide-induced neuroblastoma cell death is accompanied by proteolytic activation of nuclear Bax. *Oncogene*.

Kerr JF, Wyllie AH, Currie AR (1972) Apoptosis: a basic biological phenomenon with wide-ranging implications in tissue kinetics. *Br J Cancer* 26:239-257.

Kim H, Rafiuddin-Shah M, Tu HC, Jeffers JR, Zambetti GP, Hsieh JJ, Cheng EH (2006a) Hierarchical regulation of mitochondrion-dependent apoptosis by BCL-2 subfamilies. *Nat Cell Biol* 8:1348-1358.

Kim JB, Sig CJ, Yu YM, Nam K, Piao CS, Kim SW, Lee MH, Han PL, Park JS, Lee JK (2006b) HMGB1, a novel cytokine-like mediator linking acute neuronal death and delayed neuroinflammation in the postischemic brain. *J Neurosci* 26:6413-6421.

Korsmeyer SJ, Gross A, Harada H, Zha J, Wang K, Yin XM, Wei M, Zinkel S (1999) Death and survival signals determine active/inactive conformations of pro-apoptotic BAX, BAD, and BID molecules. *Cold Spring Harb Symp Quant Biol* 64:343-350.

Korsmeyer SJ, Shutter JR, Veis DJ, Merry DE, Oltvai ZN (1993) Bcl-2/Bax: a rheostat that regulates an anti-oxidant pathway and cell death. *Semin Cancer Biol* 4:327-332.

Korsmeyer SJ, Wei MC, Saito M, Weiler S, Oh KJ, Schlesinger PH (2000) Pro-apoptotic cascade activates BID, which oligomerizes BAK or BAX into pores that result in the release of cytochrome c. *Cell Death Differ* 7:1166-1173.

Koubi D, Jiang H, Zhang L, Tang W, Kuo J, Rodriguez AI, Hunter TJ, Seidman MD, Corcoran GB, Levine RA (2005) Role of Bcl-2 family of proteins in mediating apoptotic death of PC12 cells exposed to oxygen and glucose deprivation. *Neurochem Int* 46:73-81.

Krajewski S, Krajewska M, Ellerby LM, Welsh K, Xie Z, Deveraux QL, Salvesen GS, Bredesen DE, Rosenthal RE, Fiskum G, Reed JC (1999) Release of caspase-9 from mitochondria during neuronal apoptosis and cerebral ischemia. *Proc Natl Acad Sci U S A* 96:5752-5757.

Larner SF, Hayes RL, Wang KK (2006) Unfolded protein response after neurotrauma. *J Neurotrauma* 23:807-829.

Lee GH, Kim HK, Chae SW, Kim DS, Ha KC, Mike C, Kress C, Reed JC, Kim HR, Chae HJ (2007) Bax inhibitor-1 regulates endoplasmic reticulum stress-associated reactive oxygen species and heme oxygenase-I expression. *J Biol Chem*.

Lee MM, Hseih MT, Kuo JS, Yeh FT, Huang HM (1998) Magnolol protects cortical neuronal cells from chemical hypoxia in rats. *Neuroreport* 9:3451-3456.

Leist M, Single B, Naumann H, Fava E, Simon B, Kuhnle S, Nicotera P (1999) Inhibition of mitochondrial ATP generation by nitric oxide switches apoptosis to necrosis. *Exp Cell Res* 249:396-403.

Lin MT, Beal MF (2006) Mitochondrial dysfunction and oxidative stress in neurodegenerative diseases. *Nature* 443:787-795.

Linseman DA, Butts BD, Precht TA, Phelps RA, Le SS, Laessig TA, Bouchard RJ, Florez-McClure ML, Heidenreich KA (2004) Glycogen synthase kinase-3beta phosphorylates Bax and promotes its mitochondrial localization during neuronal apoptosis. *J Neurosci* 24:9993-10002.

Loepke AW, McCann JC, Kurth CD, McAuliffe JJ (2006) The physiologic effects of isoflurane anesthesia in neonatal mice. *Anesth Analg* 102:75-80.

Manakova S, Singh A, Kaariainen T, Taari H, Kulkarni SK, Mannisto PT (2005) Failure of FK506 (tacrolimus) to alleviate apomorphine-induced circling in rat Parkinson model in spite of some cytoprotective effects in SH-SY5Y dopaminergic cells. *Brain Res* 1038:83-91.

Mandal M, Adam L, Mendelsohn J, Kumar R (1998) Nuclear targeting of Bax during apoptosis in human colorectal cancer cells. *Oncogene* 17:999-1007.

Mandal M, Olson DJ, Sharma T, Vadlamudi RK, Kumar R (2001) Butyric acid induces apoptosis by up-regulating Bax expression via stimulation of the c-Jun N-terminal kinase/activation protein-1 pathway in human colon cancer cells. *Gastroenterology* 120:71-78.

Mandir AS, Poitras MF, Berliner AR, Herring WJ, Guastella DB, Feldman A, Poirier GG, Wang ZQ, Dawson TM, Dawson VL (2000) NMDA but not non-NMDA excitotoxicity is mediated by Poly(ADP-ribose) polymerase. *J Neurosci* 20:8005-8011.

Martin SS, Perez-Polo JR, Noppens KM, Grafe MR (2005) Biphasic changes in the levels of poly(ADP-ribose) polymerase-1 and caspase 3 in the immature brain following hypoxia-ischemia. *Int J Dev Neurosci* 23:673-686.

Mehta SL, Manhas N, Raghubir R (2007) Molecular targets in cerebral ischemia for developing novel therapeutics. *Brain Res Rev* 54:34-66.

Meng S, Qiao M, Scobie K, Tomanek B, Tuor UI (2006) Evolution of magnetic resonance imaging changes associated with cerebral hypoxia-ischemia and a relatively selective white matter injury in neonatal rats. *Pediatr Res* 59:554-559.

Mishra OP, Randis T, Ashraf QM, Iivoria-Papadopoulos M (2006) Hypoxia-induced Bax and Bcl-2 protein expression, caspase-9 activation, DNA fragmentation, and lipid peroxidation in mitochondria of the cerebral cortex of newborn piglets: The role of nitric oxide. *Neuroscience* 141(3): 1339-1349.

Morris EJ, Keramaris E, Rideout HJ, Slack RS, Dyson NJ, Stefanis L, Park DS (2001) Cyclin-dependent kinases and P53 pathways are activated independently and mediate Bax activation in neurons after DNA damage. *J Neurosci* 21:5017-5026.

Moubarak RS, Yuste VJ, Artus C, Bouharrou A, Greer PA, Menissier-de MJ, Susin SA (2007) Sequential Activation of Poly(ADP-Ribose) Polymerase 1, Calpains, and Bax Is Essential in Apoptosis-Inducing Factor-Mediated Programmed Necrosis. *Mol Cell Biol* 27:4844-4862.

Muskopf S (2006). The Rat Circulatory System. Date Retrieved 07/07.
www.biologycorner.com/bio3/rat_circulatory.html

Nakagawa T, Zhu H, Morishima N, Li E, Xu J, Yankner BA, Yuan J (2000) Caspase-12 mediates endoplasmic-reticulum-specific apoptosis and cytotoxicity by amyloid-beta. *Nature* 403:98-103.

Nakajima W, Ishida A, Lange MS, Gabrielson KL, Wilson MA, Martin LJ, Blue ME, Johnston MV (2000) Apoptosis has a prolonged role in the neurodegeneration after hypoxic ischemia in the newborn rat. *J Neurosci* 20:7994-8004.

Nishita M, Inoue S, Tsuda M, Tateda C, Miyashita T (1998) Nuclear translocation and increased expression of Bax and disturbance in cell cycle progression without prominent apoptosis induced by hyperthermia. *Exp Cell Res* 244:357-366.

Northington FJ, Ferriero DM, Martin LJ (2001) Neurodegeneration in the thalamus following neonatal hypoxia-ischemia is programmed cell death. *Dev Neurosci* 23:186-191.

Northington FJ, Graham EM, Martin LJ (2005) Apoptosis in perinatal hypoxic-ischemic brain injury: how important is it and should it be inhibited? *Brain Res Brain Res Rev* 50:244-257.

Nutt LK, Chandra J, Pataer A, Fang B, Roth JA, Swisher SG, O'Neil RG, McConkey DJ (2002a) Bax-mediated Ca^{2+} mobilization promotes cytochrome c release during apoptosis. *J Biol Chem* 277:20301-20308.

Nutt LK, Pataer A, Pahler J, Fang B, Roth J, McConkey DJ, Swisher SG (2002b) Bax and Bak promote apoptosis by modulating endoplasmic reticular and mitochondrial Ca^{2+} stores. *J Biol Chem* 277:9219-9225.

Oakes SA, Opferman JT, Pozzan T, Korsmeyer SJ, Scorrano L (2003) Regulation of endoplasmic reticulum Ca^{2+} dynamics by proapoptotic BCL-2 family members. *Biochem Pharmacol* 66:1335-1340.

Oakes SA, Scorrano L, Opferman JT, Bassik MC, Nishino M, Pozzan T, Korsmeyer SJ (2005) Proapoptotic BAX and BAK regulate the type 1 inositol trisphosphate receptor and calcium leak from the endoplasmic reticulum. *Proc Natl Acad Sci U S A* 102:105-110.

Odding E, Roebroek ME, Stam HJ (2006) The epidemiology of cerebral palsy: incidence, impairments and risk factors. *Disabil Rehabil* 28:183-191.

Oltvai ZN, Millman CL, Korsmeyer SJ (1993) Bcl-2 heterodimerizes in vivo with a conserved homolog, Bax, that accelerates programmed cell death. *Cell* 74:609-619.

Papucci L, Formigli L, Schiavone N, Tani A, Donnini M, Lapucci A, Perna F, Tempestini A, Witort E, Morganti M, Nosi D, Orlandini GE, Zecchi OS, Capaccioli S (2004) Apoptosis shifts to necrosis via intermediate types of cell death by a mechanism depending on c-myc and bcl-2 expression. *Cell Tissue Res* 316:197-209.

Pardo R, Colin E, Regulier E, Aebischer P, Deglon N, Humbert S, Saudou F (2006) Inhibition of calcineurin by FK506 protects against polyglutamine-huntingtin toxicity through an increase of huntingtin phosphorylation at S421. *J Neurosci* 26:1635-1645.

Platt MJ, Cans C, Johnson A, Surman G, Topp M, Torrioli MG, Krageloh-Mann I (2007) Trends in cerebral palsy among infants of very low birthweight (<1500 g) or born prematurely (<32 weeks) in 16 European centres: a database study. *Lancet* 369:43-50.

Plesnila N, Zhu C, Culmsee C, Groger M, Moskowitz MA, Blomgren K (2004) Nuclear translocation of apoptosis-inducing factor after focal cerebral ischemia. *J Cereb Blood Flow Metab* 24:458-466.

Polster BM, Basanez G, Etxebarria A, Hardwick JM, Nicholls DG (2005) Calpain I induces cleavage and release of apoptosis-inducing factor from isolated mitochondria. *J Biol Chem* 280:6447-6454.

Precht TA, Phelps RA, Linseman DA, Butts BD, Le SS, Laessig TA, Bouchard RJ, Heidenreich KA (2005) The permeability transition pore triggers Bax translocation to mitochondria during neuronal apoptosis. *Cell Death Differ* 12:255-265.

Pretorius E, Bornman MS (2005) Calcium-mediated apoptosis plays a central role in the pathogenesis of estrogenic chemical-induced neurotoxicity. *Med Hypotheses* 65:893-904.

Proskuryakov SY, Konoplyannikov AG, Gabai VL (2003) Necrosis: a specific form of programmed cell death? *Exp Cell Res* 283:1-16.

Putcha GV, Deshmukh M, Johnson EM, Jr. (1999) BAX translocation is a critical event in neuronal apoptosis: regulation by neuroprotectants, BCL-2, and caspases. *J Neurosci* 19:7476-7485.

Rabuffetti M, Sciorati C, Tarozzo G, Clementi E, Manfredi AA, Beltramo M (2000) Inhibition of caspase-1-like activity by Ac-Tyr-Val-Ala-Asp-chloromethyl ketone induces long-lasting neuroprotection in cerebral ischemia through apoptosis reduction and decrease of proinflammatory cytokines. *J Neurosci* 20:4398-4404.

Raffo AJ, Kim AL, Fine RL (2000) Formation of nuclear Bax/p53 complexes is associated with chemotherapy induced apoptosis. *Oncogene* 19:6216-6228.

Raju TNK (2006c) Hypoxic Ischemic Encephalopathy. Date Retrieved: 07/07. <http://www.emedicine.com/ped/topic149.htm>.

Ramadan S, Terrinoni A, Catani MV, Sayan AE, Knight RA, Mueller M, Krammer PH, Melino G, Candi E (2005) p73 induces apoptosis by different mechanisms. *Biochem Biophys Res Commun* 331:713-717.

Rao RV, Castro-Obregon S, Frankowski H, Schuler M, Stoka V, Del RG, Bredesen DE, Ellerby HM (2002) Coupling endoplasmic reticulum stress to the cell death program. An Apaf-1-independent intrinsic pathway. *J Biol Chem* 277:21836-21842.

Reed JC (2006) Proapoptotic multidomain Bcl-2/Bax-family proteins: mechanisms, physiological roles, and therapeutic opportunities. *Cell Death Differ* 13:1378-1386.

Saelens X, Festjens N, Vande WL, van GM, van LG, Vandenabeele P (2004) Toxic proteins released from mitochondria in cell death. *Oncogene* 23:2861-2874.

Salah-eldin A, Inoue S, Tsuda M, Matsuura A (2000) Abnormal intracellular localization of Bax with a normal membrane anchor domain in human lung cancer cell lines. *Jpn J Cancer Res* 91:1269-1277.

Sanges D, Comitato A, Tammara R, Marigo V (2006) Apoptosis in retinal degeneration involves cross-talk between apoptosis-inducing factor (AIF) and caspase-12 and is blocked by calpain inhibitors. *Proc Natl Acad Sci U S A* 103:17366-17371.

Sanges D, Marigo V (2006) Cross-talk between two apoptotic pathways activated by endoplasmic reticulum stress: differential contribution of caspase-12 and AIF. *Apoptosis* 11:1629-1641.

Scaffidi P, Misteli T, Bianchi ME (2002) Release of chromatin protein HMGB1 by necrotic cells triggers inflammation. *Nature* 418:191-195.

Scorrano L, Oakes SA, Opferman JT, Cheng EH, Sorcinelli MD, Pozzan T, Korsmeyer SJ (2003) BAX and BAK regulation of endoplasmic reticulum Ca²⁺: a control point for apoptosis. *Science* 300:135-139.

Segura AJ, Kostrzewa RM (2004) Neurotoxins and neurotoxic species implicated in neurodegeneration. *Neurotox Res* 6:615-630.

She QB, Chen N, Dong Z (2000) ERKs and p38 kinase phosphorylate p53 protein at serine 15 in response to UV radiation. *J Biol Chem* 275:20444-20449.

Shimizu S, Ide T, Yanagida T, Tsujimoto Y (2000) Electrophysiological study of a novel large pore formed by Bax and the voltage-dependent anion channel that is permeable to cytochrome c. *J Biol Chem* 275:12321-12325.

Shimizu S, Narita M, Tsujimoto Y (1999) Bcl-2 family proteins regulate the release of apoptogenic cytochrome c by the mitochondrial channel VDAC. *Nature* 399:483-487.

Shou Y, Li L, Prabhakaran K, Borowitz JL, Isom GE (2004) Calcineurin-mediated Bad translocation regulates cyanide-induced neuronal apoptosis. *Biochem J* 379:805-813.

Sitia R, Molteni SN (2004) Stress, protein (mis)folding, and signaling: the redox connection. *Sci STKE* 2004:e27.

Spierings D, McStay G, Saleh M, Bender C, Chipuk J, Maurer U, Green DR (2005) Connected to death: the (unexpurgated) mitochondrial pathway of apoptosis. *Science* 310:66-67.

Stefanis L (2005) Caspase-dependent and -independent neuronal death: two distinct pathways to neuronal injury. *Neuroscientist* 11:50-62.

Suzuki Y, Takahashi-Niki K, Akagi T, Hashikawa T, Takahashi R (2004) Mitochondrial protease Omi/HtrA2 enhances caspase activation through multiple pathways. *Cell Death Differ* 11:208-216.

Szegezdi E, Logue SE, Gorman AM, Samali A (2006) Mediators of endoplasmic reticulum stress-induced apoptosis. *EMBO Rep* 7:880-885.

Tabakman R, Jiang H, Shahar I, Iren-Zakay H, Levine RA, Lazarovici P (2005) Neuroprotection by NGF in the PC12 in vitro OGD model: involvement of mitogen-activated protein kinases and gene expression. *Ann N Y Acad Sci* 1053:84-96.

Tan Z, Sankar R, Tu W, Shin D, Liu H, Wasterlain CG, Schreiber SS (2002) Immunohistochemical study of p53-associated proteins in rat brain following lithium-pilocarpine status epilepticus. *Brain Res* 929:129-138.

Tanaka S, Takehashi M, Iida S, Kitajima T, Kamanaka Y, Stedeford T, Banasik M, Ueda K (2005) Mitochondrial impairment induced by poly(ADP-ribose) polymerase-1 activation in cortical neurons after oxygen and glucose deprivation. *J Neurochem* 95:179-190.

Tentori L, Portarena I, Graziani G (2002) Potential clinical applications of poly(ADP-ribose) polymerase (PARP) inhibitors. *Pharmacol Res* 45:73-85.

Terrinoni A, Ranalli M, Cadot B, Leta A, Bagetta G, Vousden KH, Melino G (2004) p73-alpha is capable of inducing scotin and ER stress. *Oncogene* 23:3721-3725.

Tsuruta F, Sunayama J, Mori Y, Hattori S, Shimizu S, Tsujimoto Y, Yoshioka K, Masuyama N, Gotoh Y (2004) JNK promotes Bax translocation to mitochondria through phosphorylation of 14-3-3 proteins. *EMBO J* 23:1889-1899.

Vanags DM, Porn-Ares MI, Coppola S, Burgess DH, Orrenius S (1996) Protease involvement in fodrin cleavage and phosphatidylserine exposure in apoptosis. *J Biol Chem* 271:31075-31085.

Vannucci RC, Lyons DT, Vasta F (1988) Regional cerebral blood flow during hypoxia-ischemia in immature rats. *Stroke* 19:245-250.

Vaux DL, Cory S, Adams JM (1988) Bcl-2 gene promotes haemopoietic cell survival and cooperates with c-myc to immortalize pre-B cells. *Nature* 335:440-442.

Walton M, Connor B, Lawlor P, Young D, Sirimanne E, Gluckman P, Cole G, Dragunow M (1999) Neuronal death and survival in two models of hypoxic-ischemic brain damage. *Brain Res Brain Res Rev* 29:137-168.

Wang Z, Cuddy M, Samuel T, Welsh K, Schimmer A, Hanai F, Houghten R, Pinilla C, Reed JC (2004) Cellular, biochemical, and genetic analysis of mechanism of small molecule IAP inhibitors. *J Biol Chem* 279:48168-48176.

Wei MC, Zong WX, Cheng EH, Lindsten T, Panoutsakopoulou V, Ross AJ, Roth KA, MacGregor GR, Thompson CB, Korsmeyer SJ (2001) Proapoptotic BAX and BAK: a requisite gateway to mitochondrial dysfunction and death. *Science* 292:727-730.

Wolter KG, Hsu YT, Smith CL, Nechushtan A, Xi XG, Youle RJ (1997) Movement of Bax from the cytosol to mitochondria during apoptosis. *J Cell Biol* 139:1281-1292.

Xiang H, Kinoshita Y, Knudson CM, Korsmeyer SJ, Schwartzkroin PA, Morrison RS (1998) Bax involvement in p53-mediated neuronal cell death. *J Neurosci* 18:1363-1373.

Yakovlev AG, Faden AI (2004) Mechanisms of neural cell death: implications for development of neuroprotective treatment strategies. *NeuroRx* 1:5-16.

Yoneda T, Imaizumi K, Oono K, Yui D, Gomi F, Katayama T, Tohyama M (2001) Activation of caspase-12, an endoplasmic reticulum (ER) resident caspase, through tumor necrosis factor receptor-associated factor 2-dependent mechanism in response to the ER stress. *J Biol Chem* 276:13935-13940.

Yu SW, Wang H, Poitras MF, Coombs C, Bowers WJ, Federoff HJ, Poirier GG, Dawson TM, Dawson VL (2002) Mediation of poly(ADP-ribose) polymerase-1-dependent cell death by apoptosis-inducing factor. *Science* 297:259-263.

Yuan J, Lipinski M, Degterev A (2003) Diversity in the mechanisms of neuronal cell death. *Neuron* 40:401-413.

Zhao Y, Chaiswing L, Velez JM, Batinic-Haberle I, Colburn NH, Oberley TD, St Clair DK (2005) p53 translocation to mitochondria precedes its nuclear translocation and targets mitochondrial oxidative defense protein-manganese superoxide dismutase. *Cancer Res* 65:3745-3750.

Zhu C, Qiu L, Wang X, Hallin U, Cande C, Kroemer G, Hagberg H, Blomgren K (2003) Involvement of apoptosis-inducing factor in neuronal death after hypoxia-ischemia in the neonatal rat brain. *J Neurochem* 86:306-317.

Zhu C, Wang X, Hagberg H, Blomgren K (2000) Correlation between caspase-3 activation and three different markers of DNA damage in neonatal cerebral hypoxia-ischemia. *J Neurochem* 75:819-829.

Zhu C, Wang X, Huang Z, Qiu L, Xu F, Vahsen N, Nilsson M, Eriksson PS, Hagberg H, Culmsee C, Plesnila N, Kroemer G, Blomgren K (2007) Apoptosis-inducing factor is a major contributor to neuronal loss induced by neonatal cerebral hypoxia-ischemia. *Cell Death Differ* 14:775-784.

Zong WX, Li C, Hatzivassiliou G, Lindsten T, Yu QC, Yuan J, Thompson CB (2003) Bax and Bak can localize to the endoplasmic reticulum to initiate apoptosis. *J Cell Biol* 162:59-69.

VITA

Martin Bartholomew Gill was born on March 24, 1976, in Bethesda, Maryland, the son of Walter John Gill, Jr. and Pennie Louise Gill. After graduating as valedictorian from St. John Vianney High in St. Louis, Missouri, in 1994, he entered The University of Missouri at Columbia as a Curator's Scholar. He received the degree of Bachelor of Arts in Psychology in 2002. He entered the Graduate School of Biomedical Sciences at The University of Texas Medical Branch at Galveston in 2003 as a Toxicology Scholar. While a student in the Neuroscience Graduate Program, he received several awards in recognition for his research, including a NIEHS pre-doctoral fellowship. In August of 2007, with his wife, Cassie, he will start a postdoctoral fellowship at Northwestern University, Feinberg School of Medicine, in Chicago, Illinois, to continue his career in research.

Permanent address: 3433 Cove View Boulevard
Galveston, Texas 77554

This dissertation was typed by Martin B. Gill.